

Locomotor system simulations
and muscle modeling
of the stick insect (*Carausius morosus*)

I n a u g u r a l - D i s s e r t a t i o n

zur

Erlangung des Doktorgrades

der Mathematisch-Naturwissenschaftlichen Fakultät

der Universität zu Köln

vorgelegt von

Marcus Blümel

aus Dinslaken

2010

Berichtersteller/in:

Prof. Dr. Ansgar Büschges

Prof. Dr. Wolfgang Walkowiak

Tag der letzten mündlichen Prüfung: 20.01.2011

DER FREUNDSCHAFT
-
UND ALL DEM GLÜCK
DAS SIE MIR SCHENKTE

Zusammenfassung

Auch heutzutage noch übertreffen so genannte "primitive Spezies" wie Insekten jede von Menschen entwickelte Fortbewegungsmaschine in Punkten Agilität, Anpassungsfähigkeit und Zuverlässigkeit - um nur einige zu nennen. Die vorliegende Arbeit beleuchtet zwei wichtige Aspekte, die wesentlich zur Überlegenheit der biologischen, terrestrischen Lokomotionssysteme beitragen, nämlich Bewegungssteuerung und Muskeleigenschaften.

Im ersten Teil wird ein neuartiger Steuerungsansatz für die Kontrolle von mehrsegmentigen Beinen vorgestellt, welcher die komplexen Berechnungen, die üblicherweise zur Kontrolle kinematischer Ketten notwendig sind, überflüssig macht. Das Steuerungsprinzip basiert auf spezifischen sensomotorischen Regeln, die aus mehreren Jahrzehnten Forschung an der Stabheuschrecke (*Carausius morosus*) gewonnen wurden. Mittels einer physikalischen Simulation des Stabheuschreckenkörpers wird gezeigt, dass die für die Stabheuschrecke bekannten Mechanismen zur Koordination von Beinsegmenten hinreichend sind, um im Mittelbein stabile, periodische Laufbewegungen zu erzeugen. Weiterhin war es mit Hilfe des Steuerungsprinzips auch möglich Vorder- und Hinterbeinbewegungen zu kontrollieren, wobei für die erfolgreiche Kontrolle des Hinterbeins eine leichte Veränderung im Regelsatz notwendig war.

Der zweite Teil dieser Arbeit, der aus drei Kapiteln besteht, behandelt die Modellierung des Extensors tibiae, eines der Hauptbeinmuskeln. Der Muskel ist das zentrale Element jeder Bewegungsform und mittlerweile ist unumstritten, dass Muskeln komplexe und sehr variable Eigenschaften haben. Die Zusammenhänge zwischen Aktivität im Motorneuron und der letztendlich resultierenden Bewegung können in der Regel nur mit Hilfe von Computermodellen und Simulationen nachvollzogen werden.

Es wird zunächst beschrieben wie das Modell eines einzelnen, individuellen Extensormuskels erstellt werden kann. Dieser Ansatz erfordert, dass alle Kennlinien, die zur Erstellung eines klassischen Hill-Modells notwendig sind, an einem einzelnen Muskel experimentell bestimmt werden können. Hierzu ist es nötig, die Anzahl und Dauer der Muskelmessungen und Stimulationen auf ein Minimum zu reduzieren, sodass der Muskel das gesamte Protokoll ermüdungsfrei überstehen kann.

Im Anschluss an die Darstellung dieses Ansatzes wird im nächsten Teil eine Anwendung der individuellen Muskelmodelle gezeigt. Muskeln von 10 verschiedenen Versuchstieren werden auf Unabhängigkeit ihrer Modellparameter hin untersucht. Tatsächlich ergeben sich bei dieser Untersuchung Abhängigkeiten in zwei Parameterpaaren - einmal zwischen zwei Parametern der statischen passiven Kraftkurve, und einmal zwischen einem Parameter der Kraft-Längenkurve und einem anderen der Kraft-Aktivierungskurve. Letztendlich lassen beide Korrelationen darauf schließen, dass das Modell noch weiter reduziert werden könnte.

Im letzten Teil werden isometrische und isotonische Simulationen mit unterschiedlichen Konfigurationen des Modells durchgeführt. Hier wird der Frage nachgegangen, inwieweit sich eine Mittelwertbildung unterschiedlicher Modellparameter auf die Leistungsfähigkeit des Modells auswirkt. Dies wird an vier unterschiedlichen Modellkonfigurationen untersucht, die sich nur im Anteil an gemittelten Parametern unterscheiden.

Es zeigt sich, dass im Vergleich zu einem Modell welches ausschließlich aus gemittelten Parametern besteht, das muskelspezifische Modell um etwa 40% besser ist.

Abstract

It is a matter of fact that even so called “primitive species” (like insects) readily outperform any human locomotive invention with respect to agility, adaptability and reliability – to name the least. The work at hand deals with two aspects that contribute to the pre-eminence of biological, terrestrial locomotor systems, namely motion control and muscle properties.

In the first part of this work, a new, biologically well-founded approach for the control of articulated legs is presented. This controller, based on the detailed physiological knowledge of the stick insect’s (*Carausius morosus*) leg control, redundantizes complex forward or backward kinematic calculations by dexterous employment of sensory feedback and muscle properties.

This section shows that the collection of segmental coordination rules (which have been studied in the stick insect for several decades) is indeed able to generate periodic, robust middle leg stepping movements in a physical simulation of the animal. Furthermore, the controller is capable of handling stepping in the front and hind leg; although for hind leg stepping minor modifications were necessary.

The second part of this work is about muscle modeling and it is divided into three chapters. Lynchpin of any motion is the muscle, and nowadays it is well-accepted that muscle properties are complex and highly variable. Hence, no trivial relationship between motor neuron activity and motion can be expected and typically, computer modeling is required to link the two.

This part therefore first describes how a model of the stick insect’s extensor tibiae muscle can be developed for individual muscles. The approach presented offers a way to measure and model all properties for the generation of a classical Hill-type model, in a single animal. Therefore it was necessary to reduce the number of measurements, stimulations and the overall time span of the experiment to a degree this muscle could take without severe loss in vitality.

After this approach has been described, the next section deals with a possible application of individual muscle modeling. The variation of muscle model parameters is investigated for 10 different individuals. The question of parameter independence is addressed, and in fact it could be shown that there is co-

variation between two different pairs of parameters. One correlation was found between two parameters modeling passive static force curve, the other between one parameter of the force-length and one of the force-activation curve. Both correlations suggest that the model can be reduced further.

In the final section, isometric and isotonic simulations were performed with different model configurations. It is investigated how far averaging parameters of different animals would influence model performance. This is studied by comparing the error produced by four different model configurations, differing in their share of averaged parameters. Compared to a model entirely composed of averaged parameters, performance of the muscle specific model improves by approximately 40%.

Contents

| | | |
|----------|---|-----------|
| 1 | Overview | 1 |
| 2 | Simulation of insect walking | 3 |
| 2.1 | Introduction | 3 |
| 2.2 | Simulation set up | 5 |
| 2.2.1 | Leg step controller | 5 |
| 2.2.2 | Simulation environment | 7 |
| 2.3 | Leg control mechanisms | 8 |
| 2.3.1 | Timing influences (middle leg) | 9 |
| 2.3.2 | Magnitude influences (middle leg) | 10 |
| 2.4 | The neural control system | 12 |
| 2.4.1 | State Transitions (timing control) | 14 |
| 2.4.2 | Activation Levels (magnitude control) | 16 |
| 2.4.3 | Neural control of the middle leg | 18 |
| 2.4.3.1 | Sideways | 18 |
| 2.4.3.2 | Forward | 22 |
| 2.4.4 | Predictions for front and hind leg | 24 |
| 2.5 | Discussion | 32 |
| 2.5.1 | Muscle model | 32 |
| 2.5.2 | Kinematics and muscle activations | 33 |
| 2.5.3 | Conclusion | 34 |
| 3 | Building an individual Hill-type model of the extensor tibiae muscle | 37 |
| 3.1 | Introduction | 37 |
| 3.2 | Materials and methods | 39 |
| 3.2.1 | Modeling tools | 39 |
| 3.2.2 | Dissection and experimental set-up | 39 |
| 3.2.3 | Nerve stimulation | 40 |
| 3.2.4 | Muscle protocols | 40 |
| 3.3 | Results | 43 |
| 3.3.1 | Passive force curve (parallel elasticity) | 43 |
| 3.3.2 | Series elasticity | 44 |

| | | |
|----------|---|-----------|
| 3.3.3 | Force-activation curve | 50 |
| 3.3.4 | Force-length curve | 51 |
| 3.3.5 | Force-velocity curve | 57 |
| 3.4 | Discussion | 61 |
| 4 | Parameter variation between individual Hill-type muscle models | 65 |
| 4.1 | Introduction | 65 |
| 4.2 | Materials and methods | 66 |
| 4.2.1 | Modeling and experimental procedures | 66 |
| 4.2.2 | Correlation analysis | 66 |
| 4.3 | Results | 67 |
| 4.3.1 | Parallel elasticity | 67 |
| 4.3.2 | Series elasticity | 68 |
| 4.3.3 | Force-activation | 69 |
| 4.3.4 | Force-length | 70 |
| 4.3.5 | Force-velocity | 72 |
| 4.3.6 | Parameter correlations | 75 |
| 4.3.6.1 | Parameters k_1 and k_2 | 75 |
| 4.3.6.2 | Parameters B and $curv_{hyp}$ | 76 |
| 4.4 | Discussion | 79 |
| 4.4.1 | Possible experimental or analysis artifacts | 79 |
| 4.4.2 | Implications of the observed correlations | 81 |
| 4.4.3 | Implications of inter-animal variability for neural control and modeling | 81 |
| 5 | Simulating and comparing individual Hill-type models | 83 |
| 5.1 | Introduction | 83 |
| 5.2 | Material and methods | 84 |
| 5.2.1 | Simulation conditions and stimulation | 84 |
| 5.2.1.1 | Simulation paradigms | 84 |
| 5.2.1.2 | Activation dynamics | 85 |
| 5.2.1.3 | Mechanical simulation | 86 |
| 5.2.1.4 | Muscle model configurations | 88 |
| 5.2.1.5 | Error calculations | 90 |
| 5.3 | Results | 91 |
| 5.3.1 | Approach outline | 91 |
| 5.3.2 | Activation dynamics | 94 |
| 5.3.2.1 | Frequency dependency | 94 |

| | | |
|----------|--|------------|
| 5.3.2.2 | Isometric and isotonic parameters | 95 |
| 5.3.3 | Performance Overview | 96 |
| 5.3.4 | Mean performance example | 97 |
| 5.3.5 | Model configuration comparison | 100 |
| 5.3.6 | Best, mean, worst performance comparison | 103 |
| 5.4 | Discussion | 104 |
| 5.4.1 | Performance of the Hill-type model | 104 |
| 5.4.2 | Activation dynamics | 105 |
| 5.4.3 | Isometric and isotonic contractions | 106 |
| 5.4.4 | SE compensation for the force-length curve | 108 |
| 5.4.5 | Perfomance of the different model configurations | 112 |
| 6 | Closure remarks | 113 |
| 6.1 | Outlook | 114 |
| | Literaturverzeichnis | 117 |

1 Overview

This section is called overview, because each chapter has its own, non repetitive introduction. At this place I would like to explain the linkage between the chapters and why they are sequenced the way they are.

This work is divided into four parts, three of them dealing with a detailed description of a model of the stick insect's (*Carausius morosus*) middle leg extensor tibiae muscle. Chapter 2, however, deals with a neuro-mechanical simulation, which sits in first place as these investigations initiated the muscle studies in the following chapters.

The simulations in chapter 2 were performed with a very simple muscle model, and led to the conclusion that proper kinematics cannot be achieved without a realistic muscle model. These experiences motivated the development of an improved extensor tibiae model. The development of this model turned out to be a long and bendy road and the model as it is presented in chapters 3-5 is the result of endless recursive trials and improvements.

In chapter 3 I present the experimental and theoretical approach that were used to build the model. It is important to understand how the data basis was acquired and what processing was used for generating the model parameters, because the approach used is quite unusual. Due to the large variation observed in these muscles, the models were based on data of individual muscles. This process involved a sophisticated experimental paradigm, which is elaborated in chapter 3.

The next chapter deals with muscle variability. The possibility to generate models of individual muscles provides a tool for investigating inter-muscle variation. Thus, chapter 4 is an application of the individual muscle modeling approach presented in chapter 3.

Finally, chapter 5 investigates the performance of the individual models. A benefit of having an individual model is that its output can be compared to the output of the muscle it was made from. This offers very sensitive performance comparison and evaluation. But the major point in chapter 5 is to investigate the effect of using averaged parameters in modeling. Four different model

1 Overview

configurations are compared, which contain different configurations of averaged parameters.

It now appears that this work primarily deals with muscle modeling, but its very own and initial motivation was based on neuro-mechanical simulation.

2 Simulation of insect walking

2.1 Introduction

Understanding biological control of animal motion, in particular walking, is an important research topic. It is interdisciplinary, challenging and its prospective results may influence biological, medical (e.g. prosthetics) and technical domains (e.g. robot design).

Animal motion involves numerous biomechanical and neuronal mechanisms (Dickinson et al., 2000; Chiel et al., 2009) and several studies have investigated the combination of neuronal control, behavior, kinematics and biomechanics (Dickinson, 2006; Novakovic et al., 2006; Ritzmann and Büschges, 2007; Grillner et al., 2008; Pearson, 2008)

A special type of these complex models are so called “musculoskeletal models”. They are mainly developed for humans - (for review see Pandy, 2001; Zajac et al., 2002; Zajac, 2002; Zajac et al., 2003) and have a variety of applications like improvement of motion physics in sports to analysis of soft tissue damages during accidents (see for example Anthony, 2002). However, some biomechanical models of invertebrate systems exist (nicely reviewed in Pearson et al., 2006; Edwards, 2010). Very prominent invertebrate models are for example the simulation of feeding behavior in *Aplysia* (Yu et al., 1999) and cockroach hind leg (Full and Ahn, 1995).

Walking is a particular challenging aspect of this research, due to its inherent circular and feed back nature. It results of an interweavement of neuronal pattern generation, electro-mechanical transformation, sensory feedback, environmental loops as well as biophysical and biomechanical constraints (Pearson, 1993b; Bässler and Büschges, 1998; Kubow and Full, 1999; Duysens et al., 2000; Holmes et al., 2006). This richness of inter-dependent mechanisms makes it difficult to design and interpret experiments and thus simulations including sensory feedback were developed (Ekeberg, 1993; Ekeberg and Pearson, 2005).

Until the end of the 1990’s, the stick insect (*Carausius morosus*), although being a model system for locomotion for several decades, has not entered the world

2 *Simulation of insect walking*

of computer simulation. Sophisticated experiments have revealed a great deal of knowledge about the neuronal and behavioral bases of walking and walking control (Bässler, 1983; Cruse, 1990; Bässler, 1993; Bässler and Büschges, 1998).

In general two types of experiments had contributed to this knowledge. On the one hand neuro-physiological studies, in particular these of sense organs and their integration into stepping cycle. But these experiments are hard to do under closed-loop conditions. The animal usually has to be fixated, dissected and frequently legs not under investigation have to be removed.

Behavioral experiments, on the other hand, are easy to do (and are inherently closed-loop). The animal is usually intact and more or less free to move, but insights into the underlying neuronal mechanisms can only be indirectly inferred and without additional experimental studies. This led to the situation that much physiological detail was known on the low level, and many behavioral observations were made on the high level, but the linkage of both was largely missing.

Thus, the desire to get a more integrated understanding of walking and its control, initiated the development of the first stick insect walking simulations at the end of 1990 (Cruse et al., 1999, 2000). These simulations fortified coordination rules derived from behavioral experiments by combining an artificial neuronal network controller with a kinematic stick insect simulation. However, these simulations did not model the neuronal mechanisms shown in the plenty of neurophysiological experiments, thus it remained an open question how the kinematic rules observed could be implemented on the neuronal level.

This issue has been approached by the development of neuro-mechanical, dynamic simulations (Hoy et al., 1990; Ekeberg, 1993; Loeb et al., 1999; Ekeberg, 2001; Ekeberg et al., 2004; Chiel et al., 2009; Pearson et al., 2006). These types of simulations combine the modeling of neuronal principles (e.g. leg control) with the Newton physics of rigid bodies and thus introduce a higher level of realism and integration. Especially it is possible to study sensory systems under closed loop conditions, preserving the full access to the detailed underlying mechanisms.

Movement in these dynamic simulations is created by force being applied to a mass. Mass motion can be further constraint in its degree of freedom to create joints. However, the dynamic paradigm prohibits the direct specification of linear or angular body velocity therefore controllers used in kinematic simulations (like the walk-net controller developed by Cruse et al.) can not be used without substantial modification.

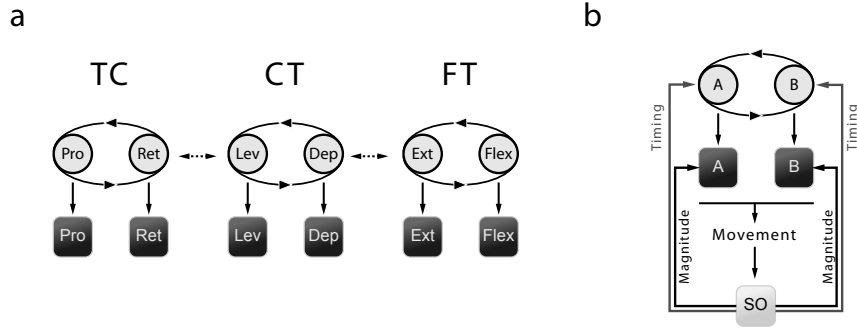


Figure 2.1: Key concepts of stick insect leg control. In panel a) is shown that each major leg segment is controlled by a dedicated CPG (one for the thorax-coxa joint (TC), one for coxa-trochanter (CT) and one for femur tibia joint (FT)). Loose coupling can infrequently be observed between these CPGs (indicated by the dashed arrows between the three oscillators). Each CPG has two mutual exclusive states (protraction (Pro) or retraction (Ret), levation (Lev) or depression (Dep) and extension (Ext) or flexion (Flex)). Switching into a state activates the associated motor system (dark squares) which consists of motor neurons and muscles.

Panel b) shows how sensory information interacts with centrally generated rhythms. The central oscillatory network (A and B in circles) generates rhythmic output and activates their associated motor system (A and B in squares). This activation generates movement which in turn is detected by sense organs (SO). These sensory signals can both change the phase of the CPG and the amplitude of motor system activity (adapted from Büschges, 2005).

In case of the stick insect many neurophysiological experiments have been performed investigating the role of central and sensory influence on motorneuron activity or muscle activation. None of these results can be easily related to angular velocities, but they can be related to muscle force. This fact makes dynamic simulations a means of choice for understanding how changes in neuronal activity effects and possibly controls movement (Lloyd and Besier, 2003; Zakotnik et al., 2006; Pearson et al., 2006; Chiel et al., 2009).

2.2 Simulation set up

2.2.1 Leg step controller

The leg stepping controller is responsible for the integration of all sensory inputs and calculates muscle activation levels based on the instantaneous combination of these signals. It is an important simplification that this controller does not keep track of its own state, all decisions made are purely due to the incoming sensory information at any time. In understanding how the controller is set up it might help to conceptually divide it into two parts. One part is responsi-

2 Simulation of insect walking

ble for selecting which muscle to activate (muscle activation *timing*), another part controls the activation amplitude of the active muscles (magnitude). This division fits well to the common hypothesis that muscle activation timing and magnitude are separately controlled (Büschges, 2005). This idea is based on findings showing that interneuronal networks are able to effect activation phasing by influencing *when* a given muscle gets activated (e.g. Bässler and Wegner, 1983; Büschges et al., 1995) while signals from sense organs are processed in parallel and effect *how strong* it is activated (e.g. Bässler and Büschges, 1998; Büschges et al., 2000).

Figure 2.1 summarizes current ideas of walking pattern generation. Central element of the controller organization is the joint oscillator (interconnected circles). It could be shown that each joint is associated with a dedicated internal oscillator (Bässler and Wegner, 1983; Büschges et al., 1995). Cycle coupling between oscillators in the absence of sensory input occurs very infrequently and proved to be weak to establish a fictive locomotion pattern for the whole limb (the coupling is indicated by the dashed arrows between the oscillators in Figure 2.1 a). Figure 2.1 a highlights this idea by presenting three basically independent oscillatory systems, one for each of the major leg joints (thorax-coxa (TC) joint, coxa-trochanter (CT) joint and femur-tibia (FT) joint). The output of the internal oscillator is fed to the motor system (motor neurons, muscles and tendons) represented by the dark boxes. Figure 2.1 b) shows the current understanding of how sensory input and central pattern generators cooperate. The CPG element controls the timing of muscle activation by either activating motor system A or B. The active motor system eventually causes a movement which in turn is detected by the sense organs (SO). They again feed back into the CPG and the motor system. The CPG uses sensory information mainly to coordinate its rhythm (it decides whether to stay in the current activity phase, or to switch and activate the antagonistic motor system). The sensory signals feeding into the motor system serve another purpose and are used to tune muscle activation level (magnitude).

The controller used here, does not have an internal oscillator and therefore will not be able to generate movements without sensory feedback. However, although internal oscillators (central pattern generators, CPG's) have been shown to be activateable in almost all rhythmic locomotor systems (Grillner, 1985; Pearson, 1993a; Marder and Bucher, 2001; Grillner, 2003; Pearson, 2004) their proportion in controlling functional motor output unclear and most likely depends on the kind of motor task. Especially in highly adaptable behaviors

like (slow) walking, sensory signals can be expected to influence the resulting motor pattern that much, that one could expect meaningful simulation results even in the absence of an internal oscillator. From a theoretical perspective, as the timing of muscle activation is strongly determined by sensory information, the CPG could be approximated with a constant arousal system, which possibly might have phasic effects on the probability of a sensor-induced activation switching, but is not capable of dictating its periodicity to the motor neurons. Therefore by omitting an internal oscillator, the probability of a sensor signal causing a switch in muscle activation is artificially increased, but the results should still be meaningful.

2.2.2 Simulation environment

The leg stepping controller operates in a three dimensional environmental simulation. This simulation includes a six legged, physical model of the stick insect, a surface to move on, gravity, body collision detection and realistic proportional body masses. The simulator code was developed by Örjan Ekeberg in the C computer language and it was exclusively adapted to the stick insect simulations performed here. Stick insect body model, starting conditions, and all other parameters were hard coded into the simulator. The leg stepping controller however, was loaded during run time as a Python script, which allowed flexible and easy experimentation with different controller versions.

| Leg | Segment | Length (mm) | Mass (mg) |
|------------------------|---------|-------------|-----------|
| Front | Coxa | 1.61 | 0.43 |
| | Femur | 17.85 | 10.30 |
| | Tibia | 17.10 | 3.30 |
| Middle | Coxa | 1.57 | 1.00 |
| | Femur | 13.47 | 8.05 |
| | Tibia | 13.20 | 1.70 |
| Hind | Coxa | 1.39 | 1.00 |
| | Femur | 15.51 | 8.60 |
| | Tibia | 16.51 | 2.70 |
| Head / Thorax /Abdomen | | 73.20 | 760.40 |

Table 2.1: Size and mass of the body elements used in the mechanical model of the stick insect simulator. Numbers are partially from Cruse, 1976 or have been measured by members of the department of animal physiology of the university Cologne.

2 Simulation of insect walking

The mechanical stick insect model consisted exclusively of rigid bodies, cylindrical in shape the caps closed with a hemisphere. Head, trunk and abdomen of the animal were approximated with a single cylinder, each leg was assembled out of three cylinders. All joints have been simplified to being hinge joints with a single degree of freedom which is a pretty accurate approximation for coxa-trochanter and femur-tibia joint, but the thorax-coxa joint is known to be more complex in reality (Cruse and Bartling, 1995). Irrespective of the fact that this joint has more than one degree of freedom, it is most of the time *operating* like a hinge joint.

Size and mass of each body part was averaged from several animals or, if available, taken from the literature (Cruse, 1976, see also Ekeberg et al., 2004). A summary of all masses and sizes used in the mechanical model can be found in Table 2.1.

As explained on page 4, motion in dynamic simulations results from the application of forces to body parts. Force in this simulation is generated by simplified Hill-type muscle model. This muscle model transforms an arbitrary unit *activation level* into a force depending on muscle length and contraction velocity. Force-length and force-velocity relations were approximated by linear fits to data of Storrer (1976).

The simulator finally provides information about joint angles and angular velocities (both crucial for muscle length and contraction velocity calculations) as well as joint torques and ground contact. This data was made available to the leg stepping controller as well, but only joint angle, velocity and ground contact signals are used during control.

Stepping is simulated with only a single leg actively moving at any time, the other legs supporting body weight and stabilize the animals position. Non-moving legs are immobilized by strong co-contraction of its muscles, the moving leg is defined friction less to allow it to slide over the ground during stance phase. This situation is comparable to classic *slippery surface* experiments or experiments performed with a tread-band (Graham and Cruse, 1981; Epstein and Graham, 1983; Gruhn et al., 2006).

2.3 Leg control mechanisms

Many sense organs and many different types of sensory information are involved in leg stepping control (Graham, 1985; Cruse, 1990; Bässler and Büschges, 1998). Historically most investigations were performed on the middle leg, thus

most detailed knowledge is available for this leg. However, not all of these known influences could be incorporated into this model, only timing and magnitude influences have been included instead. Two types of signals were of particular interest. Signals originating from the FT joint sense organs (FT angle and angular velocity) and signals encoding strain inside the leg which are crucial for proper ground contact detection. The sense organ responsible for the neuronal FT joint feedback is the femoral chordotonal organ (fCO, Bässler, 1974). Strain or load on the leg is sensed by two populations of campaniform sensillae, one located on the trochanter and another on the femur (trCS and fCS, Delcomyn, 1991; Hofmann and Bässler, 1982).

Sections 2.3.1 and 2.3.2 describe the influences of sensory information for leg stepping control which were included in the simulation. A visual summary of these results is given in Table 2.2.

2.3.1 Timing influences (middle leg)

Signals number 1 and 2 both originate from the most proximal joint, the torax-coxa (CT) joint. The strain signals however are detected on the trochanter, the adjacent leg segment, by the trochanteral campaniform sensillae (trCS). These signals influence the timing of both major joint controlling muscles (protractor coxae (PRO) and retractor coxae (RET)). An increase in strain can cause the retractor to become active if it was inactive before the same signal is able to terminate preceding protractor activity. (Note that all signals share this mutual exclusive behavior for antagonistic joint muscles.) When strain decreases again the effects are reversed. Retractor activity becomes more likely to get terminated and protractor onset is supported. The role of trCS in joint control has been investigated in detail by Akay et al. 2004.

Signals number 3 to 6 influence the coxa-trochanter (TC) joint. In analogy to the TC joint, the sense organs providing the control signals are placed on the adjacent leg segment, the femur. The femoral chordotonal organ (fCO) delivers directed position, velocity and also acceleration signals, but only the first two have verifiable effects on the timing of muscle activity. If substantial flexion velocity or a critical flexed position is detected (signals 3 and 4), it can initiate activity in the levator trochanteris (LEV) and at the same time terminate activity in the depressor trochanteris (DEP). The opposite responses can be observed for extension signals. An extending motion or an extended joint position can terminate levator activity and initiate depressor activity.

2 Simulation of insect walking

The effects of position signals can be even strong enough to lock the oscillatory network of the CT joint in one phase (for example the levation phase). The effects summarized here result from investigations of Bucher et al. (2003); Hess and Büschges (1999) and Bässler (1977).

Signals 7 to 10 effect the femur-tibia joint (FT). Two sense organs are involved in the joint control, the fCO provides movement and position information and the femoral campaniform sensillae (fCS) provide strain signals. In contrast to the control of TC and CT joint, the sense organs and the effected muscles reside on the same leg segment. A fact that is sometimes referred to as *intra joint control*, in contrast to *inter joint control* (where sense organs influence muscle activity of adjacent leg segments).

Interestingly, in case of the FT control, a logical separation between position and velocity signals can be seen. Increased flexion velocity assists the ongoing flexion by consolidating flexor tibiae (FLX) activity and decreasing the probability of extensor tibiae (EXT) becoming active (Bässler, 1976, 1988). This forms a positive feedback loop which supporting the robustness of the stance phase. Flexion can be finally terminated by position signals of the fCO. At a critical FT angle, these signals can cause the termination of flexor activity and initiate extensor activity.

Strain signals are detected by the femoral campaniform sensillae (fCS). If strain increases, which is the case in stance phase, when the leg has ground contact, flexor activity can be initiated and extensor activity terminated (Akay et al., 2004). In turn, in case load decreases (for example at the end of stance phase) fCS signals can activate extensor and terminate flexor, thus supporting the transition from stance to swing phase.

2.3.2 Magnitude influences (middle leg)

Magnitude influences have only been identified effecting the coxa-trochanter joint muscles. Motion and position signals, originating from the CFO both have similar effects on levator and depressor activation amplitude. For a flexed FT joint position or substantial flexion velocity levator activity increases and depressor activity decreases. The opposite is true for extended positions and extension motion. In this case depressor activity increases and levator activity decreases (Hess and Büschges, 1997; Bucher et al., 2003).

Signals 15-18 are generated by the trochanteral hair plates (trHP) and an internal levator receptor organ (Schmitz, 1986; Schmitz and Schöwerling, 1992). As the signals originate from the trochanter itself and effect CT controlling mus-

2.3 Leg control mechanisms

| Timing | | | | | | | | | |
|-----------|-----------------|-----|-----|-----|-----|-----|-----|-------------|-------|
| # | Signal | PRO | RET | DEP | LEV | FLX | EXT | Sense organ | Joint |
| 1 | strain increase | ⊖ | ⊕ | | | | | trCS | TC |
| 2 | strain decrease | ⊕ | ⊖ | | | | | trCS | |
| 3 | flex. motion | | | ⊖ | ⊕ | | | fCO | CT |
| 4 | flex. position | | | ⊖ | ⊕ | | | fCO | |
| 5 | ext. motion | | | ⊕ | ⊖ | | | fCO | |
| 6 | ext. position | | | ⊕ | ⊖ | | | fCO | |
| 7 | flex. motion | | | | | ⊕ | ⊖ | fCO | FT |
| 8 | flex. position | | | | | ⊖ | ⊕ | fCO | |
| 9 | strain increase | | | | | ⊕ | ⊖ | fCS | |
| 10 | strain decrease | | | | | ⊖ | ⊕ | fCS | |
| Magnitude | | | | | | | | | |
| 11 | flex. position | | | ⊖ | ⊕ | | | fCO | CT |
| 12 | flex. motion | | | ⊖ | ⊕ | | | fCO | |
| 13 | ext. position | | | ⊕ | ⊖ | | | fCO | |
| 14 | ext. motion | | | ⊕ | ⊖ | | | fCO | |
| 15 | dep. position | | | ⊖ | ⊕ | | | trHP | |
| 16 | dep. motion | | | ⊖ | ⊕ | | | trHP | |
| 17 | lev. position | | | ⊕ | ⊖ | | | trHP | |
| 18 | lev. motion | | | ⊕ | ⊖ | | | trHP | |
| | | PRO | RET | DEP | LEV | FLX | EXT | | |

Table 2.2: State transition matrix of middle leg control. This Table lists signals and their influences on muscle activation strength (magnitude) and activation phase (timing). The first column contains a number for reference in the text, second column the signal that could be identified to effect magnitude or timing (flex.: flexion, ext.: extension). The following six columns represent the six major leg muscles (PRO: protractor, RET: retractor, DEP: depressor, LEV: levator, FLX: flexor, EXT: extensor). Sense organ column denotes the sense organ the signal originates from. The final column groups the joint which is effected by the muscle activity (TC: torax-coxa joint, CT: coxa-trochanter joint, FT: femur-tibia joint).

2 Simulation of insect walking

| Signal | Description |
|---------------------|---|
| FT pos flex | A rather flexed FT joint position. |
| FT pos ext | A rather extended FT joint position. |
| $GC \wedge \neg AR$ | The combination of ground contact (GC) (additionally representing strain increase) and no conditions for active reaction (AR) being given. $\neg AR$ is “true” if FT position is rather flexed and angular velocity of FT is high. |
| $GC \wedge AR$ | The combination of ground contact (GC) (additionally representing strain increase) and active reaction (AR). AR is “true” in case FT position is rather stretched and angular velocity of FT is small. |
| $\neg GC$ | No ground contact (additionally representing decreasing or lack of strain). |
| PEP | Posterior extreme position. This refers to the TC joint position. |

Table 2.3: Summary of signals used for state transitions. Signals can be binary (like ground contact) or continuous (angles or velocities).

cles, they form a feedback loop. This feedback loop is considered as a primary component of height control of the animal (Cruse et al., 1993). Looking closer to the effects of the trHP signals shows that they build a negative feedback. When ever the trochanter moves downward or has a downward velocity, depressor activity gets decreased and levator activity increased, potentially stopping the downward motion and turning it into a levation. In turn, if an upward position or velocity is detected, levator activity decreases and depressor activity increases. Thus muscles and trHP can work like a servo controller trying to keep a certain target CT angle.

2.4 The neural control system

The knowledge outlined above have been used to set up a software controller reflecting the essential features of the biological system. The controller has three independent modules, each controlling one leg joint (see ellipses in Figure 2.1). Each module has two mutual exclusive states (circles inside the ellipses in the same Figure). As joint oscillator coupling is weak (dashed arrows), it wasn’t included into the controller. Interpreting the controller as a state machine, the combination of the three independent oscillators each being in one of two possible activity states gives an overall of 8 possible states for a three joint controller (4 states if only two joints are controlled, which is true in case of leg

sideways stepping).

The controller changes its state in dependence of six signals, representing all sensory input that is capable of influencing activity timing (section 2.3.1). The signals are listed and explained in Table 2.3.

The `FT pos flexed` and `FT pos ext` signals simply represent the measured joint angle from the mechanical simulation. The `GC^AR` and `GC^¬AR` signals are a combination of strain, ground contact, position and velocity information. Whether the leg has ground contact or not can be decided by performing a collision detection inside the mechanical simulation. As a rigid body simulator was used, there was no way to get strain information of certain position on leg segments. This problem was worked around by using ground contact information as an approximator for strain. If a leg has ground contact strain could be expected to increase in all leg segments. In turn, if the leg is being lifted, strain is likely to decrease significantly in all leg segments.

In case ground contact is detected, the controller is basically expected to switch to producing a stance phase. But, at least for the middle leg, the stance phase has two parts, controlled by a phenomenon called the active reaction. Without going into detail about the active reaction (Bässler, 1988), in short it changes flexor and extensor activation in response to FT position and velocity information. The first part of the active reaction will occur when FT position is rather extended and flexion velocity isn't too high. Under this conditions, the active reaction supports the stance phase by initiating flexor and terminating extensor activation. If either FT position is rather flexed or flexion velocity is too high, part two of active reaction ceases flexor and starts extensor activation, thus supporting stance-swing transition.

The `¬GC` signal is generated if the ground collision of the leg disappears. This signal is thus again an approximation for decreasing strain on the trochanter and femur.

The final signal (PEP) has been added to reflect a powerful influence described only on the behavioral level. Advanced retraction of the leg in combination with decreasing load or strain, supports phase transition from stance to swing (Cruse, 1985). This is done by activating levator, protractor and extensor while inactivation retractor and depressor. This influence is powerful enough to prevent stance-swing transition if load receptors or TC position receptors are manipulated to continuously send stance phase information (Bässler, 1977, 1979). Though neuronal mechanisms of this influences are not known in any detail, this effect was included into the controller as it has proven to be an

2 *Simulation of insect walking*

important part in stepping control. However, strain information could only be approximated, which didn't allow for continuous load monitoring (ground contact is a binary signal), PEP was only implemented using the retraction angle of the leg. The load detection component was not included.

2.4.1 State Transitions (timing control)

The controller was designed as a memory less state machine. Its current state is purely defined by the input signals and on present state information. As the sideways controller only needs to control a two dimensional movement, its number of states is reduced to 4. Each sub table in Table 2.4 defines which new state will result from any combination of input signal and current state. They list all theoretically possible states and transitions, however not all states or transitions will be used during a normal walking cycle.

For the hind leg, a modified set of signals was used. The active reaction signal cannot simply be transferred to the hind leg, as its kinematic differs from the more anterior legs (Cruse and Bartling, 1995). The hind leg performs an extension movement in the FT joint during stance phase. An unmodified active reaction would interfere with the inversed kinematics of the hind leg FT joint. In how far the active reaction might be modified in the hind leg had not been investigated to the time these studies were performed, thus it was decided to remove the active reaction from the list of input signals for the hind leg. This decision results in a hind leg controller that doesn't need velocity information at all and entirely relies on position and ground contact signals. In addition to the posterior extreme position (PEP) an anterior extreme position signal (AEP) was added to the hind leg (Cruse, 1979, 1985). The AEP signal was responsible to terminate the swing phase by activation of depressor trochanteris in case of advanced protraction.

2.4 The neural control system

a Middle Leg, Sideways

| Signal | Status | | | |
|-----------------------|--------|----|----|----|
| | FL | FD | EL | ED |
| FT pos flex | FD | FL | EL | ED |
| FT pos ext | FL | FD | ED | EL |
| GC \wedge \neg AR | EL | EL | EL | EL |
| GC \wedge AR | FD | FD | FL | FD |
| \neg GC | EL | ED | EL | ED |
| PEP | FL | FL | EL | EL |

b Middle Leg, Forward

| Signal | Status | | | | | | | |
|-----------------------|--------|-----|-----|-----|-----|-----|-----|-----|
| | RDF | RLF | RLE | RDE | PDF | PDE | PLF | PLE |
| FT pos flex | RLF | RLF | RLE | RLE | PLF | PLE | PLF | PLE |
| FT pos ext | RDF | RDF | RDE | RDE | PDF | PDE | PDF | PDE |
| GC \wedge \neg AR | RDE | RLE | RLE | RDE | RDE | RDE | RLE | RLE |
| GC \wedge AR | RDF | RLF | RLF | RDF | RDF | RDF | RLF | RLF |
| \neg GC | PDE | PLE | PLE | PDE | PDE | PDE | PLE | PLE |
| PEP | RLF | RLF | RLE | RLE | PLF | PLE | PLF | PLE |

c Front Leg, Forward

| Signal | Status | | | | | | | |
|-----------------------|--------|-----|-----|-----|-----|-----|-----|-----|
| | RDF | RLF | RLE | RDE | PDF | PDE | PLF | PLE |
| FT pos flex | RLF | RLF | RLE | RLE | PLF | PLE | PLF | PLE |
| FT pos ext | RDF | RDF | RDE | RDE | PDF | PDE | PDF | PDE |
| GC \wedge \neg AR | RDE | RLE | RLE | RDE | RDE | RDE | RLE | RLE |
| GC \wedge AR | RDF | RLF | RLF | RDF | RDF | RDF | RLF | RLF |
| \neg GC | PDE | PLE | PLE | PDE | PDE | PDE | PLE | PLE |
| PEP | RLF | RLF | RLE | RLE | PLF | PLE | PLF | PLE |

d Hind Leg, Forward

| Signal | Status | | | | | | | |
|-------------|--------|-----|-----|-----|-----|-----|-----|-----|
| | RDF | RLF | RLE | RDE | PDF | PDE | PLF | PLE |
| FT pos flex | RDF | RDF | RDE | RDE | PDF | PDE | PDF | PDE |
| FT pos ext | RLF | RLF | RLE | RLE | PLF | PLE | PLF | PLE |
| GC | RDE | RLE | RLE | RDE | RDE | RDE | RLE | RLE |
| \neg GC | PDF | PLF | PLF | PDE | PDF | PDF | PLF | PLF |
| PEP | RLF | RLF | RLE | RLE | PLF | PLE | PLF | PLE |
| AEP | RDF | RDF | RDE | RDE | PDF | PDE | PDF | PDE |

Table 2.4: State transition tables of the stepping controller. The left column lists the signals provided by the simulation environment and entering the controller. For details see section 2.4. The group of columns right hand side denotes the states the controller can be in. States are defined by the activity of antagonistic leg muscles.

The following shortcuts are used: F: flexion, E: extension, L: levation, D: depression, R: retraction, P: protraction. Depending on the number of joints controlled, each state is defined by two or three letters (for example: FL means flexion and levation, RDF means retraction, depression and flexion). The transition table defines which state the controller enters for each possible combination of input signal and current state. Not all states will be entered during normal stepping, however.

a) The sideways stepping is two dimensional; therefore only two joints need to be controlled, reducing the number of possible states to 4. b-d) Middle, front and hind leg transition tables. Note that in case of the hind leg, some signals differ from the usual set. See text for details about the signal set.

2 Simulation of insect walking

| State | Front leg | | Middle leg (restricted) | | Middle leg | | Hind leg | |
|-------------|--------------------------|-----------------|--------------------------|-------------|--------------------------|-------------|--------------------------|---------------------|
| | Flexor | Extensor | Flexor | Extensor | Flexor | Extensor | Flexor | Extensor |
| Flexion | 3.4 | 0.01 | 0.8 | 0.1 | 0.8 | 0.1 | 0.02 | 0.01 |
| Extension | 0.09 | 1.9 | 0.21 | 0.95 | 0.21 | 0.95 | 0.09 | 0.96 |
| | Depressor | Levator | Depressor | Levator | Depressor | Levator | Depressor | Levator |
| Depression | $1.1+d(\gamma)+h(\beta)$ | $0.2 l(\gamma)$ | $0.2+d(\gamma)+h(\beta)$ | 0 | $0.2+d(\gamma)+h(\beta)$ | 0 | $l(\gamma)+0.1 h(\beta)$ | $1.1 d(\gamma)$ |
| Levation | $0.1 d(\gamma)$ | $1.6 l(\gamma)$ | 0 | $l(\gamma)$ | 0 | $l(\gamma)$ | $0.51 l(\gamma)$ | $4 d(\gamma) + 0.1$ |
| | Protractor | Retractor | Protractor | Retractor | Protractor | Retractor | Protractor | Retractor |
| Protraction | 0.4 | 0 | 0.4 | 0.4 | 0.05 | 0 | 0.1 | 0 |
| Retraction | 0.1 | 0.4 | 0.4 | 0.4 | 0 | 0.35 | 0 | 0.9 |

Table 2.5: Muscle activation levels. Each state sets the muscle activation level for the two antagonistic muscles it controls. Activation level can be a constant value or one of the three magnitude functions ($l(x), d(x), h(x)$). The magnitude functions have a joint angle as argument. Angle abbreviations are: $\alpha =$ CT angle, $\gamma =$ FT angle.

Equations used:

$$l(x) = \max(0, 0.28 \cdot p(x) + 0.001 \cdot q(x))$$

$$d(x) = \max(0, 0.08 - 0.105 \cdot p(x) + 0.08 \cdot q(x))$$

$$h(x) = \max(0, q(x))$$

$$p(x) = \frac{(x - w_{min})}{w_{max} - w_{min}}$$

if $p(x)$ is used in $l(x)$ or $d(x)$ $w_{min} = 61$ and $w_{max} = 100$

if $p(x)$ is used in $h(x)$ $w_{min} = -40$ and $w_{max} = 80$

$$q(x) = 1 - p(x)$$

2.4.2 Activation Levels (magnitude control)

The transition tables presented in section 2.4.1 represent a formalized description of the state switching behavior of the controller. However, to make a state effect leg movement, it has to be associated with muscle activation. Usually constant activation levels have been applied to the muscles controlled by a state. All extensor, flexor, protractor and retractor activation levels are defined as constant activation level values (this holds true for all legs). However levator and depressor are subject to magnitude control (see 2.2) and therefore don't have constant activation levels. Their activation is a function of FT and CT angle. A summary of all muscle activations used for each muscle is given in Table 2.5.

Three different functions were used to modify activation amplitude. The two functions $l(x)$ and $d(x)$ are modeled after findings from Hess and Büschges (1997) and Bucher et al. (2003). They apply an activation reduction to the depressor and an activation increase to the levator when the FT joint gets flexed. Additionally an FT joint extension amplifies activation level of both muscles. Function $l(x)$ reflects the influence of FT angle to levator activation. Consequently for front and middle leg $l(x)$ was only used in states when levator is

active. For the hind leg, $l(x)$ is used during depression, as the kinematic of the hind leg FT joint is inverted. Function $d(x)$ approximates the influence of the FT angle on depressor activation, thus it is basically an inverted variation of $l(x)$ with different parameter values. In front and middle leg $d(x)$ was used in all states with active depressor, again for the hind leg, $d(x)$ was applied to the levator instead. As a consequence of being close to the center of gravity, the hind leg generally needs to produce more force. This is also reflected by the fact that for the hind leg $l(x)$ and $d(x)$ were additionally scaled by constants and offsets (see hind leg column in Table 2.5). The third amplitude modulation function used was inspired by the work of Cruse et al. (1993) investigating stick insect height control (corresponding to signals 15-18 in Table 2.2). Function $h(x)$ creates a negative feedback loop of CT joint angle to the depressor activation amplitude. It causes depressor activity to *increase* if the leg is lifted and to *decrease* for advanced downward positions. $h(x)$ is only applied to states when depressor is active. Table 2.5 contains two more functions called $p(x)$ and $q(x)$. Their purpose however is simply to transform the measured angles into a range where $l(x), d(x)$ and $h(x)$ produce desired values.

Usually the activation levels for antagonistic muscles don't show co-activation with some exceptions: In accordance with results from Büschges et al. (1994), extensor can receive tonic activation during stance phase. This was observed for the middle leg while the animal walks on a double tread-wheel. However, such co-activation could not be found for other antagonistic muscles (Epstein and Graham, 1983; Grahm and Wendler, 1981). In case of the restricted middle leg co-activation was applied to protractor and retractor. This was done in order to remove the third degree of freedom from leg movement and resemble the preparation of the restricted middle leg, where pro- and retraction is prevented by glue or insect pins.

In other places (front and hind leg) slight co-contraction was used to stiffen the joints and ensuring a reasonable range of motion. This should basically be seen as a compensation for the highly simplified muscle model used in this simulations, which was often unable to generate sufficient torque in time. Co-contraction helps in this respect, because motion can be stopped or inverted more quickly if the antagonist is already "on". The positive effects of co-contraction to motion stability are also described for the locust in Zakotnik et al. (2006).

2 Simulation of insect walking

| Middle Leg, Sideways | | Status | | | |
|----------------------|-------|--------|------|------|--|
| Signal | 4 FL | 3 FD | EL 1 | ED 2 | |
| FT pos flex | FD | (↔)FL | EL | ED | |
| FT pos ext | FL | FD | ↔ED | EL | |
| GC \wedge -AR | EL | ↔EL | EL | EL | |
| GC \wedge AR | FD | FD | FL | ↔FD | |
| -GC | (↔)EL | ED | EL | ED | |
| PEP | FL | FL | EL | EL | |

Table 2.6: Sequence of states and signals during middle leg sideways stepping. Numbers beside state names in the first row indicate the succession of states during the control loop. Arrows point from current state to next state assuming a normal sequence of signals. An alternate pathway is indicated by dashed arrows and a dashed state number label (state FL, with label 4). This alternate pathway depends on the threshold value of “FT pos flexed” (see text for details and Table 2.4 and 2.3 for shortcuts).

2.4.3 Neural control of the middle leg

In this section the sequence of events happening during a control loop are described for each leg. The middle leg was investigated in two different walking situations: Sideways and forward walking. In the sideways condition the TC joint motion is prevented (for example with dental glue or insect pins) in a way that the middle leg is moving in one plane only (Fischer et al., 2001). In this walking situation many studies have been made investigating the role of sensory feedback for walking pattern generation therefore it was important to simulate this rather artificial but well explored condition. Actually, due to the number and quality of results available for this preparation, the sideways walking condition was both starting point and reference for simulations performed. The steps and state changes described in the next sections can also be followed in Tables 2.4 and 2.7 (for the middle leg), 2.9 (front leg) and 2.11 (hind leg).

2.4.3.1 Sideways

Starting in the swing phase, where levator and extensor are both active, the flow of signals and state switches during sideways stepping of the middle leg is as follows. During swing phase the controller is in EL state (see Table 2.6, number 1). As extensor and levator are active, FT joint angle decreases during while the leg moves upwards. By looking at the set of available signals, it is obvious that the next signal coming in has to be the “Ft pos ext” signal once the FT angle decreases to 70° (see Table 2.7 for details about threshold values). This signal causes the controller to switch into the ED state (Table 2.6, number 2) by

terminating levator activity and activating depressor instead. This will cause the leg to move down and eventually touch the ground again. Ground contact with extended FT joint creates the $GC \wedge AR$ signal which passes control to the FD state (Table 2.6, number 3) . In this state depressor and flexor are active. On a tread wheel the leg would now start pulling and accelerate the wheel towards the animal. But as friction is removed inside the simulation, the leg can slide over the simulated surface and therefore FT angle also increases constantly in the simulated stance phase. As the leg approached the trunk again, the next signal will be generated, which initiates stance-swing transition. Two different signals could in theory be generated during a regular step sequence, depending on the threshold values set up. In the simulation presented here, the threshold for termination of the active reaction (AR) was chosen to be smaller (105° , see Table 2.7) than the angle for the “FT pos flex” signal (120° , see also Table 2.7). This means, the signal terminating stance phase will be $GC \wedge \neg AR$ and the controller will immediately switch back into the EL state (see Table 2.6, number 1) .

However, if threshold of “FT pos flex” would be set to be smaller than the AR threshold angle, “FT pos flex” would be the next signal to come. This signal would also restore swing phase, but it needs an additional intermediate state, the FL state (Table 2.6, dashed arrow pointing to number 4) . During this phase, levator and flexor become active together and will quickly release strain or load on the leg. Shortly after levator activity onset the leg will lose ground contact which signals the controller to enter EL state again (Table 2.6, dashed arrow pointing to number 1). So both possible variations form a control loop with slightly different kinematics however. As the kinematics of the 3-state control loop were looking more realistically it was decided to use the threshold setting generating this sequence of states.

2 Simulation of insect walking

The establishment of a stable sideways stepping pattern shows that the known sensory influences (presented in Table 2.2) can be sufficient to control simple repetitive sideways steps. In terms of the controller, a stable sideways stepping pattern can be achieved with a sub set of the implemented signals, but setting meaningful threshold values is crucial. The sensitivity of threshold values has been tested by adding random noise to joint angles and muscle activation levels. This analysis showed that for joint angles 5% error could be tolerated without losing stable inter joint coordination. In case of muscle activation noise, the controller was even more robust, tolerating changes up to 50% of muscle activation error. This analysis was performed for all subsequent simulations with similar results. Angular noise is more critical than muscle activation noise. Often models with increasing noise tend to produce shallow swing phases with premature touch-down, causing the stepping cycle to get shorter and shorter until it ends in functionless, high-frequency oscillations.

Muscle activations and kinematics are shown in Figure 2.2. The Figure has three data groups, first muscle activations, second joint angles and third tarsal coordinates in body reference frame.

In case of the sideways walking middle leg, TC (α) joint is fixated by strong co-activation of protractor and retractor. Levator and depressor show amplitude modulation (magnitude control rules) and are strictly alternating. Levator activation is strong at the beginning of the swing phase, which supports a fast lift of, and declines as beta angle increases (effect of height control rule) preventing the leg from being lifted too high. Depressor activation profile also shows magnitude control but of a more complex shape as depressor activation amplitude is modulated by CT (β) and FT (γ) angle. During stance and swing there is a small amount of co-activation in the FT joint muscles (Büschges et al., 1994)

Looking at the joint angles, obviously the TC (α) angle is held constant by the co-activation of protractor and retractor, which is also reflected in the tarsal y coordinate. CT (β) and FT (γ) joints show smooth alternating angular changes.

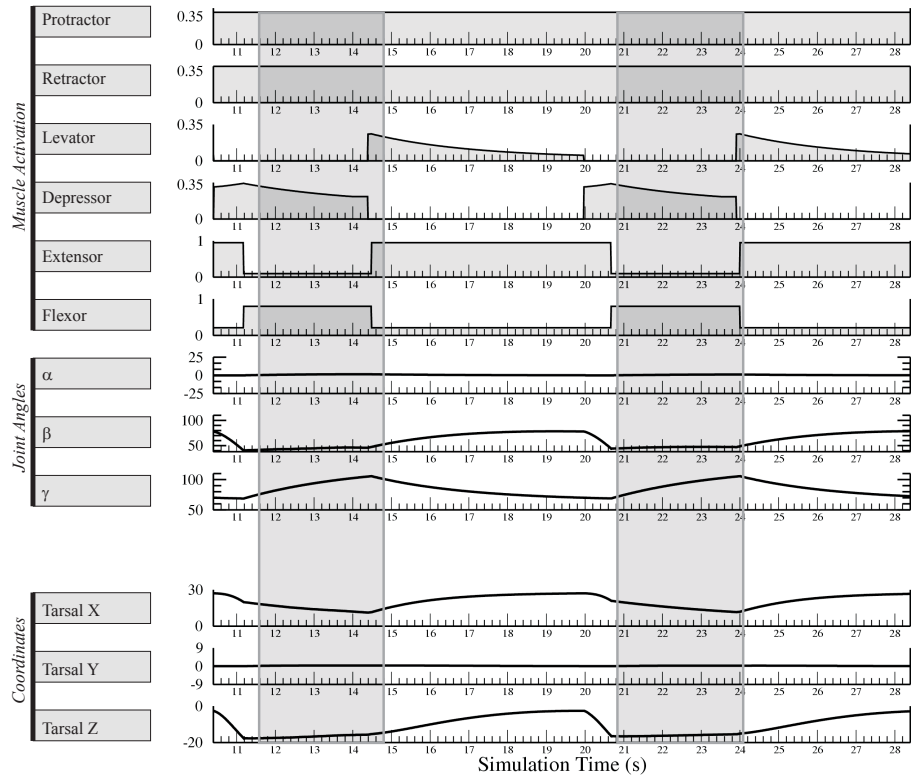


Figure 2.2: Time course of kinematics and muscle activations of the sideways stepping middle leg. First six data traces show the activations the controller generated for the major leg muscles (arbitrary units, usually between 0 and 1). Protractor (first trace) and retractor (second trace) are constantly active to prevent motion in the y axis. Levator and depressor activation is modulated by the magnitude influences (see tables 2.1 and 2.5). Next three rows show the joint angles in degrees (α =TC joint angle, β =CT joint angle, γ =FT joint angle). Note that TC (α) angle is constant during the sideways stepping simulation. In the last three traces the tarsal coordinates are shown (x values show proximal (0 mm) / distal (30 mm) tarsus positions, y corresponds to anterior (9 mm) / posterior (-9 mm) positions and z to upward (0 mm) / downward (-20 mm) positions). Time scale is the simulated time (since start of the simulation)

2 Simulation of insect walking

| a) Middle leg, sideways: | | | | Threshold values | |
|--------------------------|-------|----------------------------------|--|------------------|--------|
| Joint | State | Rule | | | |
| FT | | | | | |
| | EXT | $\neg GC \vee GC \wedge \neg AR$ | | AR: | 105° |
| | FLX | else | | PEP: | -25° |
| CT | | | | | |
| | DEP | FT pos ext | | Pos ext: | < 70° |
| | LEV | FT pos flex \vee PEP | | Pos flx: | > 120° |
| b) Middle leg, forward | | | | Threshold values | |
| Joint | State | Rule | | | |
| FT | | | | | |
| | EXT | $\neg GC \vee GC \wedge \neg AR$ | | | |
| | FLX | else | | | |
| CT | | | | | |
| | DEP | FT pos ext | | AR: | 105° |
| | LEV | FT pos flex \vee PEP | | PEP: | -25° |
| TC | | | | | |
| | RET | GC | | Pos ext: | < 70° |
| | PRO | $\neg GC$ | | Pos flx: | > 120° |

Table 2.7: Transition rules and threshold values used for middle leg stepping. a) Rules and threshold values for sideways stepping, b) rules and threshold values for forward stepping. Note: Retraction, depression and flexion decrease angular values. For a detailed description of the signals and rules see section 2.4 and table 2.3 on page 12.

2.4.3.2 Forward

The sequence of states and events for the forward walking middle leg are basically similar to the sequence observed during sideways stepping. The set of signals and their combination to transition rules is summarized in table 2.7. However, due to the added degree of freedom in motion (by releasing the TC joint) the controller has more possible states. In contrast to the situation in sideways stepping control, two states (PDF and PLF) won't become active during a normal control loop of forward walking. Actually PDF and PLF are purely hypothetical states, as there is no way of getting into one of these states from inside any other state. If analysis of forward walking is started again in the swing phase (PLE, see table 2.8, number 1), the next signal inside a normal stepping loop would therefore be "FT pos ext". This terminates levation and activates depression and control moves into the PDE state (table 2.8, number 2). Identical to the situation in sideways stepping the depression eventually brings the leg back to the surface and a strain or ground contact signal is generated ($GC \wedge AR$). In combination with the extended FT angle this passes control to the RDF state (table 2.8, number 3).

Now the leg performs the stance phase. It is pushed towards the ground by the

depressor and supports body weight. At the same time the retractor propels the trunk in respect to the tarsus and the amount flexion controls the direction of trunk. The flexion can compensate for the circular nature of pro- and retraction and thus support a more linear forward motion. Now two different pathways open up for the controller. In case flexion is strong, and reaches the threshold angle for the second part of the active reaction during stance phase, the RDE state takes over and causes an additional extension at the end of stance phase (table 2.8, number 4). This is the typical pathway also observed in the animal. As retraction continues during RDE, the leg finally reaches its PEP which then terminates depressor and starts the levation as the controller switches into the RLE state (table 2.8, number 5). Once the levator is active the leg will quickly lose ground contact which brings the system back into the PLE state.

However, the stance phase can also be terminated differently (dashed arrows). Once in RDF (table 2.8, number 3) PEP can also be reached before $GC \wedge \neg AR$ is triggered, for example if the animal walks downhill or has touched the ground with a very extended FT angle. In cases like this it can happen that the leg reaches PEP first. Following the dashed arrow, the state response to this situation is to enter RLF, which basically means to terminate depressor and activate levator instead. This causes the leg to lift which will also bring the control back into the initial swing phase state PLE.

In summary, the observed sequence of states show that the basic set of rules defined for the simplified case of sideways walking are also a functional basis for controlling the forward walking middle leg. The succession of states additionally proved to be very stable (given the correct threshold values). Once the system enters one of the five major control loop states (table 2.8, numbers 1-5), it will, given no external disturbance, fall back into the stable sequence of states producing forward walking. Additionally stable control can also be re-gained from the RLF state. Despite the stability, the control can get trapped in other state loops or fix points (where it 'waits' for a signal which cannot be generated by the current state) but a full investigation of all possible behaviors is beyond the scope of this work.

Stability investigations concerning sensitivity to changes in parameters have also been performed for the forward walking middle leg. As they are qualitatively similar for all legs, see section 2.4.3.1 on page 18 (sideways walking middle leg) for details.

Muscle activation pattern, joint angles and tarsal coordinates of the forward walking middle leg, are shown in Figure 2.3. The resulting activation pattern

2 Simulation of insect walking

| Middle Leg, Forward | | | | | | | | |
|---------------------|--------|-------|-------|-------|-------|-------|-------|-------|
| | Status | | | | | | | |
| Signal | 3 RDF | ← RLF | 5 RLE | → RDE | 4 PDF | 2 PDE | ← PLF | 1 PLE |
| FT pos flex | RLF | RLF | RLE | RLE | PLF | PLE | PLF | PLE |
| FT pos ext | RDF | RDF | RDE | RDE | PDF | PDE | PDF | PDE |
| GC \wedge -AR | RDE | RLE | RLE | RDE | RDE | RDE | RLE | RLE |
| GC \wedge AR | RDF | RLF | RLF | RDF | RDF | RDF | RLF | RLF |
| -GC | PDE | PLE | PLE | PDE | PDE | PDE | PLE | PLE |
| PEP | RLF | RLF | RLE | RLE | PLF | PLE | PLF | PLE |

Table 2.8: Sequence of states and signals for middle leg forward stepping. As there is an additional degree of freedom in comparison to the sideways walking leg, the controller now has eight states. For explanation of numbers and arrows, see Table 2.4 and 2.3 for shortcuts.

looks basically similar to the one produced by the sideways controller, however protractor and retractor are now alternatingly active. Protraction requires much less activation than retraction, as the leg has no ground contact during swing. Also levator activity is reduced; mainly because sideways stepping is associated with a much more pronounced lifting than forward walking (compare also tarsal z coordinates). Depressor, extensor and flexor activation profiles are very similar to the sideways stepping situation in Figure 2.2.

One interesting detail of the simulation can be seen in the CT (β) angle trace. During stance, beta angle rises and falls again slightly. This reflects the vertical movement of the trunk, as the leg pushes onto the surface. If FT (γ) angle approaches 90 degrees, the trunk is pushed up and beta angle increases slightly. For more flexed or more extended FT angles, the trunk comes down again and β decreases again. This behavior shows, that the leg is really supporting substantial portions of body weight during the simulated steps.

2.4.4 Predictions for front and hind leg

Predictions for the stepping control of front and hind leg are based on the idea that mechanisms and influences are similar to the ones found for the middle leg. Compared to the middle leg, knowledge of front and hind leg stepping control is rather limited (Bässler and Büschges, 1998). But the studies of middle leg stepping performed in sections 2.4.3.1 and 2.4.3.2 have shown, that the set of neural rules implemented in the controller, were sufficient to generate stable repetitive stepping movements.

Though the front leg has a slightly different geometry and shape as the middle leg, its overall kinematics during forward walking is more comparable to the

2.4 The neural control system

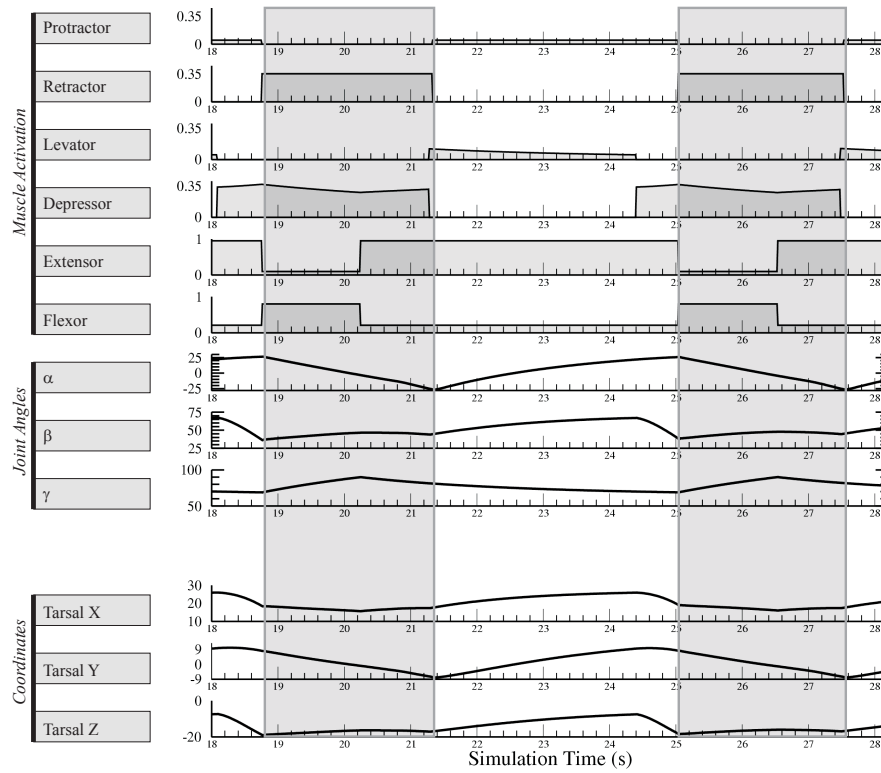


Figure 2.3: Time course of kinematics and muscle activations for the forward walking middle leg. First six data traces show the activations the controller generated for the major leg muscles (arbitrary units, usually between 0 and 1). Levator and depressor activation is modulated by the magnitude influences (see tables 2.1 and 2.5). Next three rows show the joint angles in degrees (α =TC joint angle, β =CT joint angle, γ =FT joint angle). In the last three traces the tarsal coordinates are shown. For additional details see Figure 2.2 on page 21. Time scale is the simulated time (since start of the simulation).

2 Simulation of insect walking

| Front leg, forward | | | | |
|--------------------|-------|----------------------------------|------------------|---------|
| Joint | State | Rule | Threshold values | |
| FT | | | | |
| | EXT | $\neg GC \vee GC \wedge \neg AR$ | | |
| | FLX | else | | |
| CT | | | | |
| | DEP | FT pos ext | AR: | 95° |
| | LEV | FT pos flex \vee PEP | PEP: | 10° |
| TC | | | | |
| | RET | GC | AEP: | 50° |
| | PRO | $\neg GC$ | Pos ext: | < 70° |
| | | | Pos flx: | > 94.5° |

Table 2.9: Transition rules and threshold values used for controlling front leg stepping. For a detailed description of the signals and rules see section 2.4 and table 2.3 on page 12.

middle leg than the kinematics of the hind leg. Thus the middle leg controller works without major modifications for the front leg, too. Modifications that had to be done were only in respect to threshold values (AR, PEP, AEP, Pos ext, Pos flx – see table 2.9) – no change to rules or signals was needed. The sequence of events and states is basically identical to the sequence shown for the forward stepping middle leg. Starting inside the swing phase (table 2.10, number 1) the FT joint extension introduces the swing-stance transition (table 2.10, number 2) and activates depressor. Strain, represented by ground contact initiates stance phase (table 2.10, number 3) by activation of retractor, depressor and flexor. Advanced flexion triggers the second phase of the active reaction by initiating extensor and terminating flexor with continued retraction (table 2.10, number 4). Finally the PEP signal, generated by the on-going retraction initiates stance-swing transition by activating levator (table 2.10, number 5). Once the leg loses ground contact, the swing phase is restored by returning into the PLE state (table 2.10, number 1).

Leg kinematics and muscle activations generated by the controller are shown in Figure 2.4. Note that, in contrast to the middle leg, slight co-activation was used during stance phase for protractor and retractor but not for extensor. Application of co-activation is discussed in more detail in section 2.4.2. At the beginning of the stance phase there is a short oscillation in muscle activation (approx. at 17.3 sec). This is a result of the velocity sensitivity of the active reaction rule. The controller is in PDE state, when the leg touches the ground after swing phase. If ground contact is established with sufficient downward speed the FT velocity can get high enough to activate the second part of the active reaction ($GC \wedge \neg AR$) which activates the extensor. This is mainly caused

2.4 The neural control system

by the fact that the simulated surface is frictionless; normally friction would prevent the tarsus from slipping. Nevertheless, the brief flexor activation at onset of stance is sufficient to decelerate the FT joint enough to escape from this problematic control situation and re-establish normal stance phase after the short extensor activation pulse. Another difference to middle leg control is the slightly amplified magnitude control, which can be seen by comparing the amount of modulation visible in the muscle activation traces (middle and front legs, Figure 2.3 and 2.4). This can be, at least in part, attributed to the different leg and joint geometry of the front leg – potentially also muscle properties of the front leg differ stronger from the muscle model used. Levator activation for example had to be quickly decreased after lift-off in order to prevent the leg being lifted way too much. Flexor also needed to work much harder in the front leg, than in the middle leg.

The hind leg differs that much in the way it operates, that it was obvious, that changes had to be applied to the transition rules in order to make it perform qualitatively correct movements. The hind leg cannot reach much forward swing without getting into the operating range of the middle leg. Thus its stance phase starts only marginally anterior to the point of TC joint origin. This fact makes the hind leg inoperative for pulling; its main contribution is pushing the trunk forward (Cruse and Bartling, 1995). Thus in contrast for front and middle leg, FT joint extension is an essential part of the stance phase for the hind leg. This however conflicts with the active reaction rules used for the front and middle leg, as they support flexion during most of the stance phase and extension is only allowed at the very end of stance. For this reason the velocity component of the AR rules have been removed from the hind leg controller.

| Front Leg, Forward | | Status | | | | | | | |
|--------------------|-------|--------|-------|-------|-------|-------|-------|-------|-------|
| Signal | 3 RDF | ← RLF | 5 RLE | → RDE | 4 PDF | 2 PDE | ← PLF | → PLE | 1 PLE |
| FT pos flex | RLF | RLF | RLE | RLE | PLF | PLE | PLF | PLE | PLE |
| FT pos ext | RDF | RDF | RDE | RDE | PDF | PDE | PDF | PDE | PDE |
| GC \wedge –AR | RDE | RLE | RLE | RDE | RDE | RDE | RLE | RLE | RLE |
| GC \wedge AR | RDF | RLF | RLF | RDF | RDF | RDF | RLF | RLF | RLF |
| –GC | PDE | PLE | –PLE | –PDE | PDE | PDE | PLE | PLE | PLE |
| PEP | RLF | RLF | RLE | RLE | PLF | PLE | PLF | PLE | PLE |

Table 2.10: Sequence of states and signals for front leg forward stepping. For explanation of numbers and arrows, see Table 2.4 and 2.3 for shortcuts.

2 Simulation of insect walking

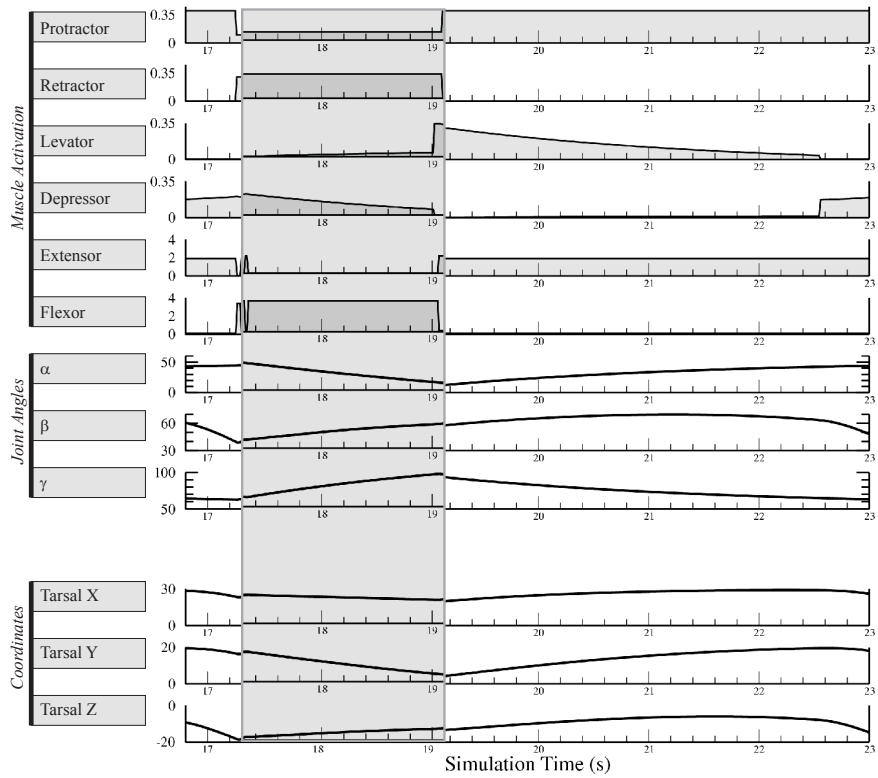


Figure 2.4: Time course of kinematics and muscle activations for the forward walking front leg. First six data traces show the activations the controller generated for the major leg muscles (arbitrary units, usually between 0 and 1). Levator and depressor activation is modulated by the magnitude influences (see tables 2.1 and 2.5). Next three rows show the joint angles in degrees (α =TC joint angle, β =CT joint angle, γ =FT joint angle). In the last three traces the tarsal coordinates are shown. Time scale is the simulated time (since start of the simulation). For additional details see Figure 2.2 on page 21.

| Hind leg, forward | | | | |
|-------------------|-------|------------------------|------------------|------|
| Joint | State | Rule | Threshold values | |
| FT | | | | |
| | EXT | GC | | |
| | FLX | \neg GC | | |
| CT | | | | |
| | DEP | FT pos flex \vee AEP | AR: | - |
| | LEV | FT pos ext \vee PEP | PEP: | -45° |
| TC | | | | |
| | RET | GC | AEP: | 5° |
| | PRO | \neg GC | Pos ext: | >90° |
| | | | Pos flx: | <55° |

Table 2.11: Transition rules and threshold values used for controlling hind leg stepping. For a detailed description of the signals and rules see section 2.4 and table 2.3 on page 12.

Hind leg control signals were reduced to ground contact and FT position signals (see table 2.11). Additionally the response rules to ground contact and FT angle have been inverted. Comparing tables 2.9 and 2.11 shows the differences. In table 2.9 (front leg) ground contact activates flexor whereas in table 2.11 (hind leg) the same signal causes a switch to extensor activity. Furthermore in case of the hind leg, FT joint flexion switches from levator to depressor activation. The opposite effect is active in front and middle leg, here FT joint extension performs this switch. TC joint muscles share the same rules in all leg, however (GC switches on retraction, lift-off does so with protraction).

In contrast to the front and middle leg, during the swing phase of the hind leg there is an FT joint flexion. Thus in early swing phase the PLF state is active (table 2.12, number 1). As swing phase proceeds, the FT angle get more and more flexed eventually triggering the FT pos flex signal. This switches into the PDF state and levator activity gets replaced by depressor activity (table 2.12, number 2); the leg starts to move downwards. Next there will be ground contact and its detection triggers the stance-swing transition for the hind leg (table 2.12 number 3). Note that hind leg stance phase is characterized by the extension of the FT joint (RDE state). Extension, depression and retraction continue until either, the posterior extreme position (PEP) is reached or FT angle gets over critically extended. Both signals (which ever comes first) make RLE the active state and thus initiate the stance swing transition. Once levator is active, ground contact will be lost quickly, and the controller returns into the PLF swing phase state (table 2.12, number 4).

2 Simulation of insect walking

| Hind Leg, Forward | | Status | | | | | | |
|-------------------|-----|--------|-------|-------|-------|-----|-------|-----|
| Signal | RDF | RLF | 4 RLE | 3 RDE | 2 PDF | PDE | 1 PLF | PLE |
| FT pos flex | RDF | RDF | RDE | RDE | PDF | PDE | PDF | PDE |
| FT pos ext | RLF | RLF | RLE | RLE | PLF | PLE | PLF | PLE |
| GC | RDE | RLE | RLE | RDE | RDE | RDE | RLE | RLE |
| -GC | PDF | PLF | PLF | PDE | PDF | PDF | PLF | PLF |
| PEP | RLF | RLF | RLE | RLE | PLF | PLE | PLF | PLE |
| AEP | RDF | RDF | RDE | RDE | PDF | PDE | PDF | PDE |

Table 2.12: Sequence of states and signals for hind leg forward stepping. For explanation of numbers and arrows, see table 2.6. The hind leg has a slightly different set of signals. See section 2.4 for details and Table 2.4 and 2.3 for shortcuts.

With only four active states, the hind leg controller is somewhat simpler than front and middle leg controller. However this is solely due to the simplified stance phase which misses the separation into FT extension and flexion phase as it is implemented in forward walking front and middle leg. Figure 2.5 shows the muscle activations and kinematics of hind leg walking controlled by the controller described above. Protractor and retractor are strictly alternating in their activity, no co-activation needed for these muscles in the hind leg. Levator and depressor, as well as extensor and flexor have small amounts of co-activation. Depressor co-activation is mainly due to the “height control” activation scaling, which increases depressor activity if beta angle increases. Additionally the hind leg has a slight flexor co-activation during stance, comparable to the one implemented in the middle leg. Noticeable is the small amount of activation needed for flexor during the swing phase. Activation is too small to be displayed in Figure 2.5 but it is not zero, as can be seen in table 2.5 on page 16. Comparing tarsal x position with FT (γ) angle, suggests that FT angular changes mainly compensate for the movement in the other joints, keeping the tarsal distance during swing and stance phase roughly constant.

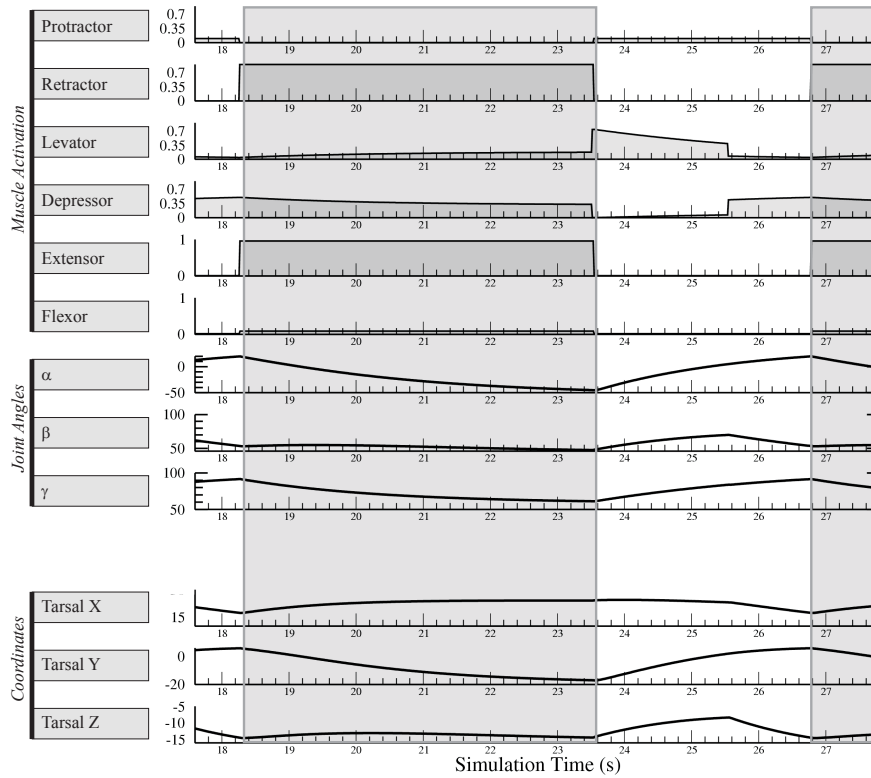


Figure 2.5: Time course of kinematics and muscle activations of the forward walking hind leg. First six data traces show the activations the controller generated for the major leg muscles (arbitrary units, usually between 0 and 1). Levator and depressor activation is modulated by the magnitude influences (see tables 2.1 and 2.5). Next three rows show the joint angles in degrees (α =TC joint angle, β =CT joint angle, γ =FT joint angle). In the last three traces the tarsal coordinates are shown. Time scale is the simulated time (since start of the simulation). For additional details see Figure 2.2 on page 21.

2.5 Discussion

First it has been tested and confirmed, that a controller, based on a rule set determined by neurophysiological experiments (neuronal controller) can be constructed. Furthermore it could be shown, that the presented set of rules is sufficient to generate stable, repetitive stepping movements in the sideways walking middle leg, which is the condition they were determined in.

A second, important question arised by these findings, was how adaptable (or general) the controller was. Therefore the controller was tested with an additional degree of freedom in middle leg forward walking, with different leg geometries in the front leg and even with geometric and kinematic changes in case of the hind leg. In all three cases it was possible to generate simple stepping movements without substantial modifications to the controller. Only in case of hind leg stepping, two state switching rules needed to be inverted. The predictions for front and hind leg therefore become testable hypothesis for new experiments. It is well possible to investigate experimentally if strain or FT position signals are reversed in the hind leg.

The result supports a conceptual paradigm for motor control of stick insect walking. This is, sensory information is capable of organizing the timing of motor output of the leg joints. Sensory signals can meaningfully switch activity in antagonistic muscles as well as shape or modulate muscle activation amplitude.

2.5.1 Muscle model

The linear muscle model approximated from sparse data of Storrer (1976) cannot be expected very accurate. It could at best give a rough indication of how much force is generated. The aspect of force development over time (activation dynamics) is completely missing in this model. However, the objective of this study was to investigate if a step cycle can be generated from the sequence of events generated by the leg sense organs. This basic statement should be possible to make even without detailed muscle models.

One drawback of the simplified muscle model can be seen in the kinematics of all legs (Figures 2.2, 2.3, 2.4 and 2.5). The movement, in particular the swing phase is very slow. This can be attributed to the linear force-velocity curve of the muscle model and prevents the muscle from producing sufficient force at higher contraction velocities.

2.5.2 Kinematics and muscle activations

The coordination of muscle activations, both of joint specific antagonists and muscles controlling different joints, is basically similar to data measured by Fischer et al. (2001) but differences are obvious. In comparison with Fischer et al. (Figure 9a) the following differences can be described:

In the walking animal protractor shows activity reaching into the stance phase and retractor starts delayed in the stance phase. Interestingly in the animal depressor motor neurons are not active during the second half of the stance phase, but as in the middle leg simulation get active shortly before start of stance. Activity of levator motor neurons is qualitative similar, but the activity in the motor neurons seems to start a bit earlier, than levator activation in the simulation. But in both cases the activity starts in late stance and terminates well before end of swing.

Levator activation during late stance could well be a special response of the animal to the artificial tread wheel walking. Animals often seem to grasp the tread wheel with their tarsal claw, and pulling it up at the end of stance phase. This behavior requires early levator motor neuron activation, but it might not be particularly natural. Furthermore the simulation is not equipped with tarsal structures, thus levator activation ultimately causes the loss of ground contact. There is no way for the simulation to significantly activate levator muscle but at the same time keep ground contact. Thus earlier activation of levator would simply lead to a shortened stance phase.

Fischer et al. (2001) did not observe extensor activity during late stance, thus the simulation differs in this respect. Also, in the simulation, extensor continues to be active until end of swing, neuronal activity however ceases slightly earlier. The difference in extensor activation profile is consequently reflected in flexor activation. Thus flexor activation in the simulation terminates earlier compared to the neuronal activation. Flexor terminates, because extensor is active in the final part of the simulated stance phase. As this was not the case in the studies Fischer et al. performed, they found activity in the flexor motor neurons throughout the complete stance phase.

In respect to tarsal movement and joint kinematics, a comparison with Cruse and Bartling (1995) reveals basic similarities of simulated middle leg and real middle leg during forward walking. As discussed above, the muscle model was not able to generate sufficient joint torque for quick movements, therefore the time scale of the stepping is much slower in the simulation, in particular the

2 *Simulation of insect walking*

swing phase is too slow even in relative comparison to stance. Swing phase is particularly sensitive to muscle force-velocity problems, because it is a rapid movement with low counter force and therefore the muscle operates in the high-velocity, low-force domain of the force-velocity curve.

As far as the set of neuronal rules and signals are concerned, it is unlikely to be complete. More mechanisms are known than have been included into the simulation and on the other hand, not all mechanisms included are neuronally explicable in sufficient detail. For example the termination of stance phase via an unknown combination of load and position information Cruse (1985) is not explained on the neuronal level. In the simulation the probably complex processing of multiple sense organs were therefore simplified to a simple position signal affecting the activity in the CT circuit. Future investigations will have to specify which relationship between load and position information is crucial for the PEP mechanism and if CT joint is the only circuit that is affected by this information.

Evaluation of front and hind leg simulation results is a bit harder than for the middle leg. Fewer investigations provide reference data for these legs. Comparing with in vivo walking, joint kinematics differ more in front and hind leg, than in middle leg.

Front and hind leg controllers were developed based on the assumption that identical underlying structures can be hypothesized for all legs. In how far this assumption holds true is unclear. Even if the general mode of operation in all legs proves to be similar, the same sensory signals might have different effects in different legs. The inversion of the rules used for hind leg stepping is one example. In how far load or position signals can have different neuronal responses is not yet clear, but preliminary results on the processing of load signals in the hind leg suggest differences in their action compared to the middle leg (Akay, Ludwar, Schmitz and Büschges, unpublished). Thus, more experiments, particularly in front and hind leg are needed to confirm the implicit hypotheses or suggest improved controller concepts.

2.5.3 Conclusion

Two major results can be summarized as result of this work. First, stepping movements (sideways and forward stepping) can be explained as a static network of immutable responses to local sensory feedback. This controlling paradigm enables to generate robust stepping without the need for compli-

cated geometric or dynamic calculations. The controller can be adapted to different leg geometries purely by changing threshold values. It can even be adapted to generated different kinematics, by few changes to its logical rules. This gives the second important result. The same basic controller can operate in different legs. Though adaptations are required for good performance, the general control paradigm proves flexible and fairly general.

Sure enough many improvements could be made for future simulations of this kind. First of all, a more realistic muscle model is needed. Especially the time constants of stick insect muscles (slow rise, slow decay, see Hooper et al., 2007) can be expected to effect the activation patterns of the joint muscles. Activation would need to start and terminate earlier, which is would make the whole activation pattern more similar to the one observed in vivo.

A realistic muscle model in combination with thorough magnitude control is the foundation for detailed comparison of joint and leg kinematics. Without having included both improvements, comparison of kinematics can only be done qualitatively.

The final important improvement regards the sense organs. Most sense organs were heavily simplified. fCS and trCS are complex cuticle strain sensors which were approximated by binary ground contact information. Similarly fCO also is a multi-parameter detector, measuring acceleration, velocity and position in a highly no-linear fashion. More realistic sense organ models would definitely help building a better controller. Additionally the controller, as implemented here has very limited capabilities of weighting competing sensory information. If increasing number or level of detail of sense organs, the controller would also need a more fine grained method of doing its state decisions. Logical rules might be replaced by a fuzzy logic, or probability functions. This would also much better reflect most of the experimental results, as these often just describe an increase in activation switch probability, rather than an absolute switch from one state to the next.

But despite all its shortcomings and simplifications, the stepping controller described here (or, in more detail in Blümel, 2004) quickly found its way into robot simulation and robot control (Lewinger et al., 2006; Lewinger and Quinn, 2009; Rutter, 2009; von Twickel et al., 2010a,b).

2 *Simulation of insect walking*

3 Building an individual Hill-type model of the extensor tibiae muscle

3.1 Introduction

Understanding neuronal mechanisms of behavior generation and control require, at least at some point, a thorough understanding of how motor patterns are translated into movements. It is well known that neuro-mechanical transformation and muscular force generation is complex and for the most part non-intuitive. Apart from the most simple muscles and motor tasks, computer models seem to be the only way of estimating how a motor pattern interacts with the real world. Different muscle models have been developed in recent times, varying in complexity and explanatory potential. Some are purely phenomenological, basically reproducing measured data (like “black box” models, for overview see for example Nigg (1995)); others are based on the fundamental biochemical and biophysical ideas of the sliding filament theory ought to explain muscle internal processes (Zahalak, 1981).

One often used model, in particular in studies of more complex motions, is the Hill-type model (Hill, 1938, 1950; Zajac, 1989). This model conceptually sits in-between black-box models, purely reproducing data sets, and models based on fundamental muscle mechanics. The Hill-type model is defined by data sets gained from a series of muscle contractions resulting in a set of curves, each describing a special, but fairly high level muscle property. Hill-type models are comparatively fast to compute and as they are based on measured data, they can be adapted to different muscles relatively easy. This makes these models attractive for a variety of modeling and simulation applications (Hannaford and Winters, 1990; Zahalak and Ma, 1990; Zajac and Winters, 1990; Alexander, 2003).

However, Hill-type models often have a delicate inherent difficulty; the amount of experimental data needed to define the crucial relationships for muscle force calculation, is too large to be measured with a single, individual muscle. Thus, frequently data sets of different animals were fused into a single model (for

3 Building an individual Hill-type model of the extensor tibiae muscle

example by averaging data sets, or by combining curves of different animals). Any type of combination is based on the assumption of independence of the combined parts. It remains unknown how far this assumption is justifiable as long as a detailed comparison of single, individual muscle Hill-type models is missing. A similar problem was described for neuron models (Golowasch et al., 2002). One particular difficulty of muscle measurements and thus modeling is the inherent variability of muscle responses (for stick insect: Hooper et al., 2006, or in case of the lobster: Thuma et al., 2003).

The idea of making Hill-type model parameter determination more efficient has been addressed before by the ISOFIT method of (Wagner et al., 2005; Siebert et al., 2007). Using the ISOFIT optimization, it is possible to determine most of the required model parameters with a single type of experiment (isovelocity contractions). However, this approach requires a pre-defined model structure, for the optimization process. If such a model structure is not available, this method cannot be used.

An alternative approach would be to first measure muscle properties in sufficient detail with different animals. This data set could be used to extract basic characteristics of the individual properties. For example it can reveal if the force-velocity curve can be adequately fitted with the Hill-hyperbola, or which function to use for approximation of the force-length curve. At this stage it is actually beneficial to be able to compare among many animals, as general principles should be extracted.

Once the types of equations to be used best are identified, they can be constrained much more efficiently. For example, if the initial studies have revealed that force-length curve, inside the physiological working range, can be modeled with a simple linear relationship, it should be sufficient to have three data points to get acceptable fits. If this principle is applied consequently to all (or most) relationships, the number of required measurements can be reduced substantially. Eventually it is possible to decrease the number of measurements that much, that they all can be performed on a single muscle.

Extensive initial studies of the extensor tibiae muscle of *Carausius morosus* have been performed by Guschlbauer et al. (2007). This work defined curves and relationships for passive force (parallel elasticity), series elasticity, force-length, force-velocity, force-activation and maximum contraction velocity in relation to activation. This section shows that it is possible to extract enough general knowledge from this data to a) develop an experimental paradigm to estimate all crucial properties for modeling in a single muscle, and b) to get

reasonable fits and thus modeling parameters from these experiments.

Thus, this section provides an approach for the estimation of Hill-type model parameters of an individual muscle. Although in total 10 muscles (of 10 different animals) have been investigated, only one is presented in detail here. The other muscles are included in mean R^2 values and standard deviations.

3.2 Materials and methods

3.2.1 Modeling tools

Calculations were performed in GnuOctave on Linux (Ubuntu 9.04, Kernel 2.6.28-15-generic, Intel Core2 T5600). Parameters were optimized using the *leasqr* routine of the *optim* package (version 1.0.3). Correlation coefficients were calculated using *corrcoef* of the statistics module. RMS values were calculated with a custom code.

3.2.2 Dissection and experimental set-up

The experiments were performed by C. Guschlbauer. They were executed at room temperature with adult female stick insects from the departmental colony. First, all legs except the right middle leg, were amputated at mid-coxa, then the animal was pinned dorsal side up on a balsa wood platform and the coxa, trochanter, and femur embedded in dental cement (ProTempII, ESPE, Seefeld, Germany). The thorax was opened longitudinally, the gut lifted from the thorax and moved to one side. Fat tissue was carefully removed.

The thoracic cavity was filled with *Carausius morosus* saline (Weidler and Diecke, 1969). Mesothoracic nerves were dissected to access nerve nl3, which contains the extensor tibiae motor axons (fast, slow and common inhibitor Bässler and Storrer, 1980). Finally the nl3 nerve was crushed near the ganglion, to remove any type of efferent information. Then the nerve was dried, lifted onto the hooks of a bipolar stimulation electrode, and isolated from the bath with vaseline (Engelhard Arzneimittel GmbH & CoKG, Niederdorfelden, Germany).

Once the thoracic dissection was completed, the femur was opened distally by cutting a small window in the dorsal cuticle. The tendon position at 90° FT angle (defined as rest length, Guschlbauer et al., 2007) was then measured and marked and was afterwards cut distal of the 90° position and connected with a

3 Building an individual Hill-type model of the extensor tibiae muscle

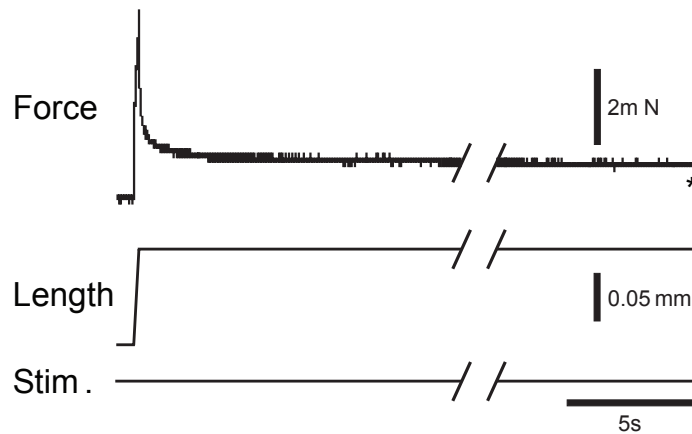


Figure 3.1: Example of a muscle response to passive stretch. Passive force (parallel elasticity) was measured by applying length ramps without stimulation. The force shows a transient peak (dynamic passive force) followed by a slow relaxation. Steady state passive force was measured at the asterisk.

hook-shaped insect pin to the lever arm of an Aurora 300 B (Aurora Scientific Inc., Ontario, Canada). After this connection was established, the muscle was reset to rest length.

3.2.3 Nerve stimulation

Motor nerve stimulation was performed using square-wave current pulses of 0.5 ms duration. This output triggered a digital pulse generator that drove a stimulation isolation unit (both from the electronics workshop at the Zoologisches Institut, Köln). These signals were then transmitted to the nerve stimulation electrode.

The current amplitude was set at least 2.5 times above the threshold that elicited visible contractions. This should ensure the activation of all three motor axons (Guschlbauer et al., 2007). Two types of stimulation patterns were used: Single pulses and tonic stimulations of 40, 60, 80, and 100 Hz of one second duration.

3.2.4 Muscle protocols

Two different types of experiments were performed. Stretching and shortening the muscle in combination with isometric stimulation was used to investigate force-length and passive force relationships. In quick-release experiments, the

3.2 Materials and methods

muscle was first isometrically stimulated at rest length, then it was allowed to contract against a constant counter force (isotonic conditions). This type of experiment was used to investigate force-velocity and series elasticity properties.

Passive force-length experiments were performed in the muscle's physiological working range. Length changes were applied with ramps (0.5 - 0.75 mm/s) from -0.2 mm to -0.1 mm to 0 mm to 0.15 mm (relative to muscle rest length). Immediately after the muscle was first shortened to -0.2 mm at the beginning of the protocol, the motor nerve was stimulated with a brief high-frequency pulse to remove muscle slack (Proske and Morgan, 1999). In response to passive stretches the muscles showed an initial rapid force increase followed by a relaxation to a steady-state value (see Figure 3.1). Passive force-length measurements were made at quasi steady-state. Because the time at which the steady-state was achieved varied for different muscle lengths, these measurements were made at the following times: 40 s after the slack-removing stimulation at the -0.2 mm length, 60 s after the stretch to the -0.1 mm length, 80 s after the stretch to the rest (0 mm) length, and 100 s after the stretch to the 0.15 mm length.

The quick release experiments were performed at muscle rest length, as shown in Figure 3.2. The motor nerve was stimulated under isometric conditions at one of the frequencies noted above. After the force had reached steady-state, the system was switched into force control mode. Muscle counter-force was set to $1/4$, $2/3$, 1.2 or 1.8 times maximal isometric force and the resulting length change observed. In case force steps were performed to smaller forces, this change consisted of an initial, extremely rapid change in muscle length followed by a brief period of oscillation (Edman, 1988) and finally a slower and continually decreasing length change (Figure 3.2). The slope of initial 25 ms of this third portion was used to construct force-velocity curves. The amplitude of the initial portion of the length change was measured by extrapolating this slope through the oscillation into its intersection with the initial portion of the length change (inset in Figure 3.2). This length was later used for determining muscle series elasticity parameters (see section 3.3.2).

The procedure above required two modifications for steps to forces larger than maximum isometric force (1.2 and 1.8 times maximum isometric force). First, data from cases with force increases in which no slope discontinuity could be identified were not included in further analysis. Second, in cases with very large force increases muscle length could achieve steady-state in less than 25 ms. If

3 Building an individual Hill-type model of the extensor tibiae muscle

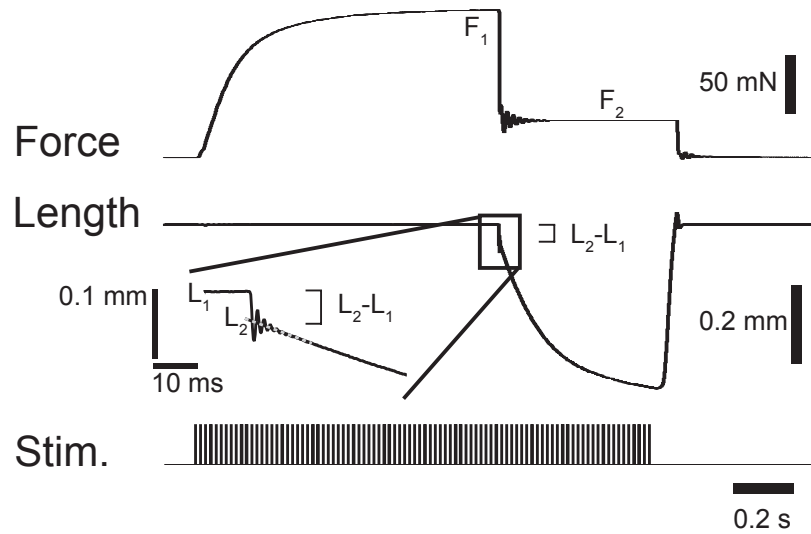


Figure 3.2: Schematic time course of a quick-release experiment for determination of series elasticity. Motor nerve was stimulated throughout the experiment. Initially the muscle was held at a given length, thus contracting isometrically. Then the Aurora is changed from position to force control and the muscle is able to contract as soon as it overcomes the defined counter force. If counter force is greater than muscle force, the muscle can get stretched in this second part of the experiment. Else, if counter force is smaller than muscle force, than the muscle will start to contract (as shown here). Shortening has a rapid, initial part, attributed to series elasticity relaxation, and a slower second part, generated by active contraction. The inset highlights the initial first part of the contraction with characteristic oscillations. The discontinuity in slope between L_1 and L_2 was important for series elastic component determination (see text for details). It corresponds to the change in series elasticity length induced by the transition from F_1 to F_2 .

this happened, the length change was determined by the following procedure: In order to get a time estimate for when to read off the length value in the position trace, the time the discontinuity took in the experiment with $1/4$ maximum isometric force at 80 Hz was measured. Then the position value at this time was used to calculate the slope (see section 3.3.2 for details).

To minimize muscle fatigue isometric experiments were performed first, isotonic experiments next, and those involving muscle lengthening were done at last. Determining force-length and force-velocity curves resulted in three measurements at 40 and 80 Hz, and five measurements at 60 Hz. The muscle fatigue was estimated by comparing isometric force of repeated measurements. Only experiments in which each force measure reached at least 80% of their respective maximal force value were used.

3.3 Results

The next sections explain which equations were used for parameter optimization and how precisely the measurements were used during the process. Once the required measurement values were extracted from the raw data, model generation could be automated and was performed by a GnuOctave script.

In order to be able to interpret the measured force values correctly, one needs to decide for an underlying model concept. Basically two concepts are commonly accepted, differing in what is connected to the series elasticity. Siebert et al. (2008) compared the properties of these different configurations. The CC model (after Siebert et al., 2008) was used here, which is shown in Figure 3.3. The type of model hypothesis is important for interpreting passive force and series elasticity measurements.

3.3.1 Passive force curve (parallel elasticity)

The terms “passive force” and “parallel elasticity” force are used synonymously here. As shown in Figure 3.3 parallel elastic spring (PE) is arranged parallel to the contractile element (CE) both connected to the series elastic spring (SE).

The passive force was measured by application of length changes to the inactive muscle. In response to lengthening the muscle produces a specific force profile, similar to the one shown in Figure 3.1. The force response can be separated into a dynamic or elastic part (the latter being prominent during lengthening) and a viscous part after the new length has been achieved. The viscous force reduction actually goes on for a very long time after muscle stretch (Guschlbauer et al., 2007) which makes it hard to define a steady force state. But force change

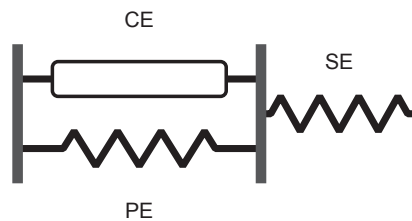


Figure 3.3: Arrangement of the functional components of the Hill-type model used here. Contractile element (CE) and parallel elasticity (PE) are both connected to the series elastic spring (SE).

3 Building an individual Hill-type model of the extensor tibiae muscle

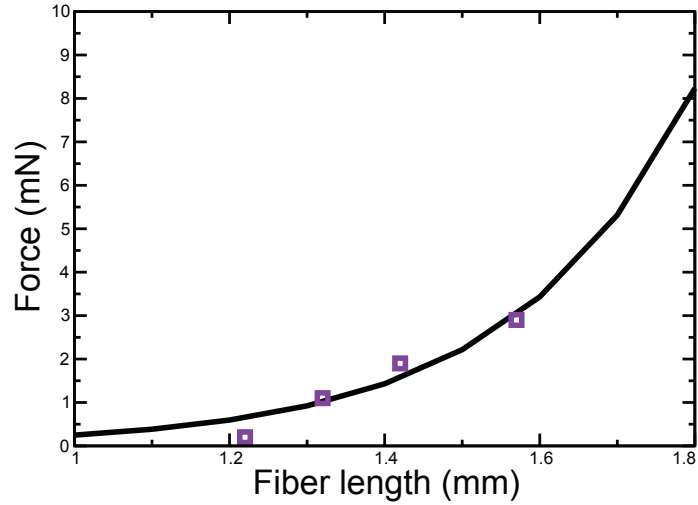


Figure 3.4: Comparison of exponential model (solid line, see equation 3.1) and measured data points of passive muscle stretch. Note that static passive force, is small (compared to active forces or dynamic passive force).

declines more and more, thus at some point the system can be assumed to be almost static.

The passive force curve results from plotting the force of several measurements over the corresponding muscle lengths. In Figure 3.4 the four measurements (squares) are presented in combination with the curve fit. The equation for fitting the data points was an exponential function, suggested by Guschlbauer et al. (2007)

$$F = k_1 \cdot e^{k_2 L}, \quad (3.1)$$

where F is muscle force, L is muscle length (which equals muscle fiber length, see Guschlbauer et al. (2007)), and k_1 and k_2 are the parameters to fit.

The parameter fit resulted in an R^2 value of 0.92. As explained above, in total 10 animals were investigated with this procedure. Across these 10 experiments the mean R^2 value was 0.94 ± 0.04 .

3.3.2 Series elasticity

Data for the determination of series elastic properties originate from the quick release experiments explained in section 3.2.4 and Figure 3.2. The experiment

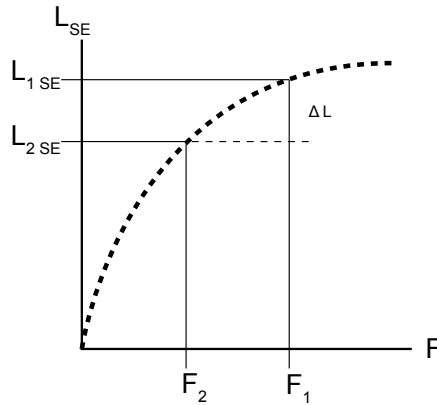


Figure 3.5: Scheme of the analytical derivation of spring constant (k_3) for series elasticity from quick release experiments. See section 3.3.2 for details of calculation.

results in two distinct length changes, an initial rapid length step and a second, slower shortening (see inset in Figure 3.2).

Consistent with the model conception underlying this work (see Figure 3.3), initial, rapid length change can be attributed exclusively to shortening of the series elastic component (SE in Figure 3.3). In this model measured muscle force is solely the force of the SE spring, and the goal of these experiments is to relate SE spring force with SE spring length. The quick release experiments, however, do not reveal SE spring length directly; only whole muscle length can be measured.

Guschlbauer et al. (2007) found a quadratic relationship between initial length change (L_2-L_1 , Figure 3.2) and F_2 (see also Figure 3.2). The quadratic relationship of these parameters corresponds to a quadratic relationship of SE spring force and SE spring length, although this conclusion is not obvious. Section 3.3.2 on page 48 contains the derivation of this conclusion.

This derivation provides a means to calculate the spring constants of the series elasticity from the quick release data. Two different ways will be described here. First, the spring constant can be analytically derived for each data set of L_1 , L_2 , F_1 and F_2 . Second, the constant can be derived by linear fitting through a plot of $\sqrt{F_2} - \sqrt{F_1}$ vs. L_2-L_1 .

Analytic solution

In Figure 3.5 the measured and required parameters are summarized. The quick release experiments provide measures for ΔL , F_1 and F_2 . L_{1SE} and L_{2SE} are unknown. However, as a quadratic relationship is assumed, it is possible to calculate the spring constant even without knowing L_{1SE} and L_{2SE} .

Equation 3.2 is the hypothesis of the quadratic spring, solved for L_{SE} in equation 3.3 where the term $\frac{1}{\sqrt{k}}$ is replaced by the variable m .

$$F = k \cdot L_{SE}^2 \quad (3.2)$$

$$L_{SE} = m \cdot \sqrt{F} \quad (3.3)$$

Equation 3.4 relates m and k to each other.

$$k = \left(\frac{1}{m}\right)^2; m = \frac{1}{\sqrt{k}} \quad (3.4)$$

With equations 3.2-3.4 it is possible to relate ΔL to F_1 , F_2 and m . ΔL is given by:

$$\Delta L_{SE} = L_{1SE} - L_{2SE} \quad (3.5)$$

However, each L_{SE} term can be expressed as a function of the corresponding force and spring constant:

$$\Delta L_{SE} = m \cdot \sqrt{F_1} - m \cdot \sqrt{F_2}, \quad (3.6)$$

solving for m , results in

$$m = \frac{\Delta L_{SE}}{\sqrt{F_1} - \sqrt{F_2}}. \quad (3.7)$$

This relates the spring constant of the series elastic spring to the forces F_1 and F_2 and the measured length difference (ΔL). Thus using equation 3.7, it is possible to calculate a distinct spring constant value for each quick release experiment. Ideally m would be identical in each experiment, but it is not. For modeling an average of all calculated spring constants was used.

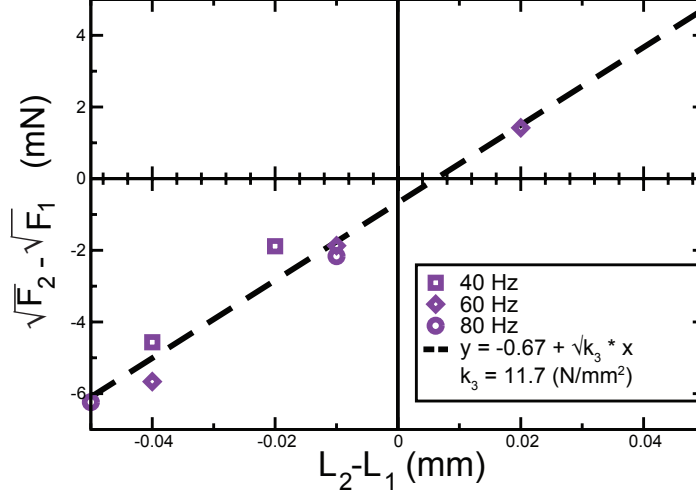


Figure 3.6: Estimating k_3 with the linear fit approach. According to equation 3.9, a linear relationship can be expected between $L_2 - L_1$ and $\sqrt{F_2} - \sqrt{F_1}$. Data of three different activation levels are shown here (squares, diamonds and circles). The linear fit shows high correlation ($R^2 = 0.96$) and k_3 is similar, but not identical to the analytical method presented above (compare section 3.3.2 and table 4.1 on page 66).

Linear fit solution

Equation 3.7 can be re-written as done in equation 3.8. Looking at equation 3.8 it becomes clear that a proportionality can be expected between ΔL and the force difference. ΔL and the difference of the square root forces are proportional to $1/m$, the reciprocal slope of the series elastic spring. Thus plotting the measured length differences against $\sqrt{F_1} - \sqrt{F_2}$ should give a linear relationship with the slope of $1/m$ (which equals \sqrt{k}) (equation 3.9).

$$m^{-1} \cdot \Delta L_{SE} = \sqrt{F_1} - \sqrt{F_2} \quad (3.8)$$

$$m^{-1} \cdot (L_{1SE} - L_{2SE}) = \sqrt{F_1} - \sqrt{F_2} \quad (3.9)$$

Figure 3.6 shows the data for the selected muscle. The strong linear correlation of the data points ($R^2 = 0.96$) further support the idea of the quadratic spring. Keeping in mind that the data points originate from experiments at different muscle activation levels. Figure 3.6 also shows that the spring constant does not change with activation level.

The quadratic spring as presented in Guschlbauer et al. (2007)

Guschlbauer et al. (2007) found the following relationship of measured length change in the quick release experiments and F_2 :

$$F_2 = k_4 \cdot (k_5 - \Delta L)^2, \quad (3.10)$$

with free parameters k_4 and k_5 and F_2 the second counter force (see F_2 in Figure. 3.2). Fitting k_4 and k_5 resulted in a very accurate description of the measured data ($R^2 > 0.99$). However, this equation is not of immediate use for modeling, as a relationship is needed describing the spring force for any given length of the series elastic spring. Thus a description in the following form is required:

$$F = k_3 \cdot L_{SE}^2, \quad (3.11)$$

with L_{SE} being the length of the series elastic component and F being its force. The following steps explain why it is allowed to assume such a spring property underlying the results shown in Guschlbauer et al. (2007). The idea is to show that the relationship between F_2 and ΔL of the quadratic spring in equation 3.11 would result in equation 3.10. Therefore ΔL is first set up, which is the result of two different counter forces pulling at the spring. The forces were called F_1 (force before the switch) and F_2 (force after switch). In terms of the spring function, these forces are associated with a certain spring length (L_{SE}). So if L_{1SE} is the spring length associated with F_1 and L_{2SE} is the spring length associated with F_2 the following relationships can be derived from equation 3.11:

$$F_1 = k_3 \cdot L_{1SE}^2 \quad (3.12)$$

$$F_2 = k_3 \cdot L_{2SE}^2 \quad (3.13)$$

$$L_{1SE} = \sqrt{\frac{F_1}{k_3}} \quad (3.14)$$

$$L_{2SE} = \sqrt{\frac{F_2}{k_3}} \quad (3.15)$$

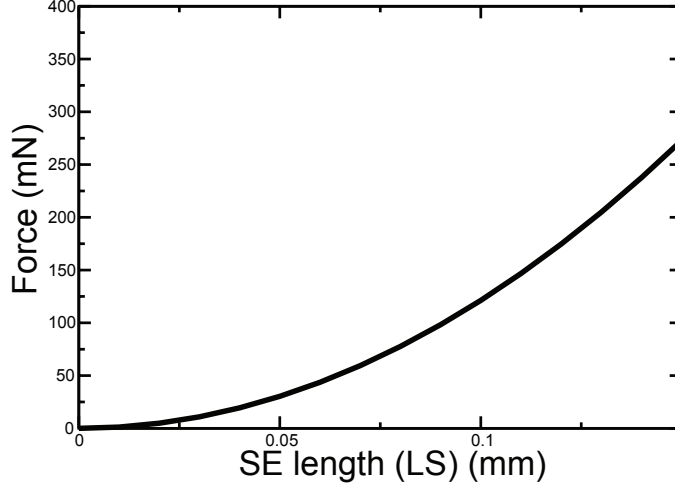


Figure 3.7: Series elastic spring model. The force the calculated quadratic spring would produce at different lengths is shown here.

With equations 3.14 and 3.15 it is possible to express ΔL :

$$-\Delta L = L_{2SE} - L_{1SE} = \sqrt{\frac{F_2}{k_3}} - \sqrt{\frac{F_1}{k_3}} \quad (3.16)$$

If the second term in equation 3.16 is replaced by a variable (for example k_5) equation 3.18 results:

$$k_5 = \sqrt{\frac{F_1}{k_3}} \quad (3.17)$$

$$-\Delta L = \sqrt{\frac{F_2}{k_3}} - k_5 \quad (3.18)$$

As it will turn out later, the k_5 defined in equation 3.17 is identical to the k_5 in equation 3.10. Equation 3.18 can now be solved for F_2 :

$$(k_5 - \Delta L) = \sqrt{\frac{F_2}{k_3}} \quad (3.19)$$

$$(k_5 - \Delta L)^2 = \frac{F_2}{k_3} \quad (3.20)$$

$$k_3 \cdot (k_5 - \Delta L)^2 = F_2 \quad (3.21)$$

3 Building an individual Hill-type model of the extensor tibiae muscle

Having solved this equation for F_2 it becomes clear that k_3 in equations 3.11-3.21 is identical to k_4 in equation 3.10

$$k_3 = k_4. \quad (3.22)$$

Thus it can be shown that the relationship of F_2 and ΔL for a spring following equation 3.11 results in

$$k_4 \cdot (k_5 - \Delta L)^2 = F_2, \quad (3.23)$$

which is exactly what has been used as a model for fitting in Guschlbauer et al. (2007). This shows that it is correct to assume a quadratic spring equation (as given in equation 3.11) from the data published in Guschlbauer et al. (2007).

Figure 3.7 finally plots the force-length relation of the series elastic spring given by the estimated k_3 value.

3.3.3 Force-activation curve

It is essential to be able to predict the force the muscle develops actively in response to motor neuron activity. The first step achieving this goal was to describe the steady-state force the muscle develops in response to varying levels of activation when held at rest length. Figure 3.8 explains this procedure. At two different stimulation frequencies the muscle produces isometric force. The asterisk denotes level of the maximum force values as it was measured. Note that muscle length is constant (at rest length) during this type of experiment.

Figure 3.9 shows the resulting force-activation data and the fitted model to it. Guschlbauer et al. (2007) fitted these data with an equation of the form:

$$F = F_{max} \cdot (1 - e^{-act/\lambda}) \quad (3.24)$$

where F_{max} is the maximum isometric force the muscle can produce at rest length, act is the stimulation frequency and λ is the ‘activation constant’. For the fits presented here, there were sufficient data points to independently determine what function best fit the data, and found that a Gompertz equation,

$$F = F_{max} \cdot e^{-e^{-a \cdot (act-b)}}, \quad (3.25)$$

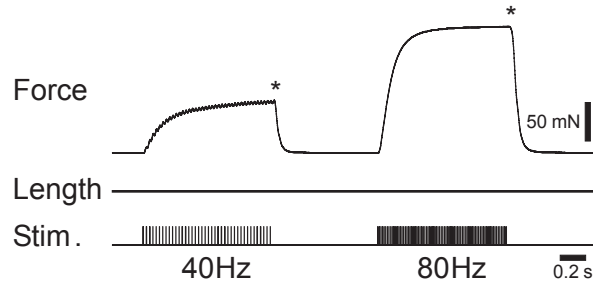


Figure 3.8: Example of experimental procedure for the determination of force-activation curve. At rest length different stimulations are performed (here 40 and 80 Hz). Force builds up isometrically (note the muscle length trace remains constant throughout the measurement) and is measured at its peak (asterisk).

gave better fits. F_{max} , a , and b are parameters determined from the fits (see Figure 3.9). One of its advantages (for example over a standard sigmoid) is that it provides a certain level of asymmetry in its asymptotes. The F_{max} parameter has a particular relevance to other modeling parts. It is the maximum isometric force the muscle can produce at full activation (corresponding to a stimulation frequency of 200 Hz). As force length and force velocity modeling were performed with normalized force (to keep the number of parameters low), estimating F_{max} accurately is crucial for the quality of these models. Thus it was important to have particular good fits for the force-activation data, as F_{max} was not measured directly, but a result of force-activation fitting.

In Figure 3.9 the fit had an R^2 value of 0.997; across the 10 experiments performed, the mean R^2 value was 0.9991 ± 0.001 .

3.3.4 Force-length curve

Despite knowing how the steady-state force varies as a function of muscle activation, it is also necessary to know how steady-state force varies at different muscle lengths. This relationship is called the “force-length” curve, or more precisely the “active force-length” curve, if it refers to muscle force generated by active contraction.

The data for setting up a force length curve originates again from steady state, isometric force measurements (similar to the measurements shown in Figure 3.8) but this time at various muscle lengths. Figure 3.10 shows an example measurement for setting up the 80 Hz force length curve. Two isometric contractions are shown at two different muscle lengths. The dashed horizon-

3 Building an individual Hill-type model of the extensor tibiae muscle

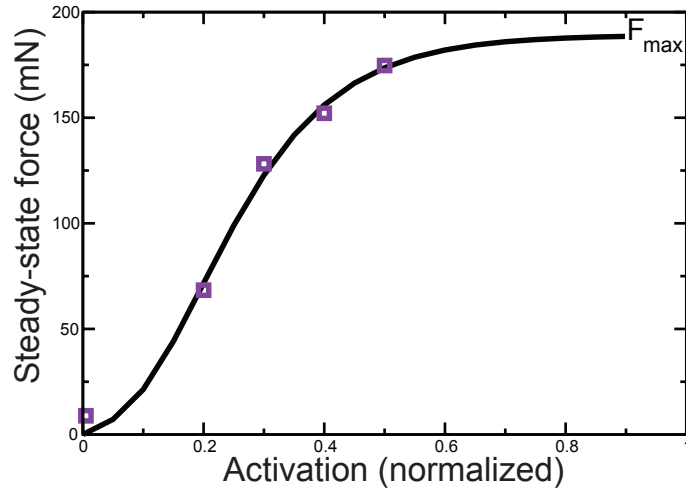


Figure 3.9: Force-activation model and related data points. Measurements as shown in Figure 3.8 result in a force-activation relationship at rest length. Four different stimulation frequencies have been applied (40, 60, 80 and 100 Hz). The first data point (left most) originates from single twitch measurements.

tal line denoted the increase in active isometric muscle force due to muscle lengthening.

In contrast to force velocity modeling, where the Hill-hyperbola (Hill, 1938) usually provides very good approximations, force length relations are more diverse in shape. Thus the first step in force length modeling was to think about a general model which is simple yet flexible enough to reproduce pertinent features of the measured curve. Several different approaches have been studied (linear, parabola, polynomial models) but one type of model proved to be very powerful although it has only a single parameter to fit to the muscle data.

Investigations of force length data of Guschlbauer et al. (2007) led to the presumption that there may exist a common maximum fiber length for all activations (see Figure 3.11a). By extrapolation this common intersection of the length axis was estimated to be approximately 2.7 mm. This idea in mind a sinusoidal model was designed which met the constraints of crossing the length axis at 2.7 mm and having a maximum amplitude of 1 (which is the maximum normalized force in the model). The solid lines in 3.11a show the behavior of the sinusoidal model when all parameters of the model were individually fit to the data points. Each line represents one activation level. The model was almost identical to the one used at last (given in equation 3.29). The only

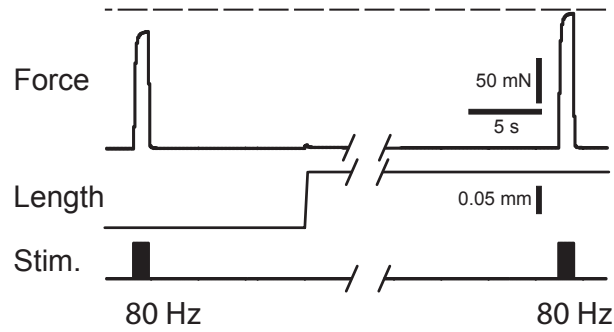


Figure 3.10: Example of force-length data measurement procedure. Muscle active force was measured at four muscle lengths at each of two activation levels (40 and 80 Hz). The data shown here are only for two muscle lengths at the 80 Hz activation level. To compensate for changes in passive force resulting from the changes in muscle length, the passive force for each length had to be subtracted from the active force. This value of passive force was measured immediately before stimulation start.

difference is that the A_{act} function (as formulated in equation 3.27) was not known at the beginning. So A_{act} simply was a parameter optimized for each activation level (thus called A_{act}^* in equation 3.26).

$$F = A_{act}^* \left[\frac{1 + \sin\left(\text{freq}_{act} \cdot \left(L - \left(\frac{\pi}{2} + 2.7 \cdot \text{freq}_{act}\right)\right)\right)}{2} \right] \quad (3.26)$$

It is visible that the model lines fit nicely to the data points up to almost 2 mm, a length way beyond the working range of the muscle (approximately 1.2-1.6 mm, see Guschlbauer et al. (2007)).

At this stage the model consisted of two parameters, one controlled the amplitude (A_{act}), the other one controls frequency (freq_{act}) of the sine wave. Both parameters were sensitive to activation, thus needed adaption to each activation level. In Figure 3.11b, the values for each parameter at the activation levels are shown. It is obvious that a) the variation of each parameter with activation is systematic, thus should be predictable and b) that both parameters (A_{act} and freq_{act}) are not independent from each other. Their relationship is drawn in Figure 3.11c. Their linear dependence makes it easy to express one parameter by a linear function of the other. Equation 3.27 expresses A_{act} as a function of freq_{act} . Equation 3.28 shows the equation used to predict the freq_{act} values in Figure 3.11b. This equation contains the curv_{hyp} parameter which is the only remaining parameter that needed to be adapted for the model to work. In Figure 3.11c, the result of the modeling is shown. In comparison to the results

3 Building an individual Hill-type model of the extensor tibiae muscle

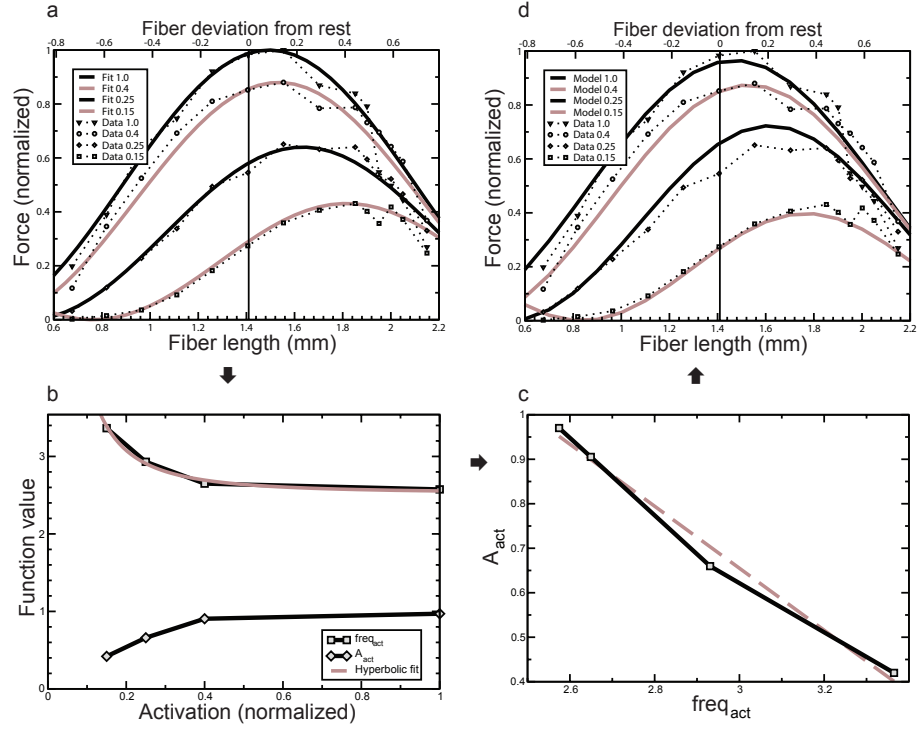


Figure 3.11: Scheme of force-length model derivation. There were 14 data points per activation level curve (total 56 measurements). a) Data from Fig. 9a of Guschlbauer et al. (2007) replotted and fit with equation 3.26. b) Plot of A_{act}^* and $freq_{act}$ of equation 3.26 vs. activation level. Note the hyperbolic variation of both parameters (equation 3.28) and the linear relationship of the two functions. c) Plot of A_{act}^* vs. $freq_{act}$ and linear fit to the data (equation 3.27). d) Curves obtained when $freq_{act}$ and A_{act} functions are used to calculate the force at any activation level. The numbers in the inset rectangles in a and b and the x-axis label in c refer to activation normalized to maximum activation (200 Hz motor nerve stimulation).

shown in panel a, the curves in d result from modeling, not from individual fits to each activation level. Thus resultant lines in panel d are not as accurate as in a, but represent a complete model for each stimulation frequency based on only one parameter (defining the ‘curvature’ of the hyperbolic function, $curv_{hyp}$).

$$A_{act} = 2.7 - 0.7 \cdot freq_{act} \quad (3.27)$$

$$freq_{act} = 2.5 + \frac{1}{(curv_{hyp} \cdot (act + 0.005))^2} \quad (3.28)$$

Equations 3.27 and 3.28 were used in the complete force length model, shown

in equation 3.29. Note that A_{act} and $freq_{act}$ are functions, not parameters.

$$F = A_{act} \left[\frac{1 + \sin \left(freq_{act} \cdot \left(L - \left(\frac{\pi}{2} + 2.7 \cdot freq_{act} \right) \right) \right)}{2} \right] \quad (3.29)$$

The terms in this equation can be understood as follows. A_{act} sets the maximum amplitude of the sine wave and depends on the level of muscle activation. The '1' and '2' in the square brackets turn all values of the sine curve positive and limit them between 0 and 1 (and thus, since the F values used here are normalized and therefore run from 0 and 1, also constrain A_{act} to lie between 0 and 1). The $freq_{act} \cdot L$ term sets sine wave frequency with $freq_{act}$ being a function of muscle activation. The $\frac{\pi}{2} + 2.7 \cdot freq_{act}$ term ensures that all sine curves produce 0 force at a muscle length of 2.7 mm and that the peak of the curves shifts to the right as activation level decreases, which was true for the muscle shown in Guschlbauer et al. (2007).

This modeling was later transferred to the individual muscles, for simplicity assuming the relation between A_{act} and $freq_{act}$ to be constant for all extensor muscles. As it turned out, it was possible to produce acceptable force-length fits under this assumption, for all ten muscles investigated. Therefore, no further study of this particular relationship was performed.

The procedure to estimate the $curv_{hyp}$ parameter was the following (for all muscles including the one presented here):

The active force-length curve was measured at four lengths at each of two activation levels (according to the method outlined in Figure 3.10 and normalized these data using the F_{max} value calculated earlier by fitting equation 3.32, see also Figure 3.9.

Afterwards the force-length model was fitted (equation 3.29) to each activation level's four data points (by optimization of $curv_{hyp}$). This gave two points (one for each activation level) on the activation / function-value plane shown in panel 3.11b. These two points were used to constrain the hyperbolic fit ('hyperbolic fit' line in Figure 3.11b), which resulted in the value of $curv_{hyp}$ in equation 3.28. Figures 3.12b and 3.12c show the resultant curves for the activation levels 0.2 and 0.4 of 200 Hz. Figure 3.12d displays the predicted curve at an activation level of 1.

It is apparent in this example that this fitting procedure, in which all equation parameters except $curv_{hyp}$ were presumed to be constant, resulted in good fits

3 Building an individual Hill-type model of the extensor tibiae muscle

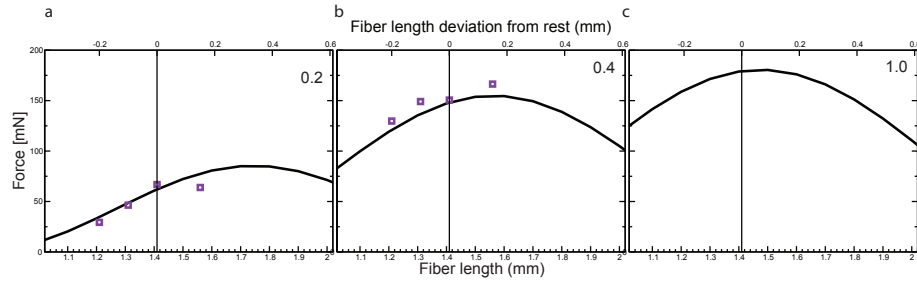


Figure 3.12: Force length curves for selected muscle. Active force-length curves calculated from four measurements each (squares in panels a and b) at the two activation levels (numbers in upper right corner of each panel). d) Predicted force-length curve for an activation of 1 (200 Hz). Normalization of force has been removed in this plot for ease of comparison with physiological data.

to the data in Figs. 3.12a ($R^2 = 0.83$) and 3.12b ($R^2 = 0.91$). When the data from the additional 9 experiments were similarly analyzed, again good fits were obtained strengthening the assumption that only $curv_{hyp}$ varied across muscles (mean $R^2 = 0.96 \pm 0.03$). How far the observed sensitivity to changes in $curv_{hyp}$ is due to a possible weak sensitivity for the A_{act} parameter has not been investigated yet. However, given the strong correlation between the two parameters and their dedicated purpose in the force-length equation (scaling and frequency), there is no reason to assume A_{act} to have considerably less effect on the curve than $freq_{act}$ (with its $curv_{hyp}$ parameter).

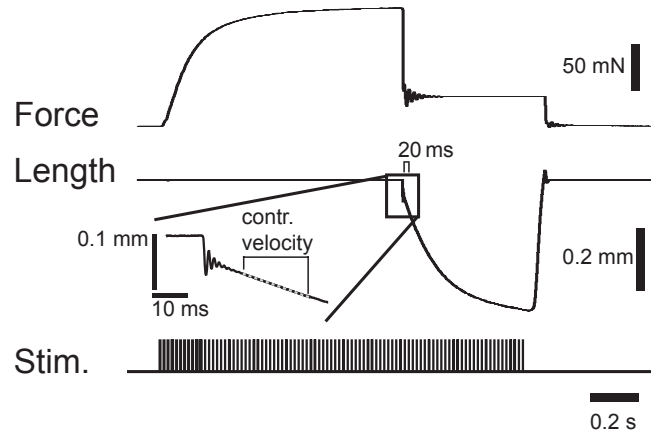


Figure 3.13: Schematic time course of a quick-release experiment for determination of the force-velocity curve. The same quick release experiments as in section 3.3.2 were used, but a different analysis was performed. The average slope during 20 ms after end of the contraction discontinuity was used to calculate the active contraction velocity of the contractile element (see inset and section 3.2.4 for details about measurement and analysis).

3.3.5 Force-velocity curve

The classic Hill hyperbola predicts the shortening force-velocity curve. Solved for force, this relationship is usually noted like equation 3.30:

$$F = \frac{c_{pos} \cdot (1 + c_{pos})}{(v/v_{max}) + c_{pos}} - c_{pos} \quad (3.30)$$

Here v is the velocity of muscle shortening, v_{max} is the maximum rate of shortening (at zero force), and c_{pos} is a constant that determines hyperbola curvature. The c_{pos} value has already been determined by Guschlbauer et al. (2007) and proved to be rather constant for all investigated muscles ($c_{neg} = 0.5$).

However, the classic formulation was made for maximum muscle activation only. It needs scaling applied to it (in some form or other) if it should be used for varying activation levels. This scaling can be as simple as a linear factor (scaling proportional to activation level) or more complex, possibly including activation dependency of other parameters, which is true for the force-velocity model presented here.

Equation 3.31 shows the scaled version of the Hill hyperbola:

3 Building an individual Hill-type model of the extensor tibiae muscle

$$F = F_A \cdot \frac{c_{pos} \cdot (1 + c_{pos})}{(v/v_{max}) + c_{pos}} - c_{pos}, \quad (3.31)$$

with F_A being equal to function 3.32

$$F_A = F_{max} \cdot e^{-e^{-a \cdot (act-b)}}. \quad (3.32)$$

The F_A function used for scaling is the force-activation relationship described in section 3.25, repeated for ease of reading (equation 3.32). In addition to simple multiplicative scaling, v_{max} is a function of activation, too. Note that both, equation 3.30 and 3.31, are valid for shortening velocities only.

The muscle force during lengthening does not follow the same relationship, as it saturates quickly for lengthening contractions, which cannot be predicted with the Hill hyperbola. The equation used for lengthening contractions is given in equation 3.33:

$$F = \frac{c_{neg} \cdot (1 + c_{neg})}{(v/v_0) + c_{neg}} - c_{neg} - F_A \quad (3.33)$$

Note that c_{neg} has a different sign than c_{pos} , which makes this hyperbolic function saturate in force for increasing lengthening velocities. This function also needs appropriate scaling in order to have both equations touch each other at zero velocity. The scaling is done by y-shifting with the final $-F_A$ term.

The process of finding appropriate v_{max} values for the shortening contraction equation and appropriate c_{neg} for the lengthening contractions was as follows:

For these contractions, all parameters are known for each activation level, except for v_{max} . v_{max} was determined from same quick release experiments (Figure 3.13) that were used in section 3.3.2 but using the initial slope of the second, slow length change (see inset in Figure 3.13). These experiments were performed using three force step changes at three activation levels. All force levels were normalized by dividing by F_{max} . v_{max} was calculated by fitting a linearly scaled version of the Hill hyperbola (equation 3.34) to the force-velocity data of each activation level.

$$F = s \cdot \frac{c_{pos} \cdot (1 + c_{pos})}{(v/v_{max}) + c_{pos}} - c_{pos} \quad (3.34)$$

The scaling factor s in this equation is simply a number, not a function, as the fitting is done separately for each activation level. This scaling could also have

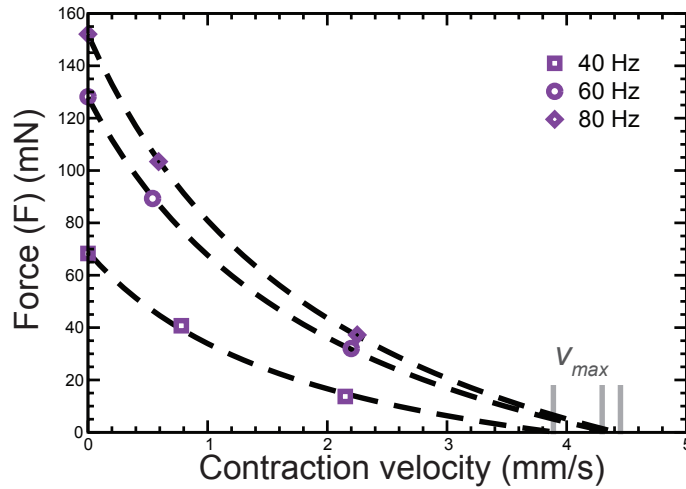


Figure 3.14: Determining maximum contraction velocity (v_{max}) for different stimulation frequencies. Equation 3.34 was fit to data resulting from quick release experiments of three different stimulation frequencies (squares (40 Hz), circles (60 Hz), diamonds (80Hz)). Each fit (dashed line) was done with activation specific s , c_{pos} and v_{max} in order to result in the best possible extrapolation of v_{max} . Thus the result of this work are the three v_{max} values in Figure 3.15.

been performed by fixing s according to the force-activation relationship (see section 3.3.3). But to maximize goodness of the fits (and hence the estimates of v_{max}) at this intermediate stage, s was instead allowed to be a free variable.

From these fits the v_{max} values (where the curves crossed the x-axis) for the various activation levels (Figure 3.14) were extrapolated. These v_{max} values were then plotted vs. activation (Figure 3.15) and fitted to an equation from Guschlbauer et al. (2007):

$$v_{max} = v_{max\infty} \cdot e^{-act/0.3} \quad (3.35)$$

in order to determine $v_{max\infty}$, which is the v_{max} at an activation of infinity. The 'activation constant' of 0.3 is taken from Guschlbauer et al. (2007). It proved to be rather constant for all investigated animals and was thus used for all muscles. As function type as well as curvature for this fit were pre-determined by Guschlbauer et al. (2007), this particular fit was not as good as it could have been without having the curvature parameter fixed. On the other hand, the single degree of freedom in this fit makes it possible to work with only three data points (as only $v_{max\infty}$ need to be optimized).

3 Building an individual Hill-type model of the extensor tibiae muscle

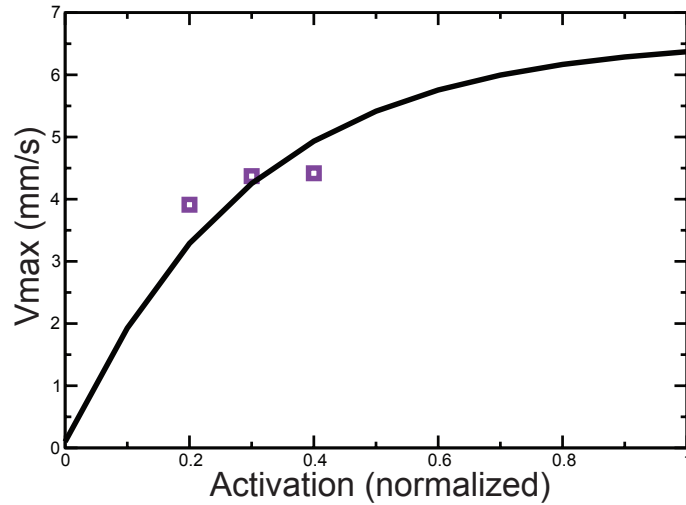


Figure 3.15: Plot of v_{max} versus activation comparing v_{max} -model and extrapolated data. v_{max} has shown to depend on muscle activation (Guschlbauer et al., 2007). This plot contains the v_{max} values determined before (squares, see Figure 3.14). The solid line represents the estimated fit through the three data points. Note, that model function and curvature were described to be constant for all muscles by Guschlbauer et al. (2007), thus only $v_{max\infty}$ could be optimized here.

As lengthening contractions are very demanding for the muscle to perform, only two of these contractions were measured (at an activation level of 0.4). Thus c_{neg} and v_0 were simply fit with equation 3.33 using the two data points from lengthening contractions (open squares in Figure 3.15).

These fitted values were then used to construct continuous force-velocity curves at different activation levels (Figure 3.16). In these plots the solid lines are the portions of the curves experimental data was available for (squares). The inset in Figure 3.16c shows the shortening contraction data points and the first lengthening contraction data point of the panel on an expanded time scale. Figure 3.16d is the predicted force-velocity curve for an activation of 1.

Quality of fit was measured separately for the shortening and lengthening portions of the curves. In the data shown, the fits for the shortening contractions (Figures 3.16 a, b, c) gave R^2 values of 0.995, 0.99997 and 0.9998; across the 10 experiments the mean R^2 values of the panels were 0.994 ± 0.007 , 0.997 ± 0.007 , and 0.998 ± 0.003 .

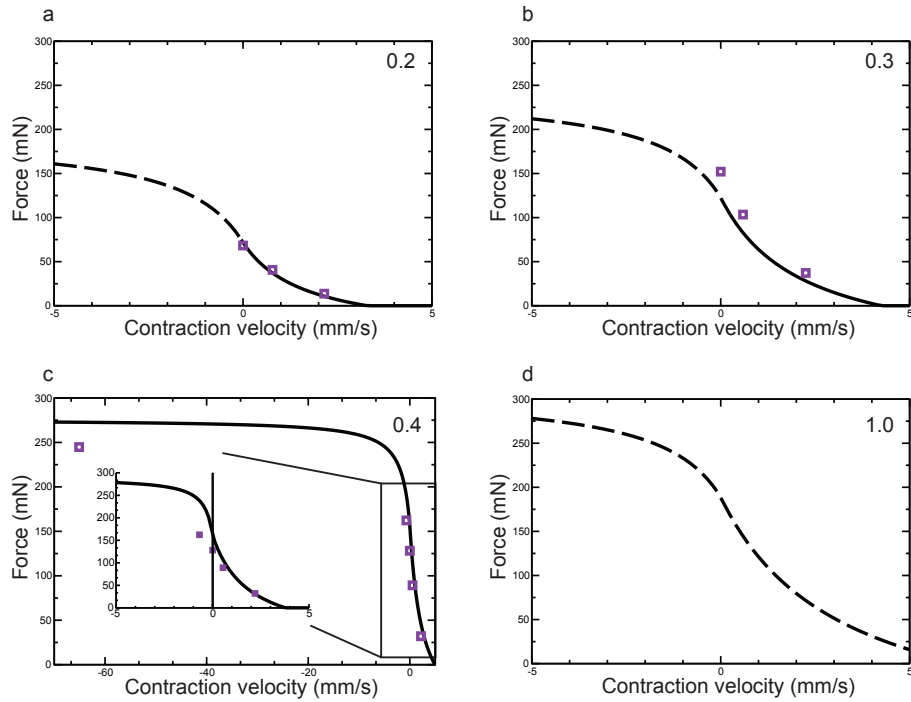


Figure 3.16: Force velocity curves of the model. The panels a-d show the force-velocity curves for shortening and lengthening contractions for different activation levels as predicted by the model (with data points measured); the activation level is noted in the upper right corner of each panel. Dashed lines denote regions where no data has been measured to compare the model to. The inset in panel c highlights the transition from lengthening to shortening contractions. Panel d contains the predicted force-velocity curve for activation level 1 (200 Hz).

3.4 Discussion

It could be shown that all the standard Hill-type parameters describing extensor muscles can be achieved with good R^2 values from a set of experimental protocols small enough to be performed on single muscles. This work, however, requires sufficient prior experiments being performed so that the general form of the functions involved can be determined (Guschlbauer et al., 2007). In order to transfer this approach to another system, these prior experiments would also need to be performed first. Nonetheless, this demonstrates that it is possible to make these determinations in single experiments, suggesting that this approach could also be followed in other systems, at least those with muscles of comparable robustness as stick insect muscles.

A possible concern with these results is that the parameter determinations were made with only 4 to 11 data points per characteristic. The R^2 values associated

3 Building an individual Hill-type model of the extensor tibiae muscle

with these determinations were uniformly high across the 10 muscles investigated, which suggests that these numbers were sufficient to well constrain the fits. It is important to note that this success strongly depended on the extensive prior knowledge of the muscles. For most characteristics the prior work already defined or suggested applicable model functions, in some cases even certain function parameters have been determined (like c_{pos} in force-velocity function).

Further this knowledge allowed to pre-determine which experiments should be performed best to find the most useful data points for constraining the various curves. Although this need for prior knowledge is time-consuming, the experiments to obtain this background data are standard, and already available in the literature for many systems. Consideration of prior work in other systems shows that the functions used in this work also apply to most other muscles. As such, the approach detailed here is again likely applicable to many other muscles.

An alternative approach to determining muscle-defining parameter values in experiments on individual muscles was provided by Wagner et al. (2005). In this work the authors subjected the muscles to iso-velocity length changes at multiple activation levels and then fitted the parameters of an existing muscle model so that the model best reproduced the muscle responses to this input. This approach fundamentally differs from the one used here as no direct measurements of muscle Hill-type characteristics were attempted, but instead were inferred once optimization was accomplished. Provided the muscle model used in Wagner et al. (2005) is sufficiently accurate, both approaches should give equivalent results, inasmuch as a given muscle has only one set of such characteristics.

The ISOFIT approach has certain advantages including the ability to measure muscle responses *in vivo*. But it has the drawback that an accurate muscle model must already be available, and it is unclear how sensitive the results obtained from it are to model details.

Although in some cases data are interpreted in terms of a muscle model here as well, the data measures itself are model-independent. As such, the approach detailed here may have advantages for investigating muscle properties in cases in which insufficient model detail or computer resources (to perform the optimizations) are available. The direct relationship between the measurements made here and well-understood and widely used descriptors of muscle characteristics is also an advantage of this approach.

3.4 Discussion

In summary, a methodology is described here, which allows specification of muscle passive force, series elasticity, force-activation, force-length, and force-velocity curves at all activations, from only 28 measurements, a small enough number to perform in experiments on single muscles. This approach allows modeling muscles individual-by-individual, and will be useful for investigating how much animal-to-animal variability is present in muscles, whether muscles from different animals must be modeled individually, and whether there are correlations among muscle parameters. These issues will be examined for the stick insect extensor muscle in the following sections.

3 *Building an individual Hill-type model of the extensor tibiae muscle*

4 Parameter variation between individual Hill-type muscle models

4.1 Introduction

Comparison of muscles contractions of from different individuals to identical neural driving suggests that considerable inter-individual variation may exist (Hooper et al., 2006; Thuma et al., 2003). Whole muscle responses result from the combined action of multiple lower-level processes, and thus these different responses presumably arise from difference in the lower-level processes. One method to characterize these lower-level processes is by modeling. Hill-type models composed of multiple equations, each of which are defined by one to several parameters, are very commonly used to predict whole muscle activity (Hannaford and Winters, 1990; Winters, 1990; Zahalak and Ma, 1990; Zajac and Winters, 1990). In prior work the values of the parameters in these equations have been determined from many experiments, with only one or a few parameters being measured in any one experiment. Since the model's parameters are never determined for any single muscle, this approach has the drawback that it is impossible to measure parameter variation across animals.

In section 3 a technique was presented, which enables to measure all parameters necessary to build a Hill-type model for an individual muscle. The individual muscle data allows to directly measure both how much variability is present between different stick insect extensor muscles and whether any of the model parameters co-vary. As it turned out, there is indeed substantial (1.3 to 17-fold) variation in model parameters across muscles. Two parameter pairs of the model co-vary. One of the pairs is present in equations modeling different muscle characteristics (force-length and force-activation curves). These two characteristics will vary in a linked fashion across muscles, and this lack of independence is a good argument to take particular care in combining data from different muscles into single models.

4 Parameter variation between individual Hill-type muscle models

| Animal | k_1 (μN) | k_2 (mm^{-1}) | k_3 (N/mm^2) | F_{\max} (mN) | A | B | $curv_{hyp}$ | $v_{max\infty}$ (mm/sec) | v_0 (mm/sec) | c_{neg} |
|----------------|----------------------------|-------------------------------|-------------------------------------|--------------------|------|------|--------------|-----------------------------|-------------------|-----------|
| A | 1.76 | 4.73 | 12.1 | 189 | 10.8 | 0.23 | 4.23 | 6.27 | 1.07 | -1.42 |
| B | 4.87 | 4.11 | 11.6 | 197 | 6.6 | 0.32 | 3.23 | 6.02 | 0.6 | -1.26 |
| C | 0.78 | 5.48 | 13.6 | 139 | 6.3 | 0.22 | 4.47 | 5.6 | 1.14 | -1.57 |
| D | 5.29 | 4.18 | 14.2 | 116 | 10.3 | 0.12 | 6.22 | 7.05 | 0.26 | -1.68 |
| E | 3.13 | 4.38 | 12.1 | 189 | 8.1 | 0.2 | 4.51 | 6.58 | 1.04 | -1.63 |
| F | 4.65 | 4.36 | 12.7 | 121 | 11 | 0.14 | 5.57 | 6.66 | 0.69 | -1.62 |
| G | 1.24 | 5.1 | 12.7 | 196 | 11.4 | 0.12 | 5.82 | 6.17 | 0.23 | -1.5 |
| H | 0.53 | 5.99 | 31.2 | 132 | 8.1 | 0.17 | 5.13 | 5.66 | 1.06 | -1.68 |
| I | 4.29 | 4.09 | 9.5 | 170 | 8.9 | 0.24 | 4.19 | 6.06 | 3.99 | -1.54 |
| J | 0.41 | 5.73 | 8.2 | 54 | 6.6 | 0.23 | 4.24 | 7 | 0.49 | -1.38 |
| | | | | | | | | | | |
| Fold-variation | 12.9 | 1.5 | 3.8 | 3.7 | 1.8 | 2.7 | 1.9 | 1.3 | 17.4 | 1.3 |

Table 4.1: Summary of all parameters and values of the model. The first row contains the parameter names used in the equations and the text. Animals in column one are identified with a capital letter (A-J). The final row lists the variation observed for a specific parameter between all animals. Variation ranges from 1.3 fold to 17.4 fold. Parameters k_1 and k_2 are used in passive force, k_3 in series elasticity, F_{\max} , A and B in force-activation, $curv_{hyp}$ in force-length and $v_{max(act=1)}$, v_0 and c_{neg} in force-velocity equations.

4.2 Materials and methods

4.2.1 Modeling and experimental procedures

Modeling and muscle experiments were performed the same way as described in section 3.2. However in this section the results of ten extensor muscles were examined.

4.2.2 Correlation analysis

The Hill-type model used here has 10 parameters. The ability in the experimental work to measure all ten of these parameters in single muscles allowed not only to describe each muscle individually, but to test for correlations among the parameters across muscles. This work was performed on ten muscles because with ten parameters ten measurements are sufficient to detect a significant correlation 87.9% of the time (J Edu Stat 14:245-253, 1989). In general individual parameters across the ten muscles were not normal distributed, which means that it was necessary to use non-parametric correlation tests. A Spearman rank correlation was therefore used with a α level of 0.00114 (to compensate for the multiple comparisons being made, nominal α was 0.05). The statistical test was kindly performed by Dr. Silvia Gruhn.

4.3 Results

It has been shown in chapter 3 that it is possible to design a Hill-type model from a set of measurements small enough to be performed on individual muscles. This allows to compare these curves across muscles and to test for correlations between curve parameters. In Table 4.1 all parameter values for all animals and their variation are presented. In the following sections it is first shown how each type of curve varies across the ten muscles examined. Then the correlations present among curve parameters and possible bases for these correlations are examined.

4.3.1 Parallel elasticity

Passive force (parallel elasticity) curves were described in section 3.3.1 (equation 3.1). Because of the exponential nature of these curves, the absolute value range across the 10 muscles was relatively small at small fiber lengths (0.4 to 0.85 mN at a fiber length of 1.2 mm, the shorter edge of the working range) and increased as fiber length increased (3 to 7.6 mN at 1.6 mm, the longer edge of the working range, Figure 4.1). Parameter k_1 showed much greater variation (12.9-fold) than k_2 (1.5-fold, see Table 4.1), but changes in k_2 have a much greater effect on how force changes with muscle length than changes in k_1 because of k_2 's position in the exponent. Note, for instance, that the steepest

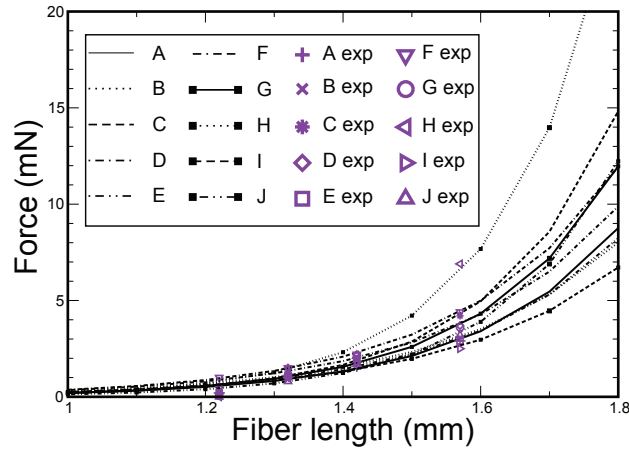


Figure 4.1: Passive force (parallel elasticity) curves. The curves show large inter-animal variation, particularly at long fiber lengths. The key identifies which data and curves come from which animal, and is used in all following figures showing data from multiple animals.

4 Parameter variation between individual Hill-type muscle models

curve in the plot (animal H) has the highest k_2 value but the second lowest k_1 value. This very strong effect of changing k_2 can also be appreciated by noting that, although animal H's curve appears very different from those of the other animals, its k_2 value was only modestly larger than that of the next-largest k_2 (5.99 vs. 5.73, see Table 4.1). Because of the exponential nature of these curves, the across-animal ranges were much smaller when expressed as fold-differences, being 2.1-fold at 1.2 mm fiber length and 2.6-fold at 1.6 mm (with this variation, of course, being solely because of the different curves having different k_2 values).

4.3.2 Series elasticity

The measurement of series elastic component was performed as described in section 3.2.4 and 3.3.2. The initial changes observed in quick release experiments are often modeled as arising from instantaneous length changes of a spring in series with the contractile element. Consideration of earlier extensor muscle data showed that for this muscle these length responses to changes in holding force were well modeled with a quadratic spring (see equation 3.2 in section 3.3.2).

Figure 4.2 shows the force of the series elastic spring for each muscle. Note that the working range for each spring is given by the maximum force the muscle can produce (usually below 200 mN). Corresponding to length values between

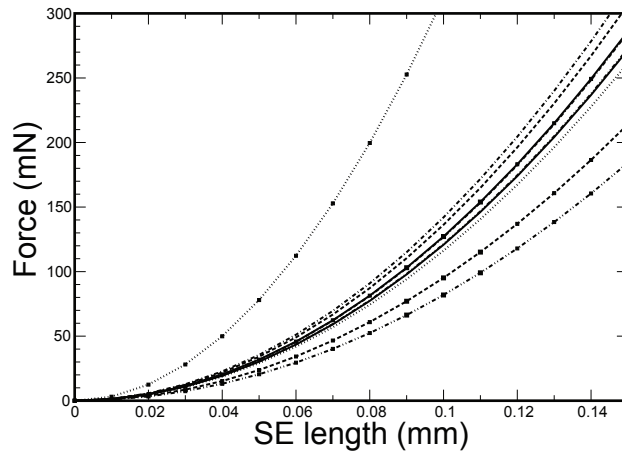


Figure 4.2: Series elasticity models for all muscles. Series elasticity shows large inter-animal variation. Note that the top curves in this figure and in Figure 4.1 are from the same animal. Although they appear to be outliers, they are no outliers in Figures 4.3-4.6.

0 and approximately 0.14 mm. These curves again showed large variation. Also variation in parameter k_3 was quite large (absolute range 8 to 31 N/mm², a 3.8-fold variation), see also Table 4.1 in section 4.3.

4.3.3 Force-activation

The force-activation curve was modeled with the Gompertz equation (eqn.3.25). Figure 4.3a shows the normalized curves and Figure 4.3b the fits scaled with individual muscle force. Even in the normalized case, in absence of inter-muscle maximum force differences (see Figure 4.3a), substantial differences in curve shape are apparent. For instance, the activation levels at which the various curves reach half-maximal force (0.5) range from 0.15 (muscle G) to 0.38 (muscle B), 2.5-fold. These changes are solely due to the different muscles having different A and B parameter values, ranging from 6.3 to 11.4 (A, 1.8-fold) and 0.12 to 0.32 (B, 2.7-fold) (see Table 4.1).

In Figure 4.3b the individual maximum muscle force is included in the plot. It is harder to see the differences in curve shape, but this representation highlights how great the real variation between muscles is. Note that for activation level 0.2 for example, the force varies from 20 mN up to approximately 130 mN. This points out how important this curve is for muscle force calculation. It also shows the large variation in maximum isometric force (F_{max}) varying from 54 to 197 mN (3.7-fold, see Table 4.1). Note that there is no correlation between muscle maximum force and the activation level at which half-maximal force

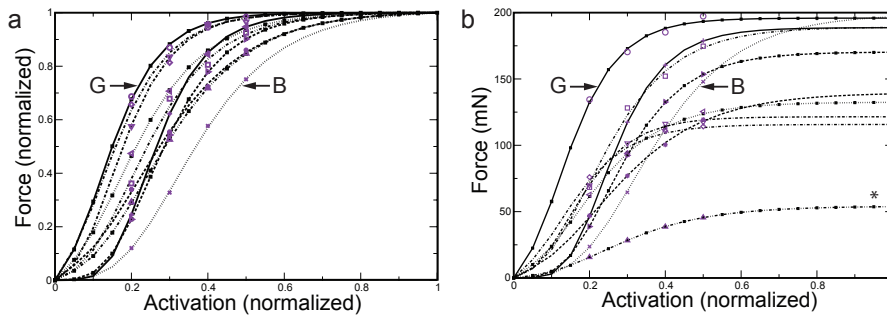


Figure 4.3: Normalized (panel a) and unnormalized force (panel b) force-activation curves. No correlation between muscle maximum force and other curve characteristics is apparent (e.g., at what activation the muscles achieved half-maximal force). ‘G’ and ‘B’ identify curves arising from the respective muscles (see Table 4.1). Note that the outlying, bottom curve in b (labeled with the asterisk) shows data from muscle J. The same muscle also produces peculiar results in Figures 4.4b2-c2 and 4.6a2-c2. But it did not give rise to the apparent outlier (top) curves in Figure 4.1 and 4.2.

4 Parameter variation between individual Hill-type muscle models

occurs, as is well shown by the F_{max} values of muscle G and B being nearly identical in maximum force (196 vs. 197 mN) despite their half-maximal force values occurring at the most different normalized activation levels for any of the ten muscles (see Figure 5.3a).

4.3.4 Force-length

Muscle force at all lengths and activations was modeled with the equations described in section 3.3.4. Considering the normalized curves (Figure 4.4 left column), it is apparent that the variation in curve shape is large for low activation levels (e.g., Figure 4.4a1).

Maximum normalized force ranges from 0.25 to 0.7 and the position of the sine peak shifts from 1.8 to 1.6 mm, see arrow.) The curves displayed in Figure 4.4a1 have $curv_{hyp}$ values from 3.23 (bottom curve) to 6.22 (top curve), a 1.9-fold range (see also Table 4.1). As activation increases the differences between the curves diminish, with the normalized curves becoming essentially identical at maximum activation (compare Figure 4.4c1).

Incorporating the muscle specific maximum force values results in the plots of absolute muscle force in the right column of Figure 4.4. In these plots the variation across animals becomes more apparent (compare Figure 4.4c1 and 4.4c2). Also the curves can now cross one another, destroying the smooth vertical and leftward displacement seen in the normalized curves (compare arrow in Figure 4.4a1). Taken together, these data show that at low activation levels both inter-muscle differences in $curv_{hyp}$ and F_{max} contribute to the different real force curves seen across the muscles, but at high activation levels the differences between the muscles are due mainly to their differing F_{max} values.

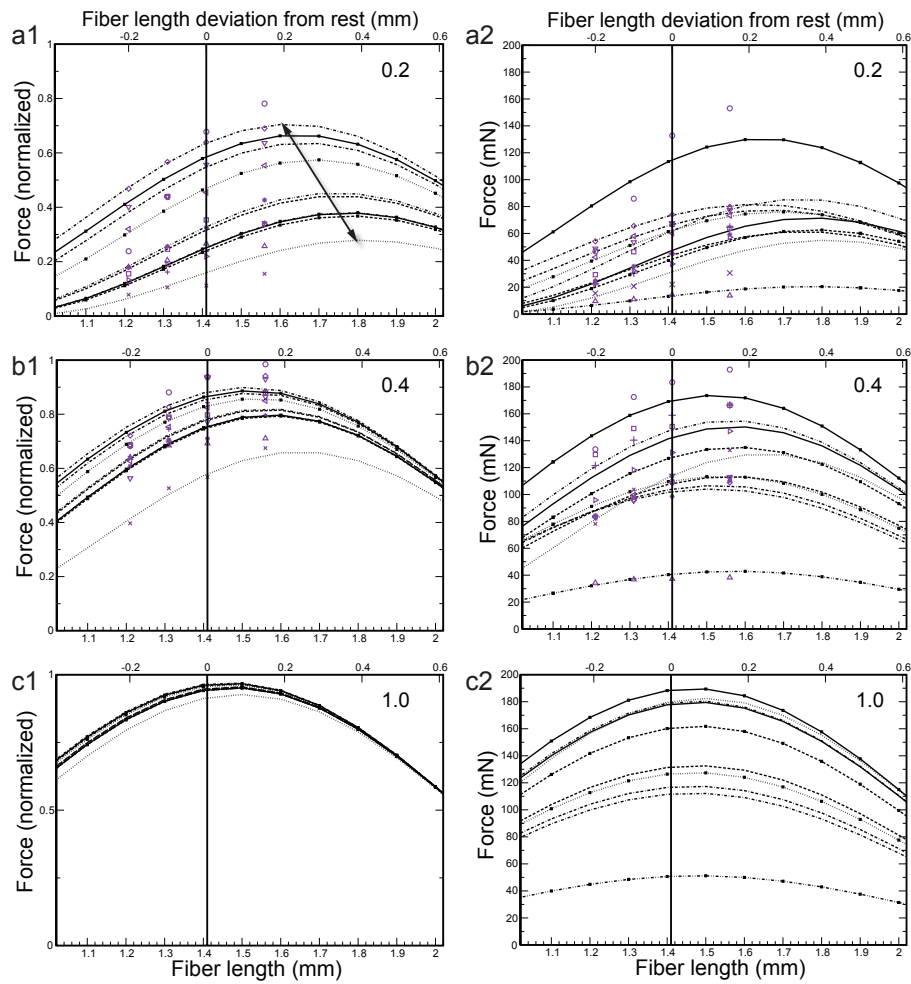


Figure 4.4: Normalized (left column, a1-c1) and unnormalized force (right column, a2-c2) force-length curves. In normalized plots, the curve peak shifts to the left with increasing activation (see arrow in a1). Unnormalized data does not show such a systematic shift and introduces curve crossings. Number in right upper corner in each panel is the activation level.

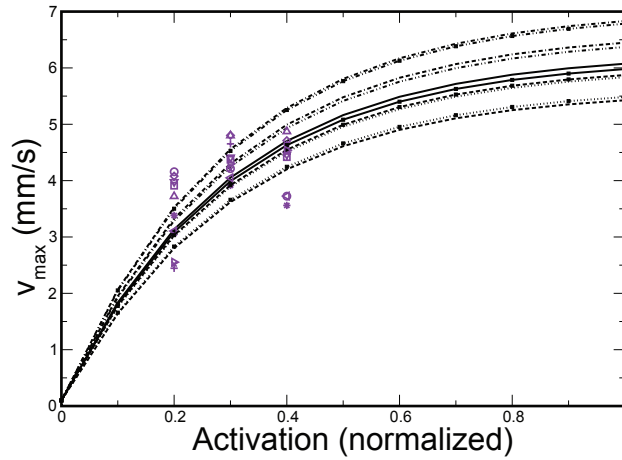


Figure 4.5: Plot of v_{max} as a function of activation. Note that curvature of the model function is fixed and has been previously defined by Guschlbauer et al. (2007), thus curves can only vary in amplitude. The v_{max} parameter shows comparatively large inter-animal variation, particularly at large activations (see also Table 4.1).

4.3.5 Force-velocity

Force-velocity curves were constructed as described in section 3.3.5. In the v_{max} models only amplitude can vary since the curvature parameter of the equation is fixed to 0.3 (compare equation 3.35). The variation is therefore small at low activations and increases with activation (Figure 4.5), ranging at maximum activation from 5.4 to 6.8 mm/s (1.8-fold), with the variation of the $v_{max\infty}$ parameter itself being somewhat larger (5.6 to 7.05 mm/s, 1.9-fold, compare Table 4.1). This difference in variation results from the fact that the model function will still increase for activation levels greater than 1. Thus the variation at activation 1 is smaller than the maximal possible variation at infinite activation.

Figure 4.6 compares the resulting force-velocity model with the measured data. Again left column shows the normalized plots, right column the plots with absolute force. In this case, as v_{max} is a muscle specific parameter, the curves also show considerable variation at low activation levels (compare panels a and b), even in the normalized display (panels a1 and b1). Maximum contraction velocity (v_{max}) ranges from 0.7 to 0.1, thus shows a 7-fold variation.

It is important to keep in mind that maximum isometric force (F_{max}) in this plot is at zero velocity, in the middle of the x-axis. In the normalized panels (a1-d1) variation of F_{max} has to decrease with increasing activation level.

4.3 Results

For activation level 1 (panel d1) all force-velocity curves cross the point (0,1), however they have a different slope due to their different v_{max} values. In the absolute force domain (right column, panels a2-d2), the variation is high for all activation levels. The curves at an activation of 1 have a force range at zero velocity of 54 to 197 mN (3.7-fold).

Since there is only sparse data for the lengthening side (negative contraction velocities) the lengthening model is fairly simple and not firmly validated. Whether the observable large variability for the lengthening contractions reflects a physiological phenomenon or merely is an artifact of the simple model type chosen, remains unclear until further experimental data is available.

With respect to the model parameters, variation ranges from 0.23 to 3.99 mm/s for v_0 (17-fold) and from -1.26 to -1.68 mm/s for c_{neg} (1.3-fold).

4 Parameter variation between individual Hill-type muscle models

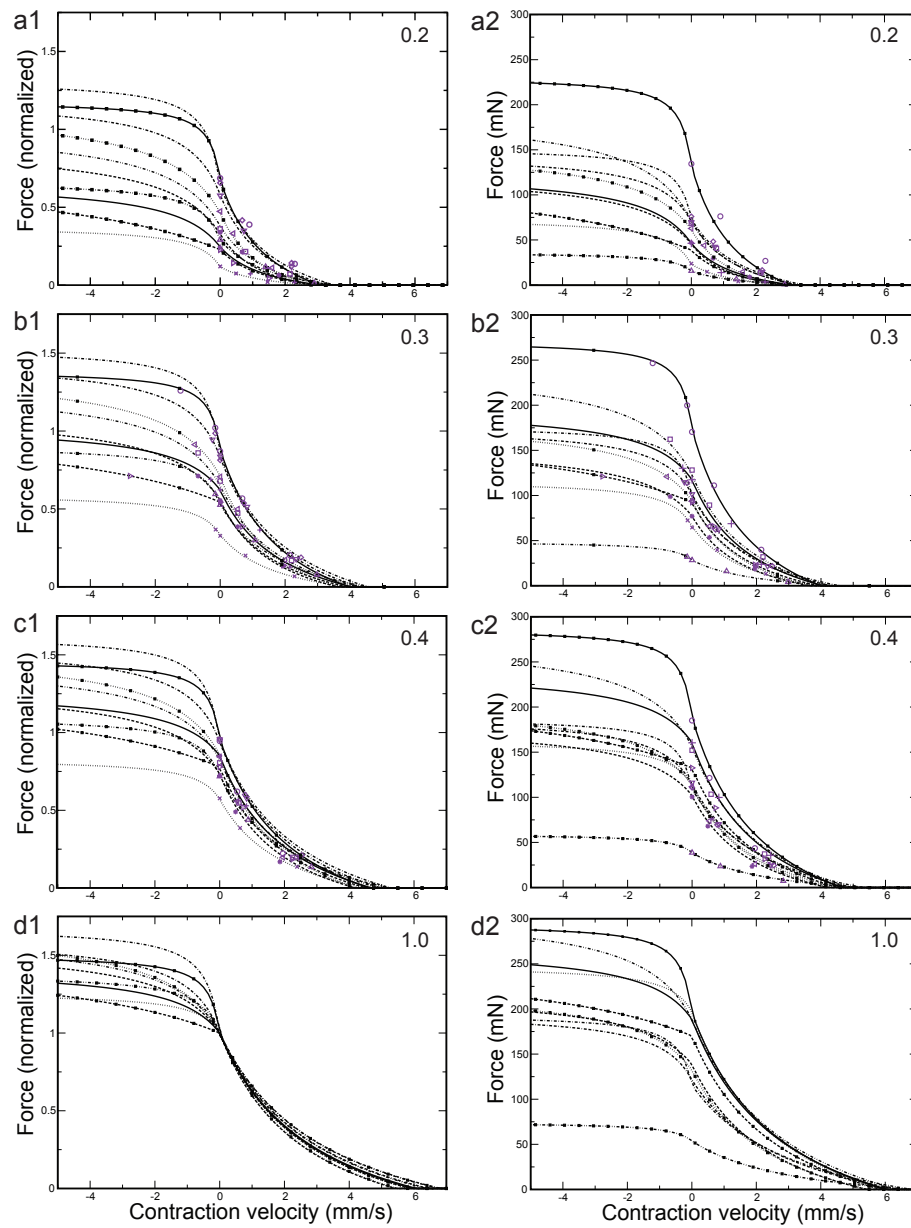


Figure 4.6: Normalized (right column) and unnormalized force (left column) force-velocity curves. In panels a-c they are plotted in together with measured data. Panels d1 and d2 show the prediction of the model for maximum activation. Numbers in right upper corner in each panel are activation level.

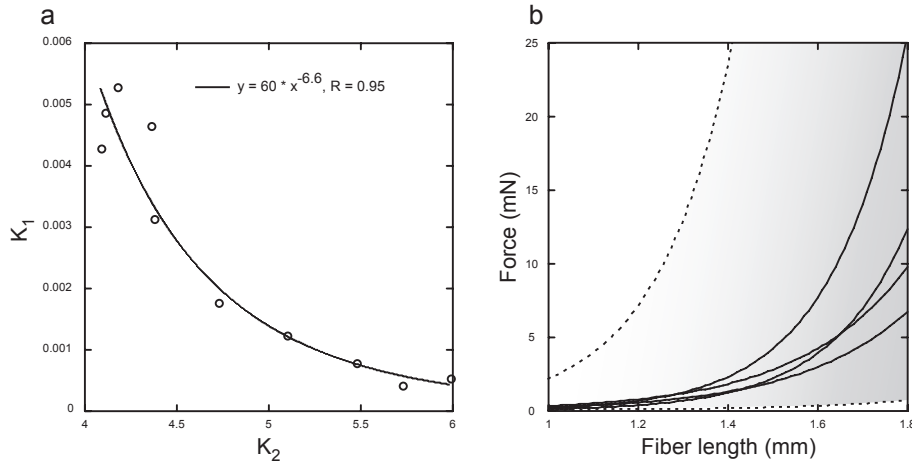


Figure 4.7: Correlation of k_1 and k_2 parameters of the passive force curve (a) and possible explanation (b). Panel a) shows that k_1 and k_2 are well correlated by a negative power function (equation and R value noted on top). b) Solid lines show data from muscles with largest and smallest k_1 and k_2 parameters (see Table 4.1). Upper dashed line shows curve with largest k_1 and k_2 parameters; bottom dashed line shows curve with smallest k_1 and k_2 parameters. The correlation shown in panel a) results in a reduced force-length area coverage, than it would without the correlation (shaded area between the dashed lines).

4.3.6 Parameter correlations

A Spearman rank test for correlation among the 10 parameters (across the 10 muscles) identified two significantly-correlated pairs of parameters k_1 and k_2 , both of passive force curve (section 4.3.1) and parameters B and $curv_{hyp}$ with B from force-activation curve (section 4.3.3) and $curv_{hyp}$ of the force-length curve (section 4.3.4).

4.3.6.1 Parameters k_1 and k_2

Plotting k_1 vs. k_2 shows that these two parameters are very well fit with a power-law relationship, with k_1 decreasing as k_2 increases (Figure 4.7).

The observed correlation of k_1 and k_2 reduces the variability of the passive force curves. The solid lines in Figure 4.7b show the four curves from Figure 4.1 that have the largest and smallest k_1 values and the largest and smallest k_2 values. The upper dashed line is the curve that would result from using the largest k_1 value and largest k_2 value and the lower dashed line is the curve that would result from using the smallest k_1 value and smallest k_2 value.

It is apparent that the actual curves occupy a much smaller area than that

4 Parameter variation between individual Hill-type muscle models

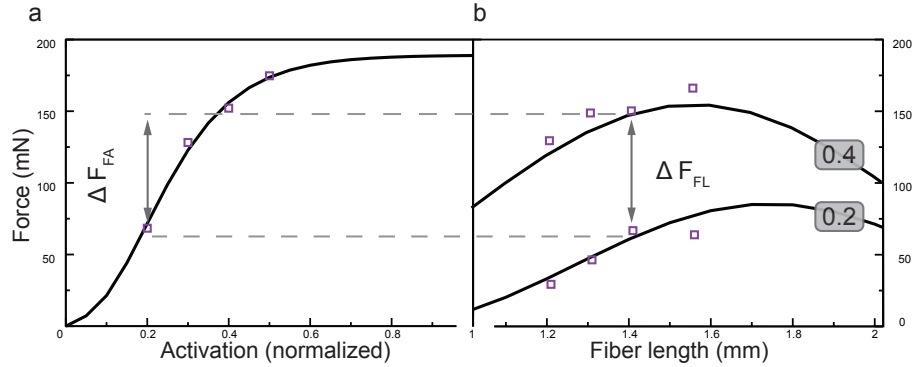


Figure 4.8: Interdependence of force-activation (a) and force-length curve (b). The force difference at positions indicated by the arrows have to match in both curves. This explains why both curves can not be expected to be independent. Numbers on the right hand side of panel b denote activation levels.

bordered by the dashed lines. Consideration of equation 3.1 shows that, at any fiber length, decreasing either k_1 or k_2 will decrease curve amplitude and increasing either k_1 or k_2 will increase curve amplitude. The amplitude of the passive force curve of a muscle with a large k_1 can thus be decreased by decreasing k_2 , and one with a large k_2 by decreasing k_1 . (Similarly, the amplitude of the passive force curve of a muscle with a small k_1 can be increased by increasing k_2 , and one with a small k_2 by increasing k_1 .)

An inverse relationship between k_1 and k_2 , as observed here, thus decreases the effects of changes in either parameter on curve amplitude. The negative correlation thus likely results in better fit accuracy (compared with keeping one of them constant).

4.3.6.2 Parameters B and $curv_{hyp}$

The second correlation, between parameter B and $curv_{hyp}$, likely results from the force-activation and force-length curve sharing data points in their derivation. Figure 4.8a1 shows one muscle's force-activation curve and Figure 4.8a2 shows the muscle's force-length curve at an activation of 0.2 and 0.4.

The data in Figure 4.8b for rest length are the same as the 0.2 and 0.4 activation data in Figure 4.8a, and therefore the difference in the force measurements at the 0.2 and 0.4 activation in Figure 4.8a (arrow) and between the 0.2 and 0.4 activation data points at rest length in Figure 4.8b (1.41 mm, arrow) must be the same. The data in the two plots are used to fit parameters in two different

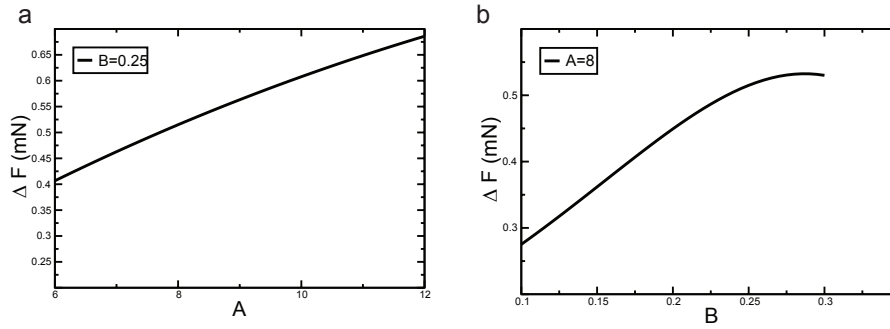


Figure 4.9: Effects of parameters A (panel a) and B (panel b) on the resulting force difference of force-activation curve (compare Figure 4.8). Increase of either parameter causes an increase in force difference in most of the physiological parameter range. Only parameter B will not increase any more for very large B values. Note, that for these investigations the other parameter (for example B in case of investigating effects of varying A) has to be fixed. The value of the fixed parameter value is given on the left top corner of each panel.

equations (Equation 3.25 for the force-activation curve, Equations 3.26-3.28 for the force-length curve). In contrast to the data points, the corresponding force differences in the fit lines do not need to be identical. That is because the other data points the models were fitted to, are not identical. However, particularly given the goodness of the curve fits, the force differences of the curve fits should be also very similar.

Why one could expect a connection between force-activation and the force-length function is explained in Figure 4.8. The crucial point is that the force-length model, is able to predict forces for all activations, and thus somehow needs to contain characteristics of the force-activation curve. In detail, two data points on the force-length curve at rest length (see arrow in Figure 4.8b) must have the same force difference as the corresponding points in the force-activation plot (see arrow in Figure 4.8a). Note, however that the force-length model has to predict these force differences for all physiological muscle fiber lengths, whereas force-activation is only determined for rest length. The force-length model predicts that these force differences are not constant for all muscle lengths, otherwise the force-length curves for different activation levels would simply be scaled copies of each other. The presented model, and of course the data of Guschlbauer et al. (2007), suggest that force-length curve scales and shifts, maybe even changes its overall shape.

These considerations favor an activation sensitive force-length model over the use of a force-activation model (at rest length) for scaling muscle force. How-

4 Parameter variation between individual Hill-type muscle models

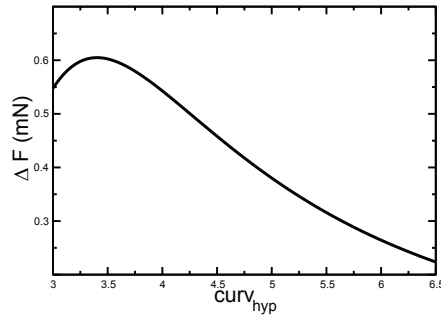


Figure 4.10: Effect of varying the $curv_{hyp}$ parameter to force difference (for rest length). Increasing $curv_{hyp}$ causes a decrease in force difference for most of the physiological parameter range. Only at the very beginning (small $curv_{hyp}$ values) the force difference increases.

ever, the force difference of the force-length model at rest length has to match the force difference of the force-activation curve (dashed lines in Figure 4.8), thus some form of correlation between the parameters of this functions could be expected.

The effects of parameters A , B and $curv_{hyp}$ on the force difference (ΔF) are presented in detail next. Figure 4.9 shows how ΔF changes in response to an increase in the parameter values A and B of the force-activation model (compare equation 3.25). These plots show that, for almost all of the physiologically relevant ranges (Table 4.1) of A and B , the force difference increases (only for very large B values the force difference will eventually decrease slightly, Figure 4.9 right hand side).

Figure 4.10 shows how ΔF reacts to increasing $curv_{hyp}$ (compare eqn. 3.26-3.28). This plot reveals that for the physiologically range of $curv_{hyp}$ values, the force difference primarily decreases (except for very small $curv_{hyp}$ values).

In respect to the interplay of force-length and force-activation model it thus follows that if $curv_{hyp}$ increases, this force difference can be kept constant by *decreasing* parameter A , B or both, and if $curv_{hyp}$ decreases, it can be kept constant by *increasing* parameter A , B or both.

Figure 4.11 correlates parameter A and B with $curv_{hyp}$. Parameter A shows a weaker correlation with $curv_{hyp}$ (panel a) than parameter B (panel b). Parameter A 's weak correlation actually is too weak to be significant in the correlation search performed and is additionally in the wrong direction to maintain the constant force difference. As such, the decrease in parameter B as $curv_{hyp}$ increases must be large enough to compensate both for the changes in $curv_{hyp}$

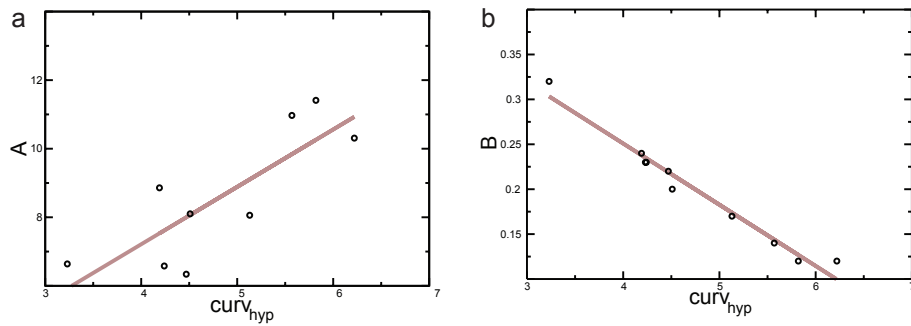


Figure 4.11: Correlations of parameters A , B and $curv_{hyp}$. Parameter A shows only weak correlation with $curv_{hyp}$ (panel a). Its correlation is too weak to be significant. Parameter B is strongly correlated (panel b).

and the associated changes that occur in parameter A .

4.4 Discussion

The protocol for determining all the parameters of the Hill-type muscle model in experiments on single muscles has been used to measure these parameters in 10 muscles and to test for correlations among the parameters. Substantial inter-individual variation have been found in all model parameters and the curves resulting from them. Also two pairs of parameters have been identified that were significantly correlated. Possible bases for these correlations were investigated.

4.4.1 Possible experimental or analysis artifacts

A particular concern in work examining variability is that the observed variation does not arise from actual differences present in the animals, but instead is the result of dissection damage or other experimental artifacts. Several observations, however, support the idea of this variation being a real phenomenon. First, only muscles that showed robust contractions which persisted without substantial force decline ($\leq 20\%$) were used in this work (see section 3.2).

Second, it might be expected that substantial damage, at least, would so much alter muscle characteristics that data from damaged muscles could no longer be well fit by the various functions chosen. However, in all cases the fits were very good (R^2 values routinely ≥ 0.95).

4 Parameter variation between individual Hill-type muscle models

Third, with few exceptions the variations produce a graded series of curves, not the division into healthy and damaged muscles that would be expected, at least for substantial damage. Consistent with this interpretation, muscles that appear to be outliers in one plot, and which might therefore be damaged muscles, are not outliers in other others (e.g., the muscle that gave the top curve in Figure 4.1 is not the muscle that gave the lowest muscle in Figure 4.3b, and neither of these muscles is the one that gave the lowest curve in Figure 4.4a2-c2).

This observation is particularly important between Figure 4.1 and 4.6, which measure passive and active force, because one type of damage that might be expected is loss of muscle fibers during dissection. This would be expected to decrease equally passive and active muscle force. The lack of correlation among these two muscle characteristics thus argues against such loss being the major source for the observed variability. Moreover, since the variability continues to be present in normalized force curves, loss of muscle fibers or similar experimental artifact affecting whole muscle force responses cannot be an explanation for it.

Fourth, the large but graded variation between animals, observed for muscle responses to identical neural driving (Hooper et al., 2006), disagrees with gross muscle damage or similar experimental artifacts.

Taken together, these arguments suggest that the observed inter-animal variation is unlikely an artifact but is truly a property of the muscles investigated.

With respect to the observed correlations, the particularly good correlations shown in Figure 4.7a and 4.11b verify the identifications of the original search among all parameters. A different concern is that the chosen 0.5 α -level was too stringent, and that biologically relevant correlations or correlations inherent to the model structure might have been missed. Figure 4.11a shows one such weak correlation, and searches of all possible combinations of the other parameters showed three other weak correlations, one between the A and B parameters ($R^2 = 0.68$), a second between parameter B and c_{neg} ($R^2 = 0.75$), and a third between $curv_{hyp}$ and c_{neg} ($R^2 = 0.73$). It is impossible from the present data to state if these correlations are real or spurious, particularly for the c_{neg} correlations, inasmuch as c_{neg} is determined from only two data points.

4.4.2 Implications of the observed correlations

One interesting aspect of the $k_1 - k_2$ correlation is its power-law shape, given that the function which k_1 and k_2 are parameters of is an exponential function. It could be that this correlation exists because it is particularly well-suited to limiting amplitude variation of an exponential function.

An important point to make about this correlation, and indeed all the functions in the phenomenological model used here, is that it is not possible to infer biological mechanisms from the types of functions that well model the biological data, or correlations among their parameters. The fact that the passive force-length data are well fit with an exponential function whose two parameters are negatively correlated does not imply that there are two linked biological processes (e.g., levels of two proteins), one represented by k_1 and the other k_2 , whose expression is inversely linked.

The other correlation, between $curv_{hyp}$ and parameter B , is due to an inherent connection between model functions. Having a force-activation curve (measured at rest length) and an activation sensitive force-length curve as components of the same model could be expected to be redundant. However, both are necessary for best modeling results. A good force-activation fit is crucial for F_{max} extrapolation. Data are easy to measure for this curve, since it is based on isometric measurements at rest length. On the other hand, the force-length model is a compromise of simplicity and accuracy. Consequently it would not be beneficial to rely only on force-length modeling. But once F_{max} has been calculated, the force-activation model might be abandoned for further modeling or simulation tasks.

As a matter of fact, the simulations performed in the next section were done without usage of the force-activation curve but the F_{max} value that was used had been calculated using the force-activation model.

4.4.3 Implications of inter-animal variability for neural control and modeling

Muscles are the drivers of movement, and thus the wide variability observed here suggests that, to produce the same movement in different animals, neural input would need to be matched to muscle properties. Although this is undoubtedly true in theory, another possibility is that movement in general, or at least in the stick insect, is not controlled on this level of detail.

4 Parameter variation between individual Hill-type muscle models

Such ‘just-good-enough’ control of movement has indeed been observed in other systems, notably in *Aplysia* feeding movements. These movements are not matched to the type of food being eaten and show great bite-to-bite variability even when eating a single food type (Hooper, 2004; Horn et al., 2004).

Further it is possible that muscle antagonist and limb biomechanics (Hooper et al., 2009) reduce the effects of muscle property variation sufficiently so that these variations do not result in functionally different movements. The consequences could be that for the neural control of actual movements this variation does not need to be concerned (in detail).

With respect to muscle models, however, the large variations reported here suggest that muscles from different animals benefit from individual-specific construction.

5 Simulating and comparing individual Hill-type models

5.1 Introduction

Muscles transform motor neuron firing into force and movement, and hence play a central role in the production of behavior. Muscle properties have therefore been intensively studied, and many models have been developed that predict muscle forces and length changes in response to motor neuron activity. These models typically require measurement of multiple characteristics.

These measurements have generally not all been made on single muscles from single individuals. Instead, one or a few characteristics have been measured from the muscle of interest in several individual animals and other sets of characteristics from other individuals. Each single characteristic is then typically obtained by some way of averaging the collected data. Then all these characteristics were combined to obtain the final model.

This approach has the potential difficulty that none of the mean characteristics could be correct for any individual animal's muscle. This concern increases if the muscles show large inter-individual variation.

Testing whether this issue leads to significant errors requires the ability to measure all muscle model characteristics on an individual-animal basis. The approach how this can be performed, is described in chapter 3. In this chapter models based on individual characteristics are compared with an averaged model (assembled from the 9 muscles investigated).

The individual models result from using parameters specific to each individual extensor muscle and the averaged models from using the mean values for all parameters averaged across the muscles.

One can expect that a good estimation of F_{max} , the maximum force a muscle can produce, would play a large role in the final simulation performance. The effect of using muscle-specific F_{max} values on model performance was also examined. This was done by comparing models using mean values for all param-

5 Simulating and comparing individual Hill-type models

eters except F_{max} , and models using muscle-specific values for all parameters except F_{max} (F_{max} being an overall muscle average value).

Surprisingly, these comparisons showed that, despite F_{max} showing large inter-individual variation, using muscle-specific F_{max} values did not improve model performance. This lack of improvement likely stems from an interaction between F_{max} and other model components.

It could also be shown that inter-individual variation in extensor muscle characteristics is large enough that using across-muscle mean values induces substantial decreases in model performance, suggesting that accurate modeling in this system (and hence possibly other muscles in this and other organisms) will benefit from individual parameter measurement.

5.2 Material and methods

Calculations were performed in GnuOctave on Linux (Ubuntu 9.04, Kernel 2.6.28-15-generic, Intel Core2 T5600). Parameters were optimized using the *leasqr* routine of the *optim* package (version 1.0.12). Normalized root mean squared deviation (NRMSD) values were calculated with custom code.

5.2.1 Simulation conditions and stimulation

Experiments and simulations were performed under both isometric and isotonic conditions. Two different stimulation protocols were used. Fixed frequency stimulations consisted of series of constant frequency pulses. Physiological stimulation consisted of a series of pulses delivered in the same patterns as real extensor motor neuron firing observed during stick insect sideways stepping. Three physiological patterns, all recorded from the same animal were applied (see Hooper et al., 2006). Physiological pattern 1 consisted of a single step, pattern 2 of two sequential steps, and pattern 3 of three sequential steps.

5.2.1.1 Simulation paradigms

A simulation paradigm is referred to as the combination of simulation condition and stimulation pattern. The data set provides three simulation paradigms: isometric contractions with fixed frequency stimulations (IM_{fixed}), isometric contractions with physiological stimulation (IM_{phys}) and isotonic contractions with physiological stimulations (IT_{phys}).

5.2.1.2 Activation dynamics

Many models of activation dynamics can be found in literature, perhaps most prominent those of Zajac and Hatze (Zajac, 1989; Hatze, 1977, 1978). Many of these models are quite complex (e.g., Zakotnik, 2006).

Complex activation is very powerful, but also tends to subsume and thus disguise Hill-type model components. Because the Hill-type model developed here is well-defined and almost fully based on experimental data, it should be maintained in its full form and a distinct separation between it and the activation component of the model should be kept. Therefore a very simple activation transfer function was used, a single-pole first-order low-pass filter. This filter was implemented recursively and had two parameters (recursion coefficients). The recursion equation is:

$$act[n] = a \cdot x[n] + b \cdot act[n - 1], \quad (5.1)$$

where n corresponds to the present, discrete moment in time, $act[n]$ is present muscle activation, $x[n]$ present stimulation input level, $act[n - 1]$ muscle activation at one time step before the present step, and a and b are the recursion coefficients. In a single-pole low-pass filter a and b are related by

$$\begin{aligned} a &= 1 - x \\ b &= x, \end{aligned} \quad (5.2)$$

where x varies between zero and one. Functionally, x determines the amplitude of decay between adjacent samples. x is referred here to as the ‘*filter*’ value. The other component of the activation module is a scaling factor, achieved by multiplying the input signal by a constant. The complete activation dynamics equation is thus

$$act[n] = (1 - filter) \cdot (scaling \cdot x[n] + filter \cdot act[n - 1]). \quad (5.3)$$

Because the square brackets indicate a given position in the time series, the filter response depends on simulation sample rate. Filter time constant independent of sample rate can be calculated from

$$d = \frac{-1}{\ln(x)} \quad (5.4)$$

$$t_{cont} = d \cdot dt, \quad (5.5)$$

where t_{const} is the time constant (the time the output signal needs to decay by $1/e$) in seconds, d is the number of samples this time corresponds to, and dt is the sample rate. A good resource for more details about digital filtering is Boug (2001).

5.2.1.3 Mechanical simulation

Muscle force depends on the equations in the Hill-type model that describe parallel elasticity, series elasticity, force-length, and force-velocity curves.

To understand how these equations interact in generating muscle force and length changes, first consider the two activation-dependent equations, force-length and force-velocity (compare sections 3.3.4 and 3.3.5). The force-length equation is straightforward, and simply gives a force for any activation and muscle length. However, muscles deliver different forces even at the same activation and length as a function of their contraction velocity; with muscle force decreasing as contraction velocity increases. The force-velocity equations describe this relationship. The force-length equation gives the force at a zero contraction velocity (the maximum force the muscle can produce at the muscle's activation level and length), and the force-velocity equations have been derived such that multiplying force-length by force-velocity gives the force the muscle produces at other contraction velocities.

Excluding series elasticity for a moment, for the remaining three model equations it is straightforward to understand how they work together. Force-length, force-velocity and activation equations form a four dimensional 'space' as force, length, activation and velocity are independent from each other. As all equations produce normalized force, their output values can simply be multiplied. This gives the following equation:

$$F_{muscle} = fl(act, l_m) \cdot fv(v_m) + pf(l_m) \quad (5.6)$$

with F_{muscle} being overall (active and passive) muscle force, fl the force resultant from the force-length relationship, fv the force produced by the force-

velocity relationship and pf being the passive force contributed by the parallel elasticity. Note that fl scales with activation, but fv does not. Thus multiplication of fl and fv already produces activation dependent force output. Therefore there is no need to include the force-activation scaling as a separate equation. This model will ‘on its own’ produce the appropriate force changes for varying activation levels.

Hill-type model components can be configured in different ways; most prominent are two configurations which differ in the position of the parallel elastic component (a detailed comparison is given in Siebert et al., 2008). The series elastic component has been placed in series to both, contractile element and parallel elastic element (like in Delp and Loan, 1995). This results in the fact that muscle force will - in the first place - cause a length change in the series elasticity. This change in length will then cause the identical change in force at the opposite end of the spring.

Although in this setup both muscle force and force at the end of the series elastic spring always have to be identical, stiffness of this spring crucially influences muscle force production. This can be understood by keeping in mind that muscle force is both length and velocity dependent. Therefore a weak series elastic spring would for example lead to a decrease in isometric muscle force and would also slow down muscle force build up.

Isometric force is decreased because the muscle shortens much more compared to a stiff series elastic spring, thus producing less force due to the nature of its force-length curve. The muscle is also expected to be slower in its force response because rapid changes in activation would cause rapid internal shortening, as the series elastic spring is comparatively easy to stretch. Rapid shortenings however can only be performed with low muscle force (as defined by the force-velocity curve). Series elastic spring therefore significantly influences muscle force amplitude and muscle force development over time.

Despite its importance, including a series elastic spring makes modeling more complicated. As it influences both length of the contractile element and contraction velocity, it introduces a feedback loop inside the modeling equations. Muscle force now depends on length and rate of length change of the series elastic spring, whereas its own length again, depends on muscle force. Though this interdependence can be solved mathematically, simulation results of models including a series elastic spring are often harder to understand.

5 Simulating and comparing individual Hill-type models

For reasons of flexibility the series elastic spring problem was not solved analytically, but rather its length was approximated using numerical integration. As muscle motion is only one dimensional (either shortening or lengthening) programming the physical simulation is fairly straightforward. Basically only four parameters need to be calculated during each time step: velocity of the contractile element, length of the contractile element, length of series elastic element and force produced by the series elastic component. This was done simply by applying Newton's law of motion ($acceleration = forces/mass$)¹. The mass was approximated with 0.2 mg (and preliminary measurements kindly performed by C. Guschlbauer confirmed that this number is in the correct order of magnitude).

Forces are the sum of contraction forces (by muscle activation), extension forces (via series elasticity stretch) and damping forces. As this model is basically composed of connected springs, it is crucial to include some term of passive damping. In the way the model equations are set up, damping is only present in the force-velocity curve (by reducing muscle force with increasing contraction velocity). But this type of implementation would not be able to prevent the concatenated springs from oscillations if muscle is not activated, therefore a small amount of additional activation independent damping was added (called passive damping). It was chosen just high enough to prevent artificial oscillations. Further to prevent the muscle from pushing if it was shorted by some external force, passive damping was additionally reduced for positive contraction velocities. Passive damping and muscle mass were constant and identical for all muscle simulations. Numerical integration was implemented by second order "improved Euler" as described in Boug (2001).

5.2.1.4 Muscle model configurations

In the course of the performed simulations the performance of four different muscle model configurations have been compared. The idea behind the different configurations was to investigate the influence of three model components in respect to simulation accuracy. These three major model components were activation dynamics, Hill model characteristics and maximum isometric muscle force (F_{max}). Each of these components could be expected to influence simulation results in a different way.

¹Of course the second law of motion should be correctly written as $F = \frac{d}{dt}(mv)$ or $F = m \cdot a$. But to highlight it's function in the calculation of *motion*, it has been re-arranged.

| MM | DP | AD | Hill | F_{max} | Muscle specific config. |
|----|----|----|------|-----------|--------------------------|
| | | ■ | ■ | ■ | Muscle Specific Settings |
| | | | | | Averaged Settings |
| ■ | ■ | | | | Constant Settings |

| MM | DP | AD | Hill | F_{max} | All averaged config. |
|----|----|----|------|-----------|--------------------------|
| | | ■ | ■ | ■ | Muscle Specific Settings |
| | | | | | Averaged Settings |
| ■ | ■ | | | | Constant Settings |

| MM | DP | AD | Hill | F_{max} | Fmax specific config. |
|----|----|----|------|-----------|--------------------------|
| | | ■ | ■ | ■ | Muscle Specific Settings |
| | | | | | Averaged Settings |
| ■ | ■ | | | | Constant Settings |

| MM | DP | AD | Hill | F_{max} | Fmax average config. |
|----|----|----|------|-----------|--------------------------|
| | | ■ | ■ | ■ | Muscle Specific Settings |
| | | | | ■ | Averaged Settings |
| ■ | ■ | | | | Constant Settings |

MM: muscle mass DP: passive damping
AD: activation dynamics Hill: Hill model
 F_{max} : maximum muscle force

Figure 5.1: Overview of the different model configurations used. Each configuration is represented by one of the tables and is assembled by three different settings. Muscle specific settings contain parameters individually optimized for each muscle. Averaged settings contain parameters that are gained by averaging muscle specific parameters over all muscles. Constant settings are immutable for all muscles. Each model is a combination of five parameters sets: The muscle mass (MM), passive damping (DP), activation dynamics (AD), Hill-type model (Hill) and maximum isometric force (F_{max}). Muscle mass and damping were constant for all model configurations.

Activation dynamics was, as described above, made of two parameters (*scaling* and *filter*) which were individually optimized for isometric and isotonic conditions. The process of determining these parameters and the reasoning for separating isometric and isotonic conditions is in detail described in the results section below.

The Hill-type model contains 7 parameters (excluding F_{max}) all acquired for individual muscles. The influence of maximum isometric force was of particular interest, thus F_{max} was extracted from the Hill-type model parameters and used as a separate model component. It was possible to compare simulations with muscle specific F_{max} with simulations using an averaged F_{max} .

5 Simulating and comparing individual Hill-type models

Figure 5.1 summarizes the four different model configurations investigated. In the muscle-specific configuration activation dynamics, Hill-type model parameters and F_{max} were used with muscle specific values. In the all-averaged configuration, the Hill-type model parameters, F_{max} and activation dynamics parameters for all muscles were averaged. However activation dynamics parameters for isometric and isotonic conditions have been averaged separately. In the all-averaged configuration there don't exist nine different models any more, but only a single one, based on the averaged data of the nine muscles. The F_{max} -specific configuration differs only in F_{max} from the all-averaged condition. The averaged F_{max} value used in the all-averaged configuration is replaced by the muscle's specific F_{max} .

The final configuration is called the F_{max} -average configuration. In this case muscle specific activation dynamics and Hill model parameters were used in combination with the averaged F_{max} value. This configuration gives, in direct comparison with the muscle-specific configuration, a good means to evaluate how much error is introduced by using averaged F_{max} . As explained above, for all four conditions muscle mass and passive damping was held constant.

5.2.1.5 Error calculations

Model performance was quantified by calculating the normalized root mean squared deviation (NRMSD) of the force or position traces between simulation and experimental data. In all cases absolute (not normalized) forces were calculated by multiplying normalized force (the intermediate model output) by either mean F_{max} (for the all-averaged and F_{max} -averaged cases) or muscle-specific F_{max} (for muscle-specific and F_{max} -specific cases). Error is expressed as percent error (NRMSD) in all figures and tables.

5.3 Results

5.3.1 Approach outline

One important task of muscle model simulations is to predict the force or movement that would result from a given stimulations pattern. In order to approach this task, two components needed be added to the Hill-type model described in chapter 3. These components are the activation dynamics and the mechanical simulation, both described in detail in the material and methods section. The flow of processing applied is presented in Figure 5.2. Simulation input was a series of unity amplitude square pulses with 1 ms duration. By means of simple threshold detection, events of action potentials from a nerve recording were transferred into unity pulses for later use as simulation input. The top row of Figure 5.2 shows an example of how the physiological pattern looks like as a pulse train.

The pulses were put into the activation dynamics filter system. As explained above, activation dynamics was based on low pass filtering of this input and only had two parameters (*filter* and *scaling*). *Scaling* is actually applied to the input signal, allowing the filter response to be greater than unity. The *filter* parameter controls the time constant of the low pass filter. Figure 5.2, second row shows an example how the impulse response of the filter would differ with large *scaling* and *filter* (top), and small *scaling* and *filter* values (middle). The hypothetical impulse is displayed at the bottom of this panel.

The output of the activation dynamics component is what's called muscle activation level. The second gray box in Figure 5.2 highlights the actual Hill-type model. Inside this model a normalized force value is calculated which depends on activation level, length and contraction velocity of the contractile element. The model consists of seven parameters ($k_1, k_2, k_3, curv_{hyp}, v_{max}, c_0, c_{neg}$) which constrain the model equations (passive force, series elastic spring, force-length, force-velocity) and are specific for each on the nine investigated muscles (muscles A-I).

The Hill-model equations all operate on normalized force, thus force output of the Hill-model is also normalized force. In order to restore absolute force values, normalized force can be multiplied with the maximum isometric force, F_{max} , which is known for each muscle.

5 Simulating and comparing individual Hill-type models

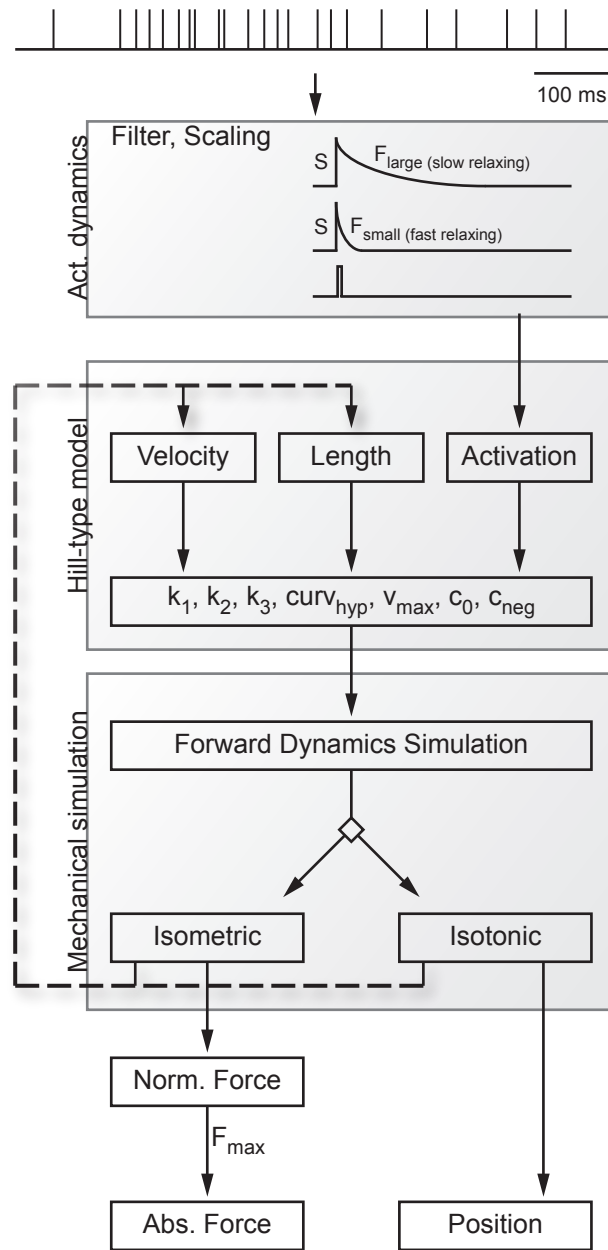


Figure 5.2: A scheme with building blocks of the simulations. Each simulation starts with a pulse pattern (unit amplitude, 1 ms durations). This pulse sequence is fed into the activation dynamics module which converts it into a continuous muscle activation value. This filtering is controlled by two variables, *filter* and *scaling*. The *filter* value controls the time constant of the impulse response, *scaling* is applied to the input before filtering. Then muscle activation is passed to the Hill-model equations. The model used here has 7 parameters ($k_1, k_2, k_3, \text{curv}_{\text{hyp}}, v_{\text{max}}, c_0$ and c_{neg}) and is described in detail in chapter 3. The output of the Hill-model is normalized force. Scaling with the muscle specific F_{max} results in absolute force.

The force calculated by the Hill-type model is an instantaneous force. As explained in materials and methods, the series elastic spring creates a feedback loop that causes the force applied at the spring to feed back onto itself. Therefore, to get realistic force development over time it is crucial to simulate the relative contractions and movements of the model components. This is done in the mechanic simulation component. Here the force produced by the Hill-type model is used to calculate the resulting acceleration of contractile element and series elastic spring. Acceleration is then integrated to get velocities and lengths of these components which consecutively feed back into the force generation.

Two different simulation environments have been investigated in this study. Under isometric conditions, the overall muscle length is constraint to be always constant. This results in the constraint of length of the contractile element plus the length of the series elastic element equalling muscle rest length at any time. The isometric simulation condition enforces this condition by stretching or squeezing the series elastic spring to the length required by this constraint which consequentially pushes or pulls on the contractile element.

The isotonic condition emulates the operation mode of the measurement tool used to gain the isotonic experimental data. Basically the length constraint for this type of simulation is comparable with the behavior of a servo motor. The muscle cannot shorten as long as its force is below a given counter force. This force was set to 40 mN for both measurements and simulations. However even a very high counter force will never stretch the muscle beyond rest length (because of the servo nature of the control). Once the muscle force exceeds the counter force, excess force will be converted into shortening movement and the muscle starts to contract. The observed acceleration will be proportional to the muscle force excess.

All force output is originally calculated as normalized force but for error analysis transformed into absolute forces. This is an important step in order to analyze the effects of changes in F_{max} to simulation quality.

5 Simulating and comparing individual Hill-type models

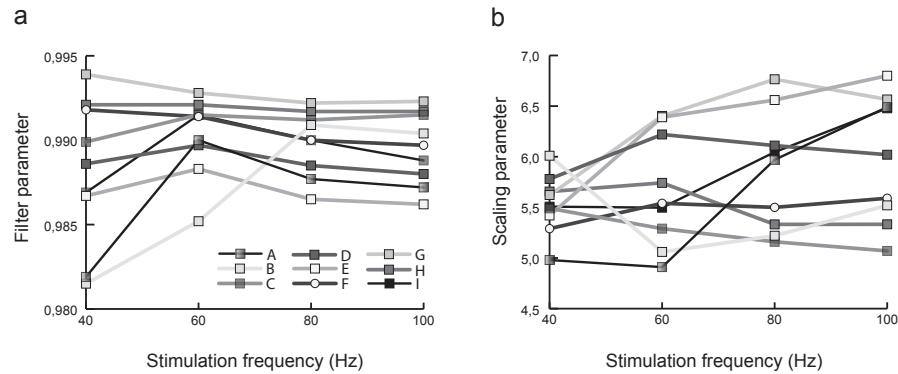


Figure 5.3: Parameters of activation dynamics model plotted over stimulation frequency. For isometric contractions *filter* and *scaling* have been optimized to each stimulation frequency (40, 60, 80 and 100 Hz). Panel a) shows that the *filter* values of different muscles can either rise or fall with increasing frequency. No systematic change with frequency could be observed. Panel b) shows the *scaling* parameter plotted over the same four stimulation frequencies. Again no systematic change of parameter value and stimulation frequency can be observed but variation of the *scaling* parameter is greater than the *filter* parameter.

5.3.2 Activation dynamics

The process of finding appropriate values for the activation dynamics component had two steps, described in this and the next section. The first step was to investigate if activation dynamics parameters show a stimulation frequency dependency.

5.3.2.1 Frequency dependency

Frequency dependent twitch scaling can be a powerful extension for activation dynamics, as for example demonstrated by Zakotnik et al. (2006) (or in more detail described in Zakotnik, 2006). In order to search for frequency dependencies, the optimal parameter values for each muscle and simulation paradigm have been determined. In the set of stimulations there had been four stimulations that were fixed frequency patterns, which were applied to the muscle (40, 60, 80 and 100 Hz). Figure 5.3 shows the optimal parameter values for each of these fixed frequency stimulations of all muscles. In six muscles the *filter* parameter hardly changes at all inside the investigated frequency range. Only muscles B, F and I showed larger variations, especially for 40 Hz (additionally 60 Hz for muscle B). Notably there seems to be no systematic variation in this parameter. Some muscles show a positive correlation of *frequency* and *filter*

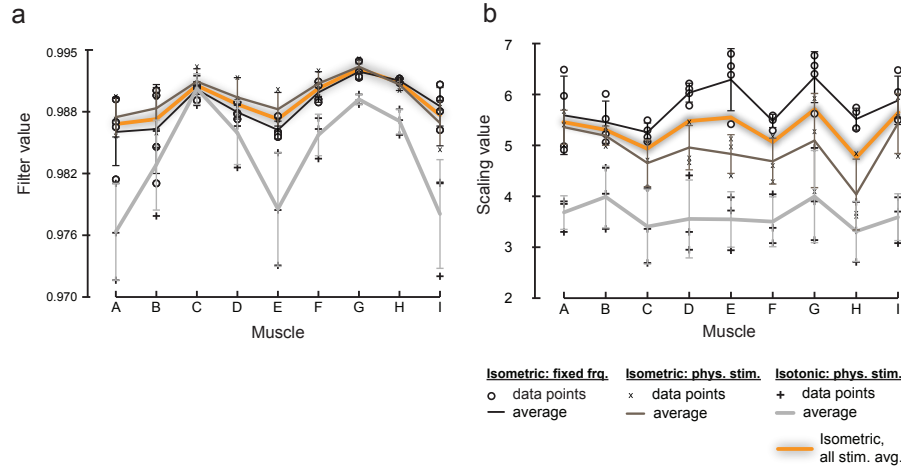


Figure 5.4: Parameters of activation dynamics of all muscles. This figure shows the individual *filter* and *scaling* parameters for IM_{fixed} , IM_{phys} and IT_{phys} stimulations of each muscle. Circles denote the parameter values resulting from the IM_{fixed} paradigm, crosses belong to the IM_{phys} and pluses to the IT_{phys} paradigm. Error bars show the standard deviation. The lines (black, dark gray and light gray) connect the mean parameter values of each paradigm. The shaded line connects the averages of both isometric conditions (IM_{fixed} and IM_{phys}). Both parameters (*filter* and *scaling*) are similar for isometric simulations and can be represented with a muscle specific mean. Parameter values for isotonic simulations are offset. Therefore isotonic simulations were performed using the averages of isotonic parameters only (light gray line).

parameter, others a slightly negative correlation. The *scaling* parameter shows greater variation, muscles A, E, F, G and I tend to increase for higher frequencies whereas the others decrease or barely change at all. It was therefore decided that, at least with this data set, it is impossible to derive a frequency dependency neither of the twitch scale nor of the twitch time constant. That is why the averaged *filter* and *scaling* parameters in the simulations were used. These averages however, were still animal specific.

5.3.2.2 Isometric and isotonic parameters

After precluding a systematic influence of stimulation frequency, it was investigated if it would be possible to use the muscle specific mean values of the activation dynamics parameters to simulate both, isometric and isotonic experiments. Figure 5.4 summarizes all data gained from the optimizations of the activation dynamics parameters for each of the three simulation paradigms (IM_{fixed} , IM_{phys} , IT_{phys}).

5 Simulating and comparing individual Hill-type models

For every muscle (A-I) it displays the optimal parameters for each paradigm (circles, crosses or pluses). Furthermore it contains the paradigm specific mean as a solid line with error bars denoting the standard deviation. This line, though connecting the averages of different muscles, should not imply a hypothetical linkage between muscles, but simply highlight the variation of the averages between the muscles. The fourth, shaded line represents IM_{fixed} and IM_{phys} values averaged to a single value (IM_{all}).

Figure 5.4a shows the optimized *filter* values of the IM_{fixed} , IM_{phys} and IT_{phys} paradigms. Obviously the *filter* values for both isometric paradigms are very similar but *filter* values for the isotonic paradigm is offset (except for muscle C). A paired Students test resulted in p values between 0.001-0.085 for all muscles except muscle C (0.22), with an overall mean p value of 0.07. This supports the idea that for isotonic conditions a different *filter* value is needed than in isometric conditions. On the other hand, the IM_{all} trace in Figure 5.4a proves that averaging the isometric parameters for each animal only introduces a small error, as the IM_{all} line is always close to the individual averages and furthermore the variation in IM_{fixed} and IM_{phys} is fairly small.

In Figure 5.4b the same is shown for the *scaling* parameter. This parameter however responds differently. Both IM paradigms diverge more and as already shown in Figure 5.3b, the variability of the data is generally greater. In particular the IM *scaling* values spread further apart, thus the error introduced by using a common mean is greater. However, IT mean is even more distinguished, clearly offset below the IM data. Statistics result in p values ranging from 0.0005-0.1 (mean 0.036). All muscles except for B and H, had a p value ≤ 0.005 , thus being significantly different from the IM values.

From the data in Figure 5.4 followed that it is necessary to use different activation dynamics parameter values for isometric and isotonic conditions. In the muscle specific model configuration the IM_{all} *filter* and *scaling* values were therefore used for all isometric simulations (fixed frequency and physiological) and *filter* and *scaling* values of IT_{phys} were used for the isotonic conditions.

5.3.3 Performance Overview

Table 5.1 lists the quality of the different muscle specific models. Three different errors are show per muscle: The overall NRMSD of all isometric and isotonic simulations in the first row and in the second and third row the isolated errors for isometric and isotonic conditions. The final column contains the mean error

| | A | B | C | D | E | F | G | H | I | Avg |
|-------------------|----------|----------|----------|----------|----------|----------|----------|----------|----------|--------------|
| NRMSD (IM and IT) | 10.3% | 15.3% | 11.9% | 15.9% | 9.4% | 8.7% | 10.8% | 11.4% | 8.6% | 11.4% |
| NRMSD IM | 10.8% | 16.2% | 8.7% | 9.7% | 8.8% | 7.7% | 10.1% | 11.2% | 8.5% | 10.2% |
| NRMSD IT | 9.1% | 13.3% | 19.2% | 30.4% | 10.8% | 11.2% | 12.5% | 11.6% | 8.9% | 14.1% |

Table 5.1: Simulation performance of all muscles. This table gives an overview of how much error each muscle produced for isometric and isotonic test conditions. The first row shows the combined error of both conditions, second row shows the error of isometric simulations and third row the error of isotonic simulations. All errors are expressed as normalized root mean square deviations (NRMSD) in per-cent. The last column shows the overall mean of each row.

of all muscles. The simulations resulted in overall error values ranging from 9-15% with a mean of slightly above 11%. The minimum error was 7.7% for muscle F, isometric mean.

Maximum error was produced by muscle D under isotonic conditions (30.4%). Further slightly better results for isometric conditions can be observed, compared to isotonic conditions (10% isometric, 14% isotonic).

5.3.4 Mean performance example

To get a more detailed idea of the simulation performance, Figure 5.5 shows the simulation results of muscle H. The decision to show muscle H, was made because its mean error is about the same as the mean error of all muscles together (11.4%, see Table 5.1).

In Figure 5.5a, four isometric force traces are shown in response to fixed frequency stimulations (40, 60, 80 and 100 Hz). Traces measured during experiments are black, simulation results are gray. As can be seen, a typical source of error is an underestimation of the force amplitude. In particular for slow stimulation frequencies (see 40 Hz trace in Figure 5.5a) the model predicts a force rise that is too slow and underestimates the maximum force.

Force rise prediction quality increases significantly for stimulation frequencies above 80 Hz. Note that muscle force frequently shows a slow long lasting increase in force and never really reaches a steady state. This phenomenon can be observed in almost all investigated muscles. The model however is not capable of reproducing this kind of second order phenomenon.

Another common difference between muscle response and simulation results is the size of the force twitches. Muscle force twitches are in general smaller than

5 Simulating and comparing individual Hill-type models

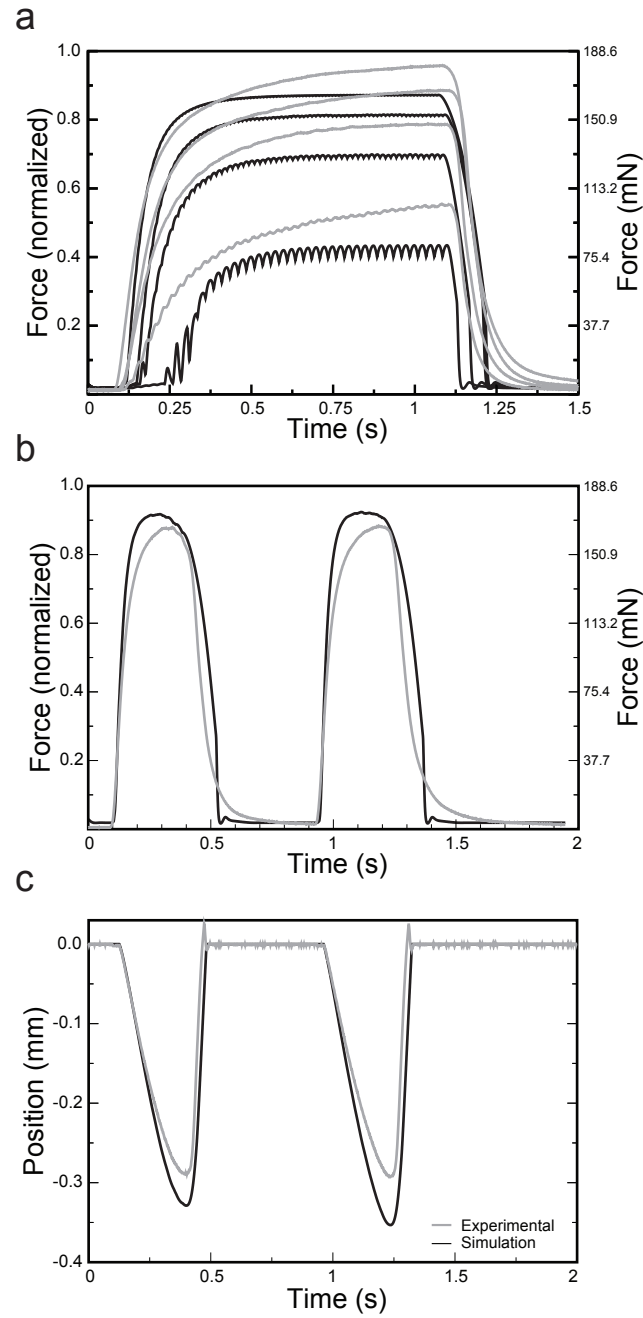


Figure 5.5: Simulation results of a muscle who's error was closest to the mean error of all muscles. This figure shows three different simulation results. In panel a) the muscle and simulation performance of the IM_{fixed} paradigm is shown for 40, 60, 80 and 100Hz. Panel b) shows the the results of the IM_{phys} paradigm, for the physiological stimulation pattern 2. And panel c) contains the results of an isotonic simulation, again with physiological stimulation pattern 2. In all panels gray lines represent experimental results and black lines simulation results.

the twitches produced by the simulation (see Figure 5.5a, 40 and 60 Hz). This difference can be mainly attributed to the simplicity of the activation dynamics filtering. Force summation is extremely sensitive to twitch time constants and although Figure 5.3a shows that twitch time constant does not vary in a specific manner, it is obvious that it does change in a way not understood yet.

Another systematic difference between the model response and the measured forces is present in the relaxation behavior. Typically the muscle relaxes noticeably slower, than the simulation. Force relaxation behavior results from a combination of twitch time constant (and the exact shape of the force decay) and internal passive damping. As you can see in the 80 and 100Hz traces in Figure 5.5a, force decline isn't still quite finished even half a second after the last spike, which is about 5 times longer than a typical single twitch will need for full relaxation. This late part of force relaxation is therefore unlikely a result of continued active force production, but produced by internal damping, which prevents the contractile element from lengthening quickly. This type of damping however, has not been investigated firmly enough to be implemented in the current model. It was thus approximated by a constant value (see material and methods for details).

Figure 5.5b shows how the response of the same muscle and the identical simulation as in Figure 5.5a to physiological stimulation input. The result of physiological stimulation pattern 2 is presented here, because it is the one condition of muscle H, that's error (10.1%) is closest to the mean error of all muscles (11.3%).

For physiological input, both muscle and simulation produce fairly smooth force traces. The simulation in this case slightly overestimates the muscle force, and also rises a bit faster than the real muscle. As far as relaxation is concerned, the same behavior as in Figure 5.5a can be observed. The muscle relaxes considerably slower than the simulation. The simulation actually shows small oscillations at the end of the relaxation phase (e.g. at 0.55 s), which indicates that passive damping in the simulation is rather small. Despite of the relaxation, the simulation reproduces the overall shape of the force trace well, sometimes showing even the same small force oscillations present in the muscle force (e.g. at 0.4 s).

Under the isotonic condition, the muscle is allowed to contract and this shortening is presented as a negative position change in Figure 5.5c. Again the result of the physiological stimulation pattern 2 is shown, as its error value (9.6%) is closest to the mean error.

5 Simulating and comparing individual Hill-type models

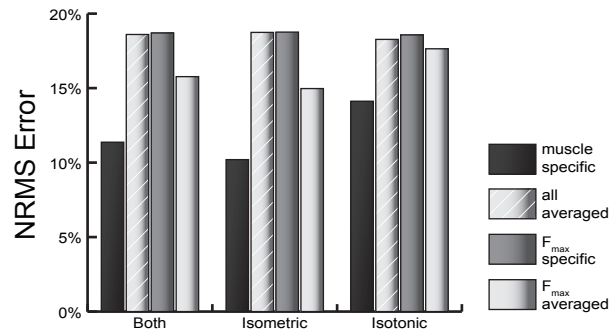


Figure 5.6: Error comparison of different muscle model configurations. This figure shows the error values (NRMSD, in per-cent) of four different muscle model configurations. (See Figure 5.1 and text for details about model configurations.) The muscle specific model proves best both in overall performance as well as in isometric and isotonic performance individually. Using the F_{max} -averaged configuration gives the second best performance. The all-averaged and F_{max} -specific models show the largest error, and both are very similar in their performance.

Typically the isotonic position responses are smoother than the isometric force responses, with the position traces in Figure 5.5c being no exception. Striking at first sight is the position overshoot of the experimental data trace. This can be interpreted as an artifact of the measurement system, and therefore shouldn't be reproduced by the model. In respect to the shape of the contraction, even the mean-quality muscle simulation presented in Figure 5.5c) nicely reproduces the time course of the contraction, only the peak amplitude was slightly overestimated. Also the passive return to the rest position though a bit late in the model, was precisely in parallel to the real muscle relaxation.

5.3.5 Model configuration comparison

The approach of generating muscle specific models offers the unique opportunity of studying the effects of using averaged parameters during modeling. In order to investigate how the model responses change by the introduction of averaged parameter values four different model configurations (see Figure 5.1) were set up and the generated errors as well as the shape of the produced force and position traces were compared. Figure 5.6 shows three error values of all four configurations. The first bar group displays the overall error, which is the error of all isometric and isotonic contraction types. The middle bar group shows the error of isometric contractions, the last group the error of isotonic contractions.

As expected, muscle specific modeling produces the smallest error, not only over all, but also in any other group. The average error of the muscle-specific configuration is 11.4%, the one of F_{max} -averaged is 15.8%, F_{max} -specific and all-averaged configurations are almost identical (18.7% and 18.6%). The F_{max} -averaged configuration is the second best in this comparison. Its NRMS error is in all three groups about 4% higher, than the error of the muscle specific configuration (which corresponds to an almost 30% increase in error compared to the muscle specific error value). Surprisingly, the error values of the other two configurations are very similar, in all three groups their error is about 18% (corresponding to a 40% increase compared to the muscle-specific configuration error).

One actually might expect the results of the F_{max} -specific configuration to be better than the ones of the all-averaged configuration, however the opposite proves true. The all-averaged configuration was actually slightly better than the combination of averaged Hill-model with muscle specific F_{max} values. This can be understood by envisioning that two independent processes influence the error in these cases. Replacing the muscle specific F_{max} with the averaged F_{max} ($F_{max\emptyset}$) usually increases the simulation error, but the increase can be ascribed either to an over-estimation *or* to an under-estimation of position or force.

The same holds for replacing the muscle specific Hill-model with an averaged model. The averaged model could also increase the error either by over or under estimation of force. Keeping this in mind, it becomes clear that the result of combining these two sources of error is at least unpredictable, because both errors have the potential to partially cancel out each other. (Actually the effects of a modified F_{max} to the error are linear, whereas the effects of changing Hill-model parameters are likely non-linear, thus the error can potentially be more sensitive to changes in these parameters.)

In case of a muscle with a weak F_{max} introduction of the averaged Hill-model could for example cause this specific muscle to become even weaker. As Hill-model parameters and F_{max} are independent an uncorrelated (see chapter 4) a muscle with weak F_{max} can very well have a ‘strong’ Hill-model. Thus there is no reason to expect the averaged Hill-model to be stronger than the one of a muscle with small F_{max} . Continuing this example, the replacement of the muscle specific Hill-model with the averaged model can cause the error to increase by a sudden underestimation of muscle force. If the muscle specific F_{max} is now additionally replaced by $F_{max\emptyset}$, the error will most likely decrease,

5 Simulating and comparing individual Hill-type models

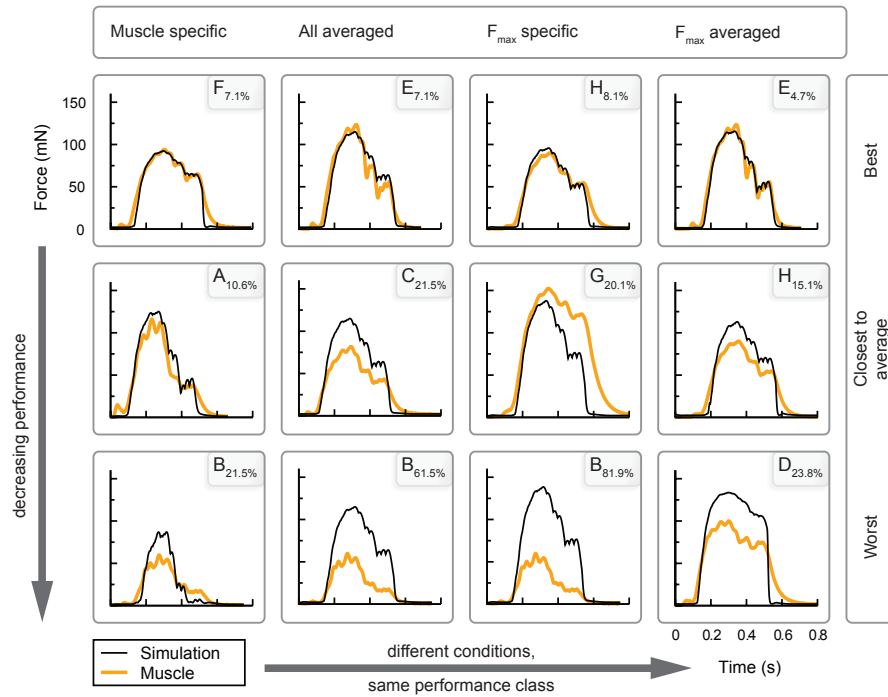


Figure 5.7: Exemplary contractions. This figure matrix contains 12 isometric contractions, provoked by the physiological simulation pattern 1. Each column contains one of the four model configurations. In the first row the best performing contraction of each condition is shown. The second row contains the contraction which is closest to the mean error of all muscles and in the third row the worst performing muscle is selected. Thus reading the figure column-wise, gives an idea of how much variation there is inside a single model configuration. Reading it left to right inside a row, compares different configurations at the same performance class (best, mean, worst). In all panels gray lines represent experimental results and black lines simulation results.

because muscle specific F_{max} of a weak muscle is almost certainly smaller than $F_{max\emptyset}$. In the data set investigated here were four muscles (A, B, D, I) where the combination of averaged Hill-model and muscle specific F_{max} resulted in an increased error compared to the all-averaged configuration. In case of the other five muscles (C, E, F, G, H), the F_{max} -specific configuration showed less error than the all-averaged configuration; but summing all errors makes error of the all-averaged configuration slightly smaller than the error of the F_{max} -specific configuration.

5.3.6 Best, mean, worst performance comparison

Although comparing errors is valuable, a different quality of information can be gained by comparing the actual force traces produced. Unfortunately reproducing all results of all muscles under all conditions and model configurations is unfeasible, thus an overview is given of only the best, the mean and the worst performing muscles and model configurations. Figure 5.7 therefore shows 12 exemplary results of the isometric physiological stimulation pattern 1. Each column contains the results of one model configuration. The first row shows the best performing muscle of each configuration, the second row shows the muscle that is closest to the overall mean and the third row shows the worst performing muscle. Therefore looking at the graphs in one column gives an idea of the variation in performance of any model configuration. On the other hand, the influence of different model configurations is accentuated by comparing the graphs row-wise.

The selected muscle and the corresponding error value are noted in the upper right corner of each graph. From looking at the first column it gets clear, that for the muscle specific model configuration the main sources of error are over estimation of force and a lack of slowness, in particular when relaxing.

The effects of introducing the averaged Hill-type model can be best studied in the third, F_{max} -specific configuration, column. Beside obvious scaling problems, the averaged Hill-type model tends to relax slightly quicker than the presented muscle specific models. Also note that the F_{max} -specific configuration is the only one where significant under estimation of force occurred.

The second column shows that the simulation response is always identical, as it should be because there is only a single, identical model for the all-averaged configuration. The all-averaged model produces a reasonable force profile which reflects the major characteristics of the real contractions. The force traces show the typical three ‘steps’, with the first peak being the strongest and the following two decreasing sequentially. The overall amplitude and the relative scaling of the force steps however are not correctly reproduced by the all-averaged model. Note that column three shows, that including F_{max} doesn’t solve the scaling problem of the all-averaged configuration, for reasons explained earlier.

5 *Simulating and comparing individual Hill-type models*

Using averaged F_{max} with a muscle specific Hill-model in column four, isn't actually as bad as one might expect. The muscle specific model and activation dynamics create force traces that even in the worst case reflect the general characteristics of the real muscle force. Sure enough, force level is offset in these cases, but this offset is only approximately 25 mN in the worst case (muscle D).

5.4 Discussion

The presented work first explains in detail how measured muscle properties were used to form a Hill-type muscle model, then it compares the results of biomechanical simulations of different muscle models. It was driven by the question how the compilation of data from different muscles effects the performance of the model. Therefore four different model types were compared, varying in their composition of individual versus averaged model components. Furthermore a simulation environment has been developed, which provides isometric and isotonic simulation conditions.

5.4.1 Performance of the Hill-type model

This is the first time that a Hill-type model of a stick insect muscle, almost exclusively based on measured muscle properties, has been built for individual muscles. Optimization of the model output to reference data was applied only to the two activation dynamics parameters, but not to parameters of the Hill-type model itself. This unusual approach offers a number of interesting insights into muscle modeling and also into muscle physiology. But the downside of this "forward modeling" approach is a limited model precision, compared to models where all or most parameters were optimized to the resulting force or movement traces.

Additionally, the extensive testing performed here, including fixed and physiological frequency stimulations as well as isometric and isotonic simulation conditions, has not been found anywhere in literature (compare also Houdijk et al., 2006).

It is important to keep these particularities in mind when evaluating model performance or discussing shortcomings and error values.

5.4.2 Activation dynamics

Activation dynamics is an important aspect for all Hill-type models. But it is exceedingly important for models excluding series elasticity and purely operating under isometric conditions. Thus, a lot of expertise has been put into powerful muscle activation models in the past (compare for example Hatze, 1978; Chou and Hannaford, 1992; Happee, 1994; Bobet and Stein, 1998; Zajac, 1989; Brown and Loeb, 2000a; Zakotnik, 2006). However, in this work none of the higher order models is used, although they were tested. Two aspects argue against the use of higher order activation dynamics.

First, substantial low pass filtering is produced by the series elastic component, which basically prevents arbitrarily high force changes. Thus, the additional complexity of higher order filters, did not improve the filtering accordingly.

From the vantage point of modeling, an even more important concern was the disguise of modeling issues by a complex activation dynamics model. Zakotnik (2006) has shown that activation dynamics in cooperation with activation dependent twitch scaling can (under certain conditions) replace most model properties (except passive damping and parallel elasticity). This poses a problem for this work as all model parameters, except the activation dynamics parameters, have been determined experimentally. Thus, using complex activation dynamics would conceptually favor ‘black box’ optimization results over measured data. Therefore the decision was made to use a simple, easily understandable, first order low pass filter for activation dynamics. Although it can almost certainly be assumed that this activation dynamics model is oversimplified, it reduces model complexity and therefore eases interpretation of modeling results. Further on, certain problems often associated with first order activation dynamics (like immediate force responses) happen to be attenuated by the inclusion of the series elastic component.

Although a rather simple activation dynamics model was used, dependencies of its parameters on activation level have been investigated (see Figure 5.3). But in contrast with the $c(f)$ relationship proposed by Zakotnik (2006) no systematic influence of stimulation frequency could be found, neither on twitch scale nor on twitch time constant. Not to say that twitch response is assumed to be invariable for stick insect extensor muscle. Moreover, in this case twitch deformation seems to be more complex. Potential supplementary candidates for twitch response alteration could be muscle length, contraction velocity, force, maybe direction of contraction, and/or history of any or all of these parameters.

5 Simulating and comparing individual Hill-type models

Length, velocity, force and direction were tested during model development, but given the sparse data set and lacking an accurate expectation none turned out promising enough to be investigated any further.

5.4.3 Isometric and isotonic contractions

Isometric contractions, especially the IM_{fixed} ones, show visible differences between simulation and reference data. The quality of the IM_{fixed} simulations is comparable to other models having experimentally pre-defined characteristics (like Yu et al., 1999 or Cole et al., 1996).

Typically, these models have not been challenged the way done here, including multiple physiological isometric and isotonic stimulations and reference data. However, if physiological conditions were important (like in Sandercock and Heckman, 1997) typically larger differences between model and reference data result.

The fact that isotonic simulations were performed with different activation dynamics parameters underlines the non-triviality of Hill-type models operating under all conditions sufficiently well. The necessity of adapting activation dynamics parameters for isotonic contractions can be explained by the requirement of the model to incorporate a new experimental situation. Under isometric conditions the measurement device and all connected gear is kept motionless. Thus, data of isometric experiments should not contain artifacts due to inertia of the measurement system, which cannot be alleged for isotonic conditions. Here additional errors can be introduced like, friction, gear slag and inertia of the lever arm.

In respect to these differences, it should not be taken for granted that the model performs almost equally well under all three conditions. This performance suggests that a reasonable model structure was chosen and that functions and the arrangement of components were basically sensible.

However, one obvious model improvement can be observed in Figure 5.5a. In most of the 10 muscles investigated, force keeps on increasing during fixed frequency stimulation. By comparing model and measured force traces it becomes clear that the model cannot reproduce this slow process of force accumulation. The origin of the continuing force increase is unclear at present, but the following influences can be involved:

The stimulation was designed to induce action potentials in the axons of all three motor neurons innervating the extensor muscle, namely fast extensor

tibiae (FETi), slow extensor tibiae (SETi), and common inhibitor (CI). The properties of the individual motor units are hard to investigate in isolation for this muscle as, for practical reasons, it is hard to stimulate the different fibers individually. In the stick insect this would require intracellular stimulation, in other systems, like the locust (*Locusta migratoria*), SETi can be exclusively stimulated extracellularly. In response to stimulation of the locust middle leg SETi motoneuron, force build-up until saturation, can take several seconds in the extensor tibiae (*Locusta migratoria*; Klein, 2009). Depending on the stimulation frequency, it can take even more than 10 seconds (Guschlbauer et al. (in prep.)).

The slow muscle fibers are a probable candidate for causing the continuous slow rise in force. Other alternatives could be facilitation or, less likely though, neuro-modulation by octopaminergic DUM neurons (Hooper et al., 2007; Weiler et al., 2005). In a more hypothetical consideration the force increase could be attributed to the passive damping component, which properties are still only superficially understood. The passive damping component can explain most viscose properties of the contractile element. During passive stretch this component can explain the creeping, slow decrease in force by gradually permitting the lengthening of the contractile element, which in turn, by shortening of the series elasticity, causes the force to decrease. The same mechanism could explain the slow force increase during active, isometric contractions. In this case, the damping would antagonize the shortening of the contractile element, and any decrease in damping would effect a stretch in the series elasticity, thus an increase in force. Once the properties of this damping are better understood, it would be a valuable addition to the model.

Another weak point of the model, which is supposably of more relevance for the actual behavior, is muscle relaxation. In Figure 5.5b, the relaxation of the simulation has a different quality than the muscle. Although both traces (model and muscle) keep staying close to each other, they differ slightly in shape. The muscle relaxation shows the typical exponential decline (Hooper et al., 2007), whereas force of the model drops more rapidly. Tuning relaxation behavior of this model is hard, as it almost completely depends on passive components (passive force, series elasticity and last but not least passive damping). The only parameter to adjust freely is passive damping, but little is known about the details of this property. Furthermore, as passive damping is constant throughout all simulations, it represents a strong compromise and needs to produce acceptable results under isometric and isotonic conditions.

5 *Simulating and comparing individual Hill-type models*

Improved passive damping would also enable the model to generate realistic, dynamic passive force responses (compare Figure 3.1) - a type of response the current model does not reproduce well.

As the dynamic passive force is substantially larger than static passive force, it is likely to become crucially important for the simulation of antagonistic muscles.

5.4.4 SE compensation for the force-length curve

Modeling often has more benefits than a prediction or verification of data. Usually the process of modeling deepens the understanding of how processes interact and highlight where a linkage of data or concepts is missing.

During the plenty of discussions and explanations the conviction emerged that for the topology of model components used here, the force-length curve needs to be corrected for the length of the series elastic spring. This model is unique in its individuality, thus it is possible to describe the force-length curve and the series elastic spring for each muscle.

The force-length characteristic has been measured over the whole muscle length (which is in case of this muscle commutable with fiber length) but in the classical Hill-type model it is attributed to the contractile element, exclusively. Zajac (1989) has already described the problem that elastic elements (a tendon in his example), which are placed in series to the contractile system, would result in a distortion of the whole muscle force-length curve. In the model described here, no tendon is modeled explicitly, as arthropod apodemes can be expected to be stiff enough to not affect muscle length (Full et al., 1998). However, the model includes a series elastic component, representing all elastic structures in series of the contractile system. Therefore the issue of force-length curve distortion is valid for the model presented here, too.

Due to the high stiffness of the series elastic spring (compare for example Figure 3.7) its influence on the force-length curve was initially neglected. From Figure 3.7 one can derive that L_{se} is at most 0.15mm at 200 mN, which is the maximum force that was produced by any muscle (dropping rapidly for decreasing forces). Thus, the length error introduced by the series elastic spring is approximately 10% at rest length (and 200 mN active force), decreasing quickly with smaller forces (recall that the average active muscle force was 161 mN). So for reasons of simplicity and comparability the simulations presented in this chapter have been performed without the series elastic spring compensation.

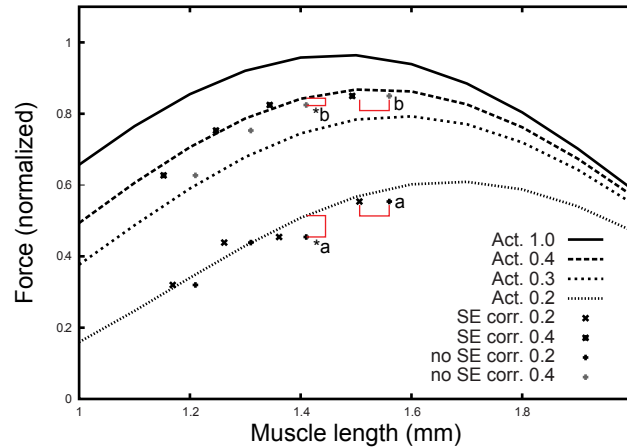


Figure 5.8: Effect of series elasticity compensation on force-length curve. This figure shows the data points of the uncompensated force-length measurements (crosses) in conjunction with the SE-compensated data points (plus symbols) and model fits to these (lines). Labels “a” and “b” highlight the horizontal distance of compensated and uncompensated data points, which increases with (increasing) force. Labels “*a” and “*b” in turn punctuate the vertical distance of the uncompensated data points to the model. Their distance decreases for increasing force level.

Nevertheless, detailed analysis of the model raises the concern that it might be conceptually spurious to use the whole muscle force-length curve as representative of the contractile elements force-length curve without SE length compensation. For this reason and to further evaluate the error introduced by this proceeding the reference muscle (H) was additionally modeled and its contractions simulated with appropriate SE length compensation.

In Figure 5.8 the effects of applying series elasticity length compensation to the whole muscle force-length curve are displayed. As the measured data points contain an additional length (length of the series elastic component), they shift towards smaller muscle lengths after the length compensation. Thus, Figure 5.8 shows both: original and compensated data points. In addition the model fit to the compensated data points is shown. To underline the influence of the length compensation, the horizontal and vertical shift is pointed out with the lines *a*, *b*, **a* and **b*. Lines *a* and *b* have identical dimensions to support recognizing that x-shift of the data increases with increasing force. Lines **a* and **b* are resized to match the distance of the original (uncompensated) data point to the model. These lines show that the amount of additional force introduced by the length compensation reduces with increasing force.

In Figure 5.9 simulation results of muscle H are compared, with an without

5 *Simulating and comparing individual Hill-type models*

series elasticity length compensation. The black lines represent the uncompensated model, the brighter ones the model with compensated force-length curve. It is obvious that the greatest differences are for fixed frequency stimulations (the most unnatural ones, by the way). Physiological stimulations, either isometric or isotonic are almost identical for both models.

Figure 5.10 quantifies the differences in error between both models. Obviously the 40 Hz isometric stimulations differ most (by little less than 10% in error). For all other conditions the difference in error is about 1-2%.

These results indicate that, although it might be a conceptual kink, using whole muscle force-length curve as approximation for the contractile elements force-length curve, it does not introduce substantial error. Which, of course, can only be claimed for the muscle investigated here, as the effect is highly sensitive to the stiffness of the series elasticity.

In literature this problem is hardly addressed, interestingly. Usually Hill-type model parameters are determined in one of the following ways: Either the whole model is optimized to a specific motor task output (like force, torque, position or joint angle) or the muscle characteristics are measured individually and finally combined into the model. The first approach seems to be more popular as the demands are mostly computational, not experimental. Usually this approach can produce muscle models non-invasively just by fitting all model parameters simultaneously to an existing data set (like arm or leg movement). In this case, the issue discussed above is nonexistent because force-length model parameters are simply adjusted to best reproduce the reference task.

However, sometimes the approach of measuring muscle characteristics directly is applied. For models designed that way, the question arises if it is necessary to compensate the measured force-length curve for possible portions of series elastic length. But unfortunately, no references have been found where it became clear that the authors were aware of this problem. In Delp and Loan (1995) and Brown and Loeb (2000b) for example, no compensation of SE length is mentioned, although their model explicitly contains a series elastic element. In Yu et al. (1999) it remains unclear if any compensation has been applied. The normalization of the force-length curve does certainly not resolve this issue. Similar uncertainty of force-length curve treatment can be found in Rosen et al. (1999) or Meijer et al. (1998). The issue is, however, well represented in more theoretical modeling articles like Zajac (1989) or Winters (1990). The latter points out explicitly that whole muscle force-length curves are not identical with contractile element force-length curves.

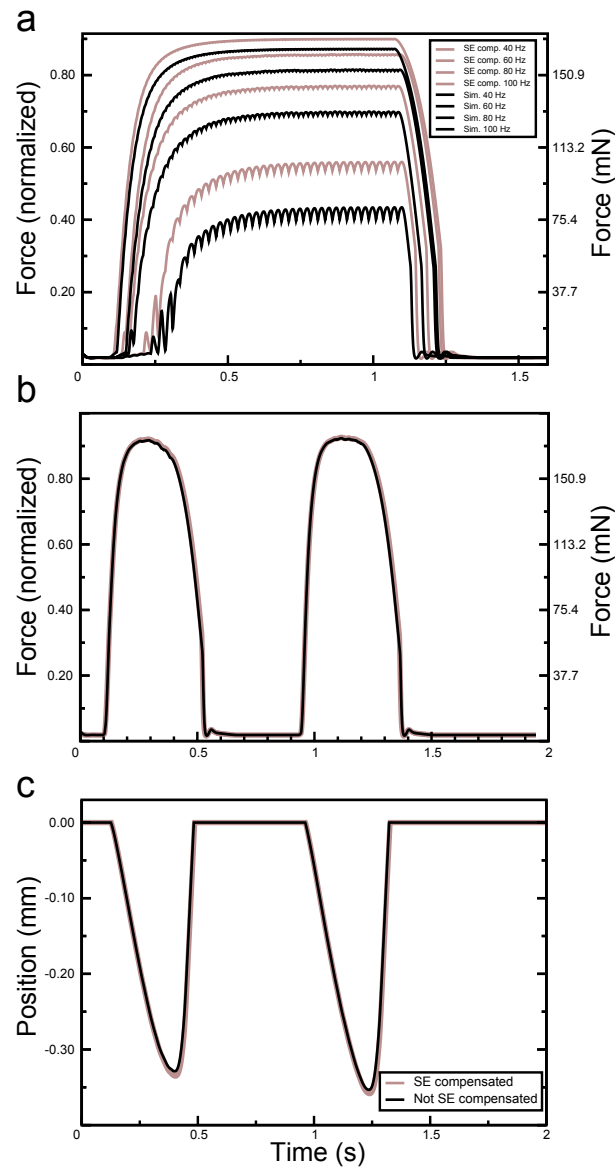


Figure 5.9: Simulation results of the SE-compensated model. Contractions of muscle H (same as in Figure 5.5) with a force-length curve compensated for series elasticity length was simulated. In each panel, darker traces represent the uncompensated model, lighter ones the SE-compensated model. In panel a) SE compensation causes higher force output of the model, as could be expected by theory (compare Fig. 5.8). Note however, that force increase diminishes quickly with increasing force. In panels b) and c) there is virtually no difference any more between both models. The SE-compensated model produces slightly more force, and thus (in panel c) contracts a bit further, but both are actually almost indistinguishable.

5.4.5 Performance of the different model configurations

The comparison of different model configuration revealed that about 40% improvement can be achieved by using muscle specific parameters instead of averaged ones. Furthermore, it turned out that the F_{max} specific configuration performs worse than the all-averaged configuration. An implication of this finding could be that particular care should be taken if averaged and specific data is combined in a single model. At least in the case presented here, it is preferable not to combine the averaged Hill-model kernel with muscle specific refinements (like F_{max}). However, this effect is related to the prediction of muscle specific data. More precise, muscle H's F_{max} -specific model is inferior in predicting muscle H's reference data (compared to the all-averaged model), but it has not been investigated how good or bad this configuration reproduces random muscle data. The question which type of model would best reproduce a random extensor muscle, could guide future work in this area. Further outlooks include the improvement of passive properties in particular damping and the associated viscous properties, as well as the inclusion of history dependent effects, which are known to be prominent in many muscles, including this one (Rassier and Herzog, 2004; Guschlbauer, 2009).

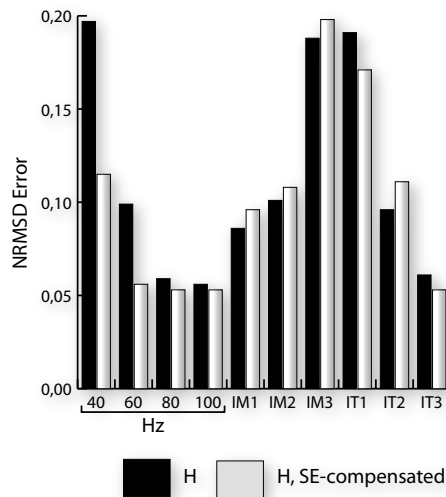


Figure 5.10: Comparing the error of the SE-length compensated model with uncompensated one. Displayed are all simulation conditions of muscle H (IM and IT shortcuts correspond to the isometric and isotonic simulation configurations with physiological stimulation patterns). Note that there is no obvious, systematic error reduction gained by SE length compensation.

6 Closure remarks

Although this work focuses on muscle modeling, it rose from a background of neuro-mechanical simulation. The idea to gain new insights into the complex field of motion generation and control had been a primary driving force throughout this work. A muscle model, at least a Hill-type model, has no particular value of its own - it is made for being used inside a simulation, eventually.

The type of model described and evaluated here is based on the strategy of «forward engineering», meaning that all but three parameters of this model are based on experimental data. This procedure puts a high burden on the general model architecture. A model is a «model» because it simplifies reality thus it is inherently imperfect (Brown and Loeb, 2000b). Constraining many model parameters by experimental values distinctly reveals shortcomings and simplifications of the model.

This approach is not chosen frequently, for at least two reasons: First, the required experiments (and dissections) are simply not possible in many systems, for ethical or physiological reasons. Second, the model performance is supposed to be better the more parameters can be optimized to the output of interest. For example, studies investigating human movements (van Soest et al., 1993; Pandy, 2001; Barrett et al., 2002; Thelen et al., 2003) usually optimize the whole model to best reproduce the desired output.

The approach of «forward engineering» a Hill-type model with this level of complexity has several issues. First of all, it is a very demanding task. Muscle physiology has to be understood well enough to perform the experiments reliably. Enough data need to be measured for each of the model curves, such that it is possible to get an impression of the general shape of the curve. Furthermore, the dependencies between curves and parameters have to be uncovered and need to be described by model curves.

Whenever muscles are investigated in more detail, additional dependencies of the classic Hill-type model curves seem to appear, like the length-dependent coupling of activation and velocity investigated by Shue and Crago (1998) or dependence of maximum shortening velocity on activation (Chow and Darling, 1999). And even more, fundamental assumptions of the Hill-type model can

6 Closure remarks

be questioned such as the uniqueness of force-velocity relationship (Katz, 1939; Joyce and Rack, 1969; van Ingen Schenau et al., 1988), or the «yielding» effect (Joyce et al., 1969) as well as the purely conceptional entities of series elasticity and activation level. However, biophysically oriented modeling approaches, like the distribution moment (DM) model (Zahalak, 1981, 1986; Zahalak and Ma, 1990), are significantly more complex and its parameters are fairly hard to estimate.

However, a lot is learned about muscle properties and its modeling by going this way. The idea to develop this model inspired new experiments and plenty of valuable discussions. Working through the complexities of muscle force production also means expunging the frequent misconception of motion being equivalent to muscle stimulation frequency (compare also Thuma et al., 2003). In this respect, modeling is always beneficial; even if the model would not meet all expectations, the experience gained by its creation is undoubtedly valuable.

6.1 Outlook

The field of neuro-mechanical simulation has been evolving constantly in the past years. Software tools have improved and today hardware acceleration enhances not only computer games, but also this particular type of simulation. In the long run, this work, its results as well as the expertise and experience gained during the modeling and simulation development, should result in an improved neuro-mechanical simulation of the stick insect. A powerful simulation framework, which has already been developed during the initial period of this work, is already awaiting service.

Abbreviations

| | |
|--------------------|--|
| A, B | parameters in rest length force-activation curve |
| A_{act} | maximum amplitude of force-length curves |
| act | muscle activation |
| c_{neg} | curvature of Hill hyperbola for lengthening contractions |
| c_{pos} | curvature of Hill hyperbola for shortening contraction |
| $curv_{hyp}$ | curvature of hyperbola relating $freq_{act}$ and act |
| ΔL | length change after force step |
| F | force |
| F_{max} | maximum isometric force at rest length |
| $F_{max\emptyset}$ | averaged isometric force at rest length (mean of all muscles) |
| $freq_{act}$ | frequency parameter on the force-length model |
| k_1, k_2 | parallel elasticity model constants |
| k_3 | passive steady-state force length |
| k_4, k_5 | constants used in fits to Guschlbauer et al. 2007 |
| SE | series elasticity |
| CE | contractile element |
| v | velocity of muscle shortening |
| v_0 | equivalent of v_{max} , but a constant, in Hill hyperbola for lengthening contractions |
| v_{max} | maximum velocity of muscle shortening (at 0 force) |
| $v_{max \infty}$ | v_{max} at an activation of infinity |
| $v_{max(act=1)}$ | v_{max} at an activation of 1 |

Literaturverzeichnis

- Akay T, Haehn S, Schmitz J, and Büschges A. Signals from load sensors underlie interjoint coordination during stepping movements of the stick insect leg. *Journal of Neurophysiology*, 2004.
- Alexander R. M. Modelling approaches in biomechanics. *Philos Trans R Soc Lond B Biol Sci*, 358(1437):1429–1435, Sep 2003.
- Anthony C. M. Mechanical modelling of soft tissue. a literary review. *Department of mechanical Engineering, Imperial College of Science, Technology and Medicine*, pages 1–56, 2002.
- Barrett R, Soest van A. J, and Neal R. A computer-graphics model of muscle activation and contraction dynamics. *Sports Biomech*, 1(1):105–121, Jan 2002.
- Bässler U. Vom chordotonalorgan gesteuerte reaktionen bei der stabheuschrecke carausius morosus: Messung der, von der tibia erzeugten kraft im aktiven tier. *Kybernetik*, 1974.
- Bässler U. Reversal of a reflex to a single motoneuron in the stick insect carausius morosus. *Biological Cybernetics*, 1976.
- Bässler U. Sensory control of leg movements in the stick insect carausius morosus. *Biological Cybernetics*, 1977.
- Bässler U. Interactions of central and peripheral mechanisms during walking in first instar stick insects extatosoma tiaratum. *Physiol. Entomol.*, 4: 193–199, 1979.
- Bässler U. *Neural Basis of Elementary Behavior in Stick Insects*. Springer-Verlag, Berlin, Heidelberg, New York, 1983.
- Bässler U. Functional principles of pattern generation for walking movements of stick insect forelegs: The role of the femoral chordotonal organ afferences. *Journal of Experimental Biology*, 1988.
- Bässler U. The femur-tibia control system of stick insects - a model system for the study of the neural basis of joint control. *Brain Research Reviews*, 1993.

- Bässler U and Büschges A. Pattern generation for stick insect walking movements - multisensory control of a locomotor program. *Brain Research Reviews*, 1998.
- Bässler U and Storrer J. The neural basis of the femur-tibia-control system in the stick insect *carausius morosus*. 1. motoneurons of the extensor tibiae muscle. *Biological Cybernetics*, 38:107–114, 1980. in Ansgars Lit.
- Bässler U and Wegner U. Motor output of the denervated thoracic ventral nerve cord in the stick insect *carausius morosus*. *Journal of Experimental Biology*, 1983.
- Blümel M. Elektrophysiologische untersuchungen und simulationen zur schrittmustererzeugung bei der stabheuschrecke *carausius morosus*. Master's thesis, Universität Köln, Zoologisches Institut, 2004.
- Bobet J and Stein R. B. A simple model of force generation by skeletal muscle during dynamic isometric contractions. *IEEE Trans Biomed Eng*, 45(8): 1010–1016, Aug 1998.
- Boug D. M. *Physics for Game Developers*. O'Reilly Media, November 2001.
- Brown I. E and Loeb G. E. Measured and modeled properties of mammalian skeletal muscle: Iv. dynamics of activation and deactivation. *J Muscle Res Cell Motil*, 21(1):33–47, Jan 2000a.
- Brown I and Loeb G. A reductionist approach to creating and using neuromusculoskeletal models. In Winters J and P. Crago P, editors, *Biomechanics and Neuro-Control of Posture and Movement*, chapter 10, pages 148–163. Springer-Verlag, New York, 2000b.
- Bucher D, Akay T, Dicaprio R, and Büschges A. Interjoint coordination in the stick insect leg-control system: The role of positional signaling. *Journal of Neurophysiology*, 89:1245–1255, 2003.
- Büschges A, Kittmann R, and Schmitz J. Identified nonspiking interneurons in leg reflexes and during walking in stick insect. *Journal of Comparative Physiology*, 174:685–700, 1994.
- Büschges A, Schmitz J, and Bässler U. Rhythmic patterns in the thoracic nerve cord of the stick insect induced by pilocarpine. *Journal of Experimental Biology*, 198:435–456, 1995.
- Büschges A, Sauer A, and Bässler U. Flexibility of a proprioceptive feedback system results from its “parliamentary” (distributed) organisation.

- In Cruse H, Dean J, and Ritter H, editors, *Prerational Intelligence: Adaptive Behavior and Intelligent Systems Without Symbols and Logic.*, pages 267–286. Kluwer Publ., cruse,h. and dean,j. and ritter,h. edition, 2000.
- Büschges A. Sensory control and organization of neural networks mediating coordination of multisegmental organs for locomotion. *J Neurophysiol*, 93(3):1127–1135, Mar 2005.
- Chiel H. J, Ting L. H, Ekeberg O, and Hartmann M. J. Z. The brain in its body: motor control and sensing in a biomechanical context. *J Neurosci*, 29(41):12807–12814, Oct 2009.
- Chou C. P and Hannaford B. Dual stable point model of muscle activation and deactivation. *Biol Cybern*, 66(6):511–523, 1992.
- Chow J. W and Darling W. G. The maximum shortening velocity of muscle should be scaled with activation. *J Appl Physiol*, 86(3):1025–1031, Mar 1999.
- Cole G. K, Bogert van den A. J, Herzog W, and Gerritsen K. G. Modelling of force production in skeletal muscle undergoing stretch. *J Biomech*, 29(8):1091–1104, Aug 1996.
- Cruse H. On the function of the legs in the free walking stick insect *carausius morosus*. *J. Comp. Physiol.*, 112:235–262, 1976.
- Cruse H. The control of the anterior extreme position of the hindleg of a walking insect. *Physiol. Entomol.*, 4:121–124, 1979.
- Cruse H. Which parameters control the leg movement of a walking insect? ii. the start of the swing phase. *Journal of Experimental Biology*, 116:357–362, 1985.
- Cruse H. What mechanisms coordinate leg movement in walking arthropods? *Trends Neurosci*, 13(1):15–21, Jan 1990.
- Cruse H and Bartling C. Movement of joint angles in the legs of a walking insect, *carausius morosus*. *Journal of Insect Physiology*, 41:761–771, 1995.
- Cruse H, Schmitz J, Braun U, and Schweins A. Control of body height in a stick insect walking on a treadwheel. *Journal of Experimental Biology*, 181:141–155, 1993.
- Cruse H, Dean J, Kindermann T, and Schmitz J. Walknet - a decentralized architecture for the control of walking behavior based on insect studies. In

- Palm G, editor, *Hybrid Information Processing in Adaptive Autonomous Vehicles*. Springer, 1999.
- Cruse H, Bartling C, Dean J, Kindermann T, Schmitz J, and Schumm M. *A Simple Neural Network for the Control of a Six-Legged Walking System*. Springer, 2000.
- Delcomyn F. Activity and directional sensitivity of leg campaniform sensillae in a stick insect. *J. Comp. Physiol.*, 168:113–119, 1991.
- Delp S. L and Loan J. P. A graphics-based software system to develop and analyze models of musculoskeletal structures. *Comput Biol Med*, 25(1): 21–34, Jan 1995.
- Dickinson M, Farley C, Full R, Koehl M, Kram R, and Lehman S. How animals move: An integrative view. *Science*, 288:100–106, 2000.
- Dickinson M. Insect flight. *Curr Biol*, 16(9):R309–R314, May 2006.
- Duysens J, Clarac F, and Cruse H. Load-regulating mechanisms in gait and posture: Comparative aspects. *Phys. Rev.*, 80:83–133, 2000.
- Edman K. A. Double-hyperbolic force-velocity relation in frog muscle fibres. *J Physiol*, 404:301–321, Oct 1988.
- Edwards D. H. Neuromechanical simulation. *Front Behav Neurosci*, 4, 2010.
- Ekeberg O. Modeling of interactions between neural networks and musculoskeletal systems. In Schutter de , editor, *Computational Neuroscience, Realistic Modeling for Experimentalists*, pages 317–335. CRC-Press, 2001.
- Ekeberg O. A combined neuronal and mechanical model of fish swimming. *Biological Cybernetics*, 56, 5-6:363–374, 1993.
- Ekeberg O and Pearson K. Computer simulation of stepping in the hind legs of the cat: an examination of mechanisms regulating the stance-to-swing transition. *J Neurophysiol*, 94(6):4256–4268, Dec 2005.
- Ekeberg O, Blümel M, and Büschges A. Dynamic simulation of insect walking. *Arthropod Struct Dev*, 33(3):287–300, Jul 2004.
- Epstein S and Graham D. Behavior and motor output of stick insects walking on a slippery surface. i. forward walking. *Journal of Experimental Biology*, 105:215–229, 1983.
- Fischer H, Schmidt J, and Büschges A. Pattern generation for walking and searching movements of a stick insect leg i. coordination of motor activity. *Journal of Neurophysiology*, 85:241–353, 2001.

- Full and Ahn . Static forces and moments generated in the insect leg: comparison of a three-dimensional musculo-skeletal computer model with experimental measurements. *J Exp Biol*, 198(Pt 6):1285–1298, 1995.
- Full , Stokes , and a . Energy absorption during running by leg muscles in a cockroach. *J Exp Biol*, 201 (Pt 7):997–1012, Apr 1998.
- Golowasch J, Goldman M. S, Abbott L. F, and Marder E. Failure of averaging in the construction of a conductance-based neuron model. *J Neurophysiol*, 87(2):1129–1131, Feb 2002.
- Graham D. Pattern and control of walking insects. *Advances in insect physiology*, 18:31–140, 1985.
- Graham D and Cruse H. Coordinated walking of stick insects on a mercury surface. *Journal of Experimental Biology*, 92:229–241, 1981.
- Graham D and Wendler G. The reflex behavior and innervation of the tergo-coxal retractor muscles of the stick insect *carausius morosus*. *Journal of Comparative Physiology*, 143:81–91, 1981.
- Grillner S. Neurobiological bases of rhythmic motor acts in vertebrates. *Science*, 228(4696):143–149, Apr 1985.
- Grillner S. The motor infrastructure: from ion channels to neuronal networks. *Nat Rev Neurosci*, 4(7):573–586, Jul 2003.
- Grillner S, Wallén P, Saitoh K, Kozlov A, and Robertson B. Neural bases of goal-directed locomotion in vertebrates—an overview. *Brain Res Rev*, 57 (1):2–12, Jan 2008.
- Gruhn M, Hoffmann O, Dübbert M, Scharstein H, and Büschges A. Tethered stick insect walking: a modified slippery surface setup with optomotor stimulation and electrical monitoring of tarsal contact. *J Neurosci Methods*, 158(2):195–206, Dec 2006.
- Guschlbauer C. *Characterisation of the biomechanical, passive, and active properties of femur-tibia joint leg muscles in the stick insect Carausius morosus*. PhD thesis, Universität zu Köln, 2009.
- Guschlbauer C, Scharstein H, and Büschges A. The extensor tibiae muscle of the stick insect: biomechanical properties of an insect walking leg muscle. *J Exp Biol*, 210(Pt 6):1092–1108, Mar 2007.
- Hannaford B and Winters J. *Actuator Properties and Movement Control: Biological and Technonogical Models In: Multiple Muscle Systems: Biomecha-*

- nics and Movement Organization*, chapter 7, pages 102–120. Springer, New York, 1990.
- Happee R. Inverse dynamic optimization including muscular dynamics, a new simulation method applied to goal directed movements. *J Biomech*, 27(7): 953–960, Jul 1994.
- Hatze H. A myocybernetic control model of skeletal muscle. *Biol Cybern*, 25 (2):103–119, Jan 1977.
- Hatze H. A general myocybernetic control model of skeletal muscle. *Biol Cybern*, 28(3):143–157, Feb 1978.
- Hess D and Büschges A. Sensorimotor pathways involved in interjoint reflex action of an insect leg. *Journal of Neurobiology*, 33:891–913, 1997.
- Hess D and Büschges A. Role of proprioceptive signals from an insect femur-tibia joint in patterning motoneuronal activity of an adjacent leg. *Journal of Neurophysiology*, 81:1856–1865, 1999.
- Hill A. The heat of shortening and the dynamic constants of muscle. *Proc R Soc Lond B Biol Sci*, 126:136–195, 1938.
- Hill A. The series elastic component of muscle. *Proc R Soc Lond B Biol Sci*, 141:104–117, 1950.
- Hofmann T and Bässler U. Anatomy and physiology of trochanteral campaniform sensilla in the stick insect *cuniculina impigra*. *Physiol. Entomol.*, 7: 413–426, 1982.
- Holmes P, Full R, Koditschek D, and Guckenheimer J. The dynamics of legged locomotion: Model, analyses and challenges. *SIAM Review*, 48:207–304, 2006.
- Hooper S. L. Variation is the spice of life. focus on "cycle-to-cycle variability of neuromuscular activity in aplysia feeding behavior". *J Neurophysiol*, 92 (1):40–41, Jul 2004.
- Hooper S. L, Guschlbauer C, Uckermann von G, and Büschges A. Natural neural output that produces highly variable locomotory movements. *J Neurophysiol*, 96(4):2072–2088, Oct 2006.
- Hooper S. L, Guschlbauer C, Uckermann von G, and Büschges A. Slow temporal filtering may largely explain the transformation of stick insect (*ca-rausius morosus*) extensor motor neuron activity into muscle movement. *J Neurophysiol*, 98(3):1718–1732, Sep 2007.

- Hooper S. L, Guschlbauer C, Blümel M, Rosenbaum P, Gruhn M, Akay T, and Büschges A. Neural control of unloaded leg posture and of leg swing in stick insect, cockroach, and mouse differs from that in larger animals. *J Neurosci*, 29(13):4109–4119, Apr 2009.
- Horn C, Zhurov Y, Orkhova I, Proekt A, Kupfermann I, Weiss K, and Brenzina V. Cycle-to-cycle variability of neuromuscular activity in aplysia feeding behavior. cycle-to-cycle variability of neuromuscular activity in aplysia feeding behavior. *J Neurophysiol*, 91:157–180, 2004.
- Houdijk H, Bobbert M. F, and Haan de A. Evaluation of a hill based muscle model for the energy cost and efficiency of muscular contraction. *J Biomech*, 39(3):536–543, 2006.
- Hoy M. G, Zajac F. E, and Gordon M. E. A musculoskeletal model of the human lower extremity: the effect of muscle, tendon, and moment arm on the moment-angle relationship of musculotendon actuators at the hip, knee, and ankle. *J Biomech*, 23(2):157–169, 1990.
- Joyce G. C and Rack P. M. Isotonic lengthening and shortening movements of cat soleus muscle. *J Physiol*, 204(2):475–491, Oct 1969.
- Joyce G. C, Rack P. M, and Westbury D. R. The mechanical properties of cat soleus muscle during controlled lengthening and shortening movements. *J Physiol*, 204(2):461–474, Oct 1969.
- Katz B. The relation between force and speed in muscular contraction. *J Physiol*, 96(1):45–64, Jun 1939.
- Klein C, Biomechanische Eigenschaften des Extensor tibiae bei *Locusta migratoria*: Vergleich des Kraftbeitrags unterschiedlicher Muskelfasertypen zur Kraft-Längen-Beziehung. Bachelorthesis, Department of Zoology, Universität zu Köln, 2009.
- Kubow T and Full R. The role of the mechanical system in control: A hypothesis of selfstabilization in hexapedal runners. *Phil. Trans. R. Soc. London*, B:849–861, 1999.
- Lewinger W and Quinn R. A small, autonomous, agile robot with an on-board, neurobiologically-based control system. In *Intelligent Robots and Systems, 2009. IROS 2009. IEEE/RSJ International Conference on*, 2009.
- Lewinger W. A, Rutter B. L, Blümel M, Büschges A, and Quinn R. D. Sensory coupled action switching modules (scasm) generate robust, adaptive step-

- ping in legged robots. In *CLAWAR 2006: 9th International Conference on Climbing and Walking Robots*, 2006.
- Lloyd D. G and Besier T. F. An emg-driven musculoskeletal model to estimate muscle forces and knee joint moments in vivo. *J Biomech*, 36(6):765–776, Jun 2003.
- Loeb G. E, Brown I. E, and Cheng E. J. A hierarchical foundation for models of sensorimotor control. *Exp Brain Res*, 126(1):1–18, May 1999.
- Marder E and Bucher D. Central pattern generators and the control of rhythmic movements. *Curr Biol*, 11(23):R986–R996, Nov 2001.
- Meijer K, Grootenboer H. J, Koopman H. F, Linden van der B. J, and Huijing P. A. A hill type model of rat medial gastrocnemius muscle that accounts for shortening history effects. *J Biomech*, 31(6):555–563, Jun 1998.
- Nigg B. M. *Biomechanics of the Musculo-skeletal System*. Wiley and Sons, 1995.
- Novakovic V. A, Sutton G. P, Neustadter D. M, Beer R. D, and Chiel H. J. Mechanical reconfiguration mediates swallowing and rejection in *aplysia californica*. *J Comp Physiol A Neuroethol Sens Neural Behav Physiol*, 192(8):857–870, Aug 2006.
- Pandy M. G. Computer modeling and simulation of human movement. *Annu Rev Biomed Eng*, 3:245–273, 2001.
- Pearson K. G. Role of sensory feedback in the control of stance duration in walking cats. *Brain Res Rev*, 57(1):222–227, Jan 2008.
- Pearson K, Ekeberg O, and Büschges A. Assessing sensory function in locomotor systems using neuro-mechanical simulations. *Trends Neurosci*, 29(11):625–631, Nov 2006.
- Pearson K. G. Generating the walking gait: role of sensory feedback. *Prog Brain Res*, 143:123–129, 2004.
- Pearson K. Common principles of motor control in vertebrates and invertebrates. *Annu. Rev. Neurosci.*, 16:265–297, 1993a.
- Pearson K. Common principles of motor control in vertebrates and invertebrates. *Annu. Rev. Neurosci.*, 16:265–297, 1993b.
- Proske U and Morgan D. L. Do cross-bridges contribute to the tension during stretch of passive muscle? *J Muscle Res Cell Motil*, 20(5-6):433–442, Aug 1999.

- Rassier D. E and Herzog W. Considerations on the history dependence of muscle contraction. *J Appl Physiol*, 96(2):419–427, Feb 2004.
- Ritzmann R. E and Büschges A. Adaptive motor behavior in insects. *Curr Opin Neurobiol*, 17(6):629–636, Dec 2007.
- Rosen J, Fuchs M. B, and Arcan M. Performances of hill-type and neural network muscle models-toward a myosignal-based exoskeleton. *Comput Biomed Res*, 32(5):415–439, Oct 1999.
- Rutter B. *Robotic models of neuromechanical step generation in insects*. PhD thesis, CASE Western Reserve University, Department of Mechanical and Aerospace Engineering, 2009.
- Sandercock T. G and Heckman C. J. Force from cat soleus muscle during imposed locomotor-like movements: experimental data versus hill-type model predictions. *J Neurophysiol*, 77(3):1538–1552, Mar 1997.
- Schmitz J. Properties of the feedback system controlling the coxa-trochanter joint in the stick insect *carausius morosus*. *Biological Cybernetics*, 55: 35–42, 1986.
- Schmitz J and Schöwerling H. No effects of coxo-trochanteral proprioceptors on extensor tibiae morot neurons in posture control. In *Proceedings of the 20th Göttingen Neurobiology Conference*, 1992.
- Shue G. H and Crago P. E. Muscle-tendon model with length history-dependent activation-velocity coupling. *Ann Biomed Eng*, 26(3):369–380, 1998.
- Siebert T, Sust M, Thaller S, Tilp M, and Wagner H. An improved method to determine neuromuscular properties using force laws - from single muscle to applications in human movements. *Hum Mov Sci*, 26(2):320–341, Apr 2007.
- Siebert T, Rode C, Herzog W, Till O, and Blickhan R. Nonlinearities make a difference: comparison of two common hill-type models with real muscle. *Biol Cybern*, 98(2):133–143, Feb 2008.
- Storrer J. *Systematische Untersuchungen am “Kniesehenreflex” der Stabheuschrecke Carausius morosus Br. (Orthoptera)*. PhD thesis, Universität Kaiserslautern, 1976.
- Thelen D. G, Anderson F. C, and Delp S. L. Generating dynamic simulations of movement using computed muscle control. *J Biomech*, 36(3):321–328, Mar 2003.

- Thuma J, Morris L, Weaver A, and Hooper S. Lobster (*panulirus interruptus*) pyloric muscles express the motor patterns of three neural networks, only one of which innervates the muscle. *J Neurosci*, 23:8911–8920, 2003.
- Ingen Schenau van G. J, Bobbert M. F, Ettema G. J, Graaf de J. B, and Huijing P. A. A simulation of rat edl force output based on intrinsic muscle properties. *J Biomech*, 21(10):815–824, 1988.
- Soest van A. J, Schwab A. L, Bobbert M. F, and Ingen Schenau van G. J. The influence of the biarticularity of the gastrocnemius muscle on vertical-jumping achievement. *J Biomech*, 26(1):1–8, Jan 1993.
- Twickel von A, Büschges A, and Pasemann F. Deriving neural network controllers from neuro-biological data – implementation of a single-leg stick insect controller. *under review*, 2010a.
- Twickel von A, Marcus Blümel A. B, and Pasemann F. Does implementation of a muscle model improve performance and robustness of neural control of stepping? *in prep*, 2010b.
- Wagner H, Siebert T, Ellerby D. J, Marsh R. L, and Blickhan R. Isofit: a model-based method to measure muscle-tendon properties simultaneously. *Biomech Model Mechanobiol*, 4(1):10–19, Aug 2005.
- Weidler D and Diecke F. The role of cations in the central nervous system of the herbivorous insect *carausius morosus*. *Zeitschrift für vergleichende Physiologie*, 1969.
- Weiler V, Mentel T, and Büschges A. Activity of modulatory neurons during leg movements in the stick insect. In *Neurowissenschaftliche Gesellschaft 5: 65B*, 2005.
- Winters J. *Hill-Based Muscle Models: A Systems Engineering Perspective*. In: *Multiple Muscle Systems: Biomechanics and Movement Organization*, chapter 5, pages 69–93. Springer, New York, 1990.
- Yu S. N, Crago P. E, and Chiel H. J. Biomechanical properties and a kinetic simulation model of the smooth muscle i2 in the buccal mass of *aplysia*. *Biol Cybern*, 81(5-6):505–513, Nov 1999.
- Zahalak G. I. A comparison of the mechanical behavior of the cat soleus muscle with a distribution-moment model. *J Biomech Eng*, 108(2):131–140, May 1986.

- Zahalak G. I and Ma S. P. Muscle activation and contraction: constitutive relations based directly on cross-bridge kinetics. *J Biomech Eng*, 112(1): 52–62, Feb 1990.
- Zahalak G. I. A distribution-moment approximation for kinetic theories of muscular contraction. *Mathematical Biosciences*, 55(1-2):89 – 114, 1981. ISSN 0025-5564.
- Zajac F. E. Muscle and tendon: properties, models, scaling, and application to biomechanics and motor control. *Crit Rev Biomed Eng*, 17(4):359–411, 1989.
- Zajac F and Winters J. *Modeling Musculoskeletal Movement Systems: Joint and Body Segmental Dynamics, Musculoskeletal Actuation, and Neuromuscular Control In: Multiple Muscle Systems: Biomechanics and Movement Organization*, chapter 8, pages 121–148. Springer, New York, 1990.
- Zajac F. E. Understanding muscle coordination of the human leg with dynamical simulations. *J Biomech*, 35(8):1011–1018, Aug 2002.
- Zajac F. E, Neptune R. R, and Kautz S. A. Biomechanics and muscle coordination of human walking. part i: introduction to concepts, power transfer, dynamics and simulations. *Gait Posture*, 16(3):215–232, Dec 2002.
- Zajac F. E, Neptune R. R, and Kautz S. A. Biomechanics and muscle coordination of human walking: part ii: lessons from dynamical simulations and clinical implications. *Gait Posture*, 17(1):1–17, Feb 2003.
- Zakotnik J. *Biomechanics and neural control of targeted limb movements in an insect*. PhD thesis, Universität Bielefeld, Februar 2006.
- Zakotnik J, Matheson T, and Dürr V. Co-contraction and passive forces facilitate load compensation of aimed limb movements. *J Neurosci*, 26(19): 4995–5007, May 2006.

Acknowledgements

In deep gratefulness to all my friends and colleagues that supported me throughout the past years, I would like to thank in particular:

*My supervisor
Prof. Dr. Ansgar Büschges,*

•

Prof. Scott L. Hooper,

•

*Dr. Brandon Rutter and Arndt von Twickel
You both inspired me in countless, thrilling discussions.*

•

*All members
(and not less the former members) of the Büschges lab,
whom I had the pleasure to become acquainted with.*

•

*Katja Hellekes
for wearing your heart on your sleeve.*

•

*Eugénio de Oliveira
for spreading the touch of Brazilian joy of living, in combination with
admirable commitment to research.*

*Especially I like to thank
Dr. Christoph Guschlbauer,
for collaborating so closely in all the years, for the extraordinary experiments
he conducted, his peerless physiological expertise as well as for endless
gossiping, discussing and, above all, for his friendship.*

•

Particular, additional gratitude goes to

Katja Wiegemann

*for accompanying me through my years of study, research and lifes ups and
downs, since 1995.*

•

Dr. Manuela Rehtanz and Dr. Jörg Albert

for your exhilarant, motivating, and sometimes vital correnpondence.

•

Finally, I am deeply indebted to :

*Klaus W. Blümel,
not only for proof reading but also*

for your impassionate involvement in countless discussions.

•

*And thank you «so much a few»
Kristina Paeschke
there,for,that,you,maked,my,englisch,readably...*

Erklärung

Ich versichere, dass ich die von mir vorgelegte Dissertation selbstständig angefertigt, die benutzten Quellen und Hilfsmittel vollständig angegeben und die Stellen der Arbeit - einschließlich Tabellen, Karten und Abbildungen -, die anderen Werken im Wortlaut und Sinn nach entnommen sind, in jedem Einzelfall als Entlehnung kenntlich gemacht habe; dass diese Dissertation noch keiner anderen Fakultät oder Universität zur Prüfung vorgelegen hat; dass sie - abgesehen von oben angegebenen Teilpublikationen - noch nicht veröffentlicht worden ist sowie, dass ich eine solche Veröffentlichung vor Abschluss des Promotionsverfahrens nicht vornehmen werde. Die Bestimmungen dieser Promotionsordnung sind mir bekannt. Die von mir vorgelegte Dissertation ist von Prof. Dr. Ansgar Büschges betreut worden.

